DISSERTATION

IMPROVING HYDROLOGIC MODELING OF RUNOFF PROCESSES USING DATA-

DRIVEN MODELS

Submitted by

Heechan Han

Department of Civil and Environmental Engineering

In partial fulfillment of the requirements

For the Degree of Doctor of Philosophy

Colorado State University

Fort Collins, Colorado

Spring 2021

Doctoral Committee:

    Advisor: Ryan Morrison

    Neil S. Grigg
    Ryan T. Bailey
    Stephanie Kampf

ABSTRACT

IMPROVING HYDROLOGIC MODELING OF RUNOFF PROCESSES USING DATA-DRIVEN MODELS

Accurate rainfall–runoff simulation is essential for responding to natural disasters, such as floods and droughts, and for proper water resources management in a wide variety of fields, including hydrology, agriculture, and environmental studies. A hydrologic model aims to analyze the nonlinear and complex relationship between rainfall and runoff based on empirical equations and multiple parameters. To obtain reliable results of runoff simulations, it is necessary to consider three tasks, namely, reasonably diagnosing the modeling performance, managing the uncertainties in the modeling outcome, and simulating runoff considering various conditions.

Recently, with the advancement of computing systems, technology, resources, and information, data-driven models are widely used in various fields such as language translation, image classification, and time-series analysis. In addition, as spatial and temporal resolutions of observations are improved, the applicability of data-driven models, which require massive amounts of datasets, is rapidly increasing. In hydrology, rainfall–runoff simulation requires various datasets including meteorological, topographical, and soil properties with multiple time steps from sub-hourly to monthly. This research investigates whether data-driven approaches can be effectively applied for runoff analysis. In particular, this research aims to explore if data-driven models can 1) reasonably evaluate hydrologic models, 2) improve the modeling

performance, and 3) predict hourly runoff using distributed forcing datasets. The details of these three research aspects are as follows:

First, this research developed a hydrologic assessment tool using a hybrid framework, which combines two data-driven models, to evaluate the performance of a hydrologic model for runoff simulation. The National Water Model, which is a fully distributed hydrologic model, was used as the physical-based model. The developed assessment tool aims to provide easy-to-understand performance ratings for the simulated hydrograph components, namely, the rising and recession limbs, as well as for the entire hydrograph, against observed runoff data. In this research, four performance ratings were used. This is the first research that tries to apply data-driven models for evaluating the performance of the National Water Model and the results are expected to reasonably diagnose the model's ability for runoff simulations based on a short-term time step.

Second, correction of errors inherent in the predicted runoff is essential for efficient water management. Hydrologic models include various parameters that cannot be measured directly, but they can be adjusted to improve the predictive performance. However, even a calibrated model still has obvious errors in predicting runoff. In this research, a data-driven model was applied to correct errors in the predicted runoff from the National Water Model and improve its predictive performance. The proposed method uses historic errors in runoff to predict new errors as a post-processor. This research shows that data-driven models, which can build algorithms based on the relationships between datasets, have strong potential for correcting errors and improving the predictive performance of hydrologic models.

Finally, to simulate rainfall-runoff accurately, it is essential to consider various factors such as precipitation, soil property, and runoff coming from upstream regions. With

improvements in observation systems and resources, various types of forcing datasets, including remote-sensing based data and data-assimilation system products, are available for hydrologic analysis. In this research, various data-driven models with distributed forcing datasets were applied to perform hourly runoff predictions. The forcing datasets included different hydrologic factors such as soil moisture, precipitation, land surface temperature, and base flow, which were obtained from a data assimilation system. The predicted results were evaluated in terms of seasonal and event-based performances and compared with those of the National Water Model. The results demonstrated that data-driven models for hourly runoff forecasting are effective and useful for short-term runoff prediction and developing flood warning system during wet season.

ACKNOWLEDGMENTS

Above all things, I would like to thank my Lord, Jesus Christ, who always gives me strength and unconditional love. This is my true confession; your countless help and guidance made me overcome challenges of work and manage every single process of this dissertation.

I am pleased to note my appreciation to all of those who helped me complete this dissertation research. First, a heartfelt thanks to my parents and my brother`s family who have supported my study abroad for six years. You all have shown me great love and trust; each of your being is my power, thus, I am able to stand still wherever I am.

A special thanks to my wife, who has always shared tears and laughter with me and whose love and support have helped me stand still in the swirls of studying and dwelling abroad. You are the greatest encourager in every single day of my study.

My deepest appreciation to my advisor, mentor, and committee chair, Dr. Ryan Morrison, whose insight and spirit of compassion in regard to research and mentoring has guided my graduate study successfully. Your bright input paved the way for me to continue my graduate work. Your generosity, consistent caring, and encouragement empowered me as a graduate student with the potential to expand learning. Your persistent guidance and help have been essential for the completion of my dissertation.

I want to thank my committee members, Dr. Neil Grigg, Dr. Ryan Bailey, and Dr. Stephanie Kampf, for advice and support. I also appreciate that their great lecture, insight, wisdom, compassion, and warmth have strongly motivated me to enlarge perspective of my dissertation.

I would also like to thank my first advisor, Dr. Jorge Ramirez, who encouraged me during the first four years of my graduate study. Your deepest interest and desire regarding

research have strongly motivated me to continue my graduate work. Your class has provided me with the greatest input and inspiration that changed my whole perspective of research. Now I pray that you are resting well in heaven.

I give many thanks to my entire faculty, who provide me with a chance to gain bright insights and knowledge at the graduate school.

Last, I express my warmest thanks to my friends who have always been beside me, and whose trust has become a power in every single day of my life.

<div align="right">

Heechan Han

Fort Collins, Colorado

</div>

DEDICATION

To my Lord,

I can do everything through you who strengthen me.

To my parents, Changkyuk and Heeboon

To my wife, Jinju

To my daughter, Kaylee and son, Noah

To my brother, Heejun and his family, Jinyoung, Sowon, and Shalom

TABLE OF CONTENTS

LIST OF TABLES

LIST OF FIGURES

Chapter 1

Introduction

This chapter introduces the objectives of this research and the application of data-driven models for developing an integrated runoff analysis system. It includes the background of rainfall–runoff modeling, hydrologic assessment, uncertainties in hydrologic models, and data-driven models. The objectives and structure of this dissertation are also presented.

Surface runoff is water from various sources, including precipitation and snowmelt, that flows over the land surface. It is a major driving force of natural disasters (such as floods and droughts), sediment transportation, soil contamination and erosion, and water resources management. Estimating surface runoff is important in several fields including hydrology, agriculture, and environmental studies. Thus, accurate rainfall–runoff modeling is an important task in such fields.

Several rainfall–runoff analysis methods have been developed to simulate the flow and volume of runoff. Hydrologic models that aim to simulate the water cycle (e.g., surface runoff,

base flow, groundwater flow, soil moisture, and evapotranspiration) generated from precipitation are based on various theoretical and empirical formulas. Many types of hydrologic models have advanced from lumped models, which aim to provide forecast information at an outlet point using characteristics across an entire watershed, to distributed models, which are based on spatially varying characteristics across the watershed (Liang et al., 1994; Arnold et al., 1998; Singh and Woolhiser, 2002; Kim et al., 2019).

Hydrologic models can include 1D, 2D, and 3D simulation capabilities (Xiang et al., 2020). The 1D model is mainly used to understand the spatial–temporal changes in the characteristics of rivers and their impacts on the surrounding environment. It aims to simulate the water flow to estimate the average velocity and water depth at each cross section. The MIKE11 is 1D software that simulates the water level, water quality, and transport of sediment in rivers (Wang et al., 2014). The 2D model is used to solve steady and unsteady flow equations in which water flows both longitudinally and latitudinally. The Soil and Water Assessment Tool (SWAT) is a typical 2D hydrologic model, which has been integrated with the ArcGIS interface to allow 2D based simulations that are widely used in the agricultural field (Arnold et al., 1998). The MIKE SHE and MIKE3 provide 3D simulations of surface flow and sediment in various fields, and they require high-quality physical data for calculating physical equations (Devia et al., 2015; Xiang et al., 2020).

In 2016, the National Water Model (NWM), which is a fully distributed hydrologic model, was developed. The NWM aims to enhance the flood forecasting capability of the National Oceanic and Atmospheric Administration (NOAA) hydrologic prediction system (Han et al., 2019; Kim et al., 2019). It is based on the community Weather Research and Forecasting Hydrologic (WRF-Hydro) modeling system, which produces various hydrologic analysis and

prediction products, including gridded fields of surface runoff, soil moisture, snowpack, shallow groundwater levels, inundated area depths, and evapotranspiration, as well as estimates of river flow and velocity for approximately 2.7 million river reaches defined by the seamless National Hydrography Dataset (NHD) Plus v2.0 (Kim et al., 2019).

As various hydrologic models are developed, studies on improving their runoff modeling performance are essential. In addition, for precise hydrologic analysis and prediction, comprehensive and accurate evaluations are necessary to reduce the model errors and improve performance. The trend of studies aimed at improving the performance of numerous hydrologic models is increasing; however, the methods for evaluating and diagnosing the capability of models for hydrologic analysis and minimizing errors have remained simple. A hydrologic evaluation method should reasonably determine the reliability of outputs and present objective indices that are understandable to users. The limitations of the current hydrologic evaluation methods must be overcome, and a new tool that can objectively assess the performance of any hydrologic model is required.

After determining the uncertainty inherent in the modeling result by diagnosing the model capability, it is also necessary to reduce the uncertainty in the model and improve its performance. Thus, a question arises as to how well or how adequate is the match between the real and simulated results from the model (Abebe and Price, 2004). Owing to incomplete information in the models, differences (errors) will always exist between the simulated results from the model and the corresponding observations. Therefore, one challenge is to reduce the errors in the model predictions consistently such that the physically-based hydrologic model can be used for its intended purpose.

Error analysis in hydrologic modeling has become a popular research topic over the last three decades (Shrestha and Solomatine, 2009). According to Montanari and Brath (2004), errors in hydrologic modeling outputs originate from several causes, such as input uncertainty, parameter uncertainty, and model uncertainty. Correcting errors in a hydrologic model is essential to obtain accurate forecasting results. Moreover, errors associated with the quality of input data affect the model in the operation stage and errors in the observations translate to the model through its outputs (Abebe and Price, 2003). Calibration of a model is the process of improving its performance by adjusting its parameters, which works as a pre-process for the modeling. However, it is inadequate for minimizing the errors of the model because there are errors from other sources, which are not covered in the calibration process. The main goal of forecasting errors in hydrologic models is to find the error relationship between various factors such as precipitation, runoff from upstream, and outcome from the model.

In addition, the main objective of hydrologic models is to simulate and predict runoff based on the rainfall–runoff relationship. However, accurate runoff modeling is a challenge because runoff forecasting is a complex dynamic process characterized by spatial and temporal variations. In addition, rainfall–runoff relationships are complex and nonlinear processes influenced by various factors such as rainfall, soil moisture, temperature, and other climatic characteristics. Physically-based hydrologic models cannot handle non-stationary and nonlinear factors involved in hydrologic modeling.

There are two main methods to predict runoff. The first method is physically-based hydrologic modeling. The physically-based model simulates the water flow process from rainfall to runoff. It requires various inputs, such as topography data and model parameters, which are not always available and could be difficult to obtain. In addition, the model parameters should be

calibrated as they significantly influence the output (Le et al., 2019). Furthermore, it is difficult to find the parameters that fit the model, as they are regionally dependent. As a result, physically-based models may not show good performance especially in areas where the data available are limited (Le et al., 2019).

Because of the limitations of physically-based models, many researchers have shifted to the second method for forecasting runoff, which is data-driven modeling (Yan et al., 2019). This method uses the statistical relationships between datasets instead of simulating physical processes. Data-driven approaches are based on the functional relationship between independent (e.g., input) and dependent (e.g., target) datasets (Kim et al., 2019; Liang et al., 2019). They include algorithms that allow machines to improve their performance over time based on relationships between datasets. During the past two decades, data-driven models contributed significantly to the advancement of hydrologic analysis in providing good performance and cost-effective solutions (Mosavi et al., 2018). The commonly used method of data-driven modeling is the artificial neural network (ANN), which was introduced by Rosenblatt (1958). A data-driven model can provide an alternative approach for forecasting hydrologic variables such as runoff, rainfall, groundwater, water level, and soil moisture. Currently, various studies have applied data-driven models to simulate and predict hydrologic variables (Solomatine and Dulal, 2003; Jothiprakash and Magar, 2012; Lin et al., 2013; Tsai et al., 2014; Chang and Tsai, 2016; Ba et al., 2018; Hu et al., 2018; Feng et al., 2019; Bui et al., 2020; Choi et al., 2020; Fan et al., 2020; Xiang et al., 2020). These studies found that data-driven models have good performance for hydrologic forecasting, and the models can be effective alternatives to physically-based models. Furthermore, for evaluating and diagnosing a model's ability for hydrologic analysis and minimizing errors in its output, data-driven approaches can be used.

However, studies about the application of data-driven models on developing new methods for improving runoff modelling processes, including evaluation of models` performance, improvement of models` performance by error prediction and correction, and prediction runoff considering distributed forcing datasets, have rarely been conducted. Thus, in this dissertation, methods using data-driven models were developed to improve the runoff modelling processes as follows: 1) developing a new hydrologic assessment tool based on hybrid framework of data-driven models to provide easy-to-understand evaluation ratings on the physically-based hydrologic model, 2) building a post-processor error correction tool for improving hydrologic modelling performance, and 3) forecasting hourly runoff by considering distributed forcing datasets. The NWM, which is used for flood forecasting over the Continental United States (CONUS), was selected as the hydrologic model, and the Russian River basin in California, USA was used as a case study.

The dissertation is organized as follows: Chapter 2 presents a literature review of previous studies related to each topic of the dissertation. In Chapter 3, the data-driven models used are described, including how the models are applied to develop the tools for evaluating and improving the NWM and forecast runoff. Chapter 4 presents the development of a composite evaluation method based on multiple error indices for the hydrologic assessment using data-driven approaches. This method provides easy-to-understand evaluation ratings on the reliability of the NWM and it was used to evaluate the performance of the NWM in the San Francisco Bay area. Chapter 5 discusses the application of data-driven approaches in developing a post-processor tool for improving the performance of the NWM based on error prediction. The developed tool was used to estimate errors with 1–18 h of lead time to correct forecasted runoff generated from the NWM. Finally, Chapter 6 presents the technique of forecasting runoff using

data-driven models and distributed forcing datasets in the Russian River basin and shows the comparison results with the NWM performance.

As observation systems such as radar and satellites are rapidly progressing, it is necessary to develop an efficient method for hydrologic analysis. Furthermore, as the resolution of observed data becomes more sophisticated, a method for supporting the data processing capability of hydrologic models is essential. This dissertation attempts to show the applications of data-driven approaches for three tasks, namely, diagnosing the model ability, improving the model performance, and forecasting runoff, which can serve as references for more sophisticated and reliable hydrologic analysis.

Chapter 2

Literature Reviews

This literature review includes studies on hydrologic assessment, error prediction, and runoff forecasting using data-driven models, as well as the limitations of previous studies.

2.1 Development of a Hydrologic Assessment Tool (HAT) Using Data-Driven Models

Because hydrologic models are created to physically simulate water flow in time and space, it is essential to develop methods for accurately evaluating the performance of these models. There are various types of hydrologic models, including lumped based models, which use aggregate characteristics of an entire watershed to simulate the water flow at one outlet point, and distributed models, which account for spatially varying features of the watershed (Liang et al., 1994; Arnold et al., 1998; Singh and Woolhiser, 2002; Cosgrove et al., 2018; Kim et al., 2019). However, the methods for hydrologic assessment have not yet evolved and still depend on several common error indices (Kim et al., 2019).

There are two main methods widely used for evaluating hydrologic models, namely, graphical and statistical approaches (Green and Stephenson, 1986; Legates and McCabe, 1999; Coffey et al., 2004). The graphical evaluation method involves comparing the observed and simulated hydrograph results from the hydrologic model (ASCE, 1993). According to Kim et al. (2019), the graphical method has the advantage of being able to easily detect the difference between two datasets without additional interpretations. However, the method is subjective, which can lead to inconsistent evaluation results of modeling performance by users.

The statistical evaluation method generally uses various statistical metrics. It is easy to understand the modeling performance, but it has the disadvantage that it cannot present standardized ratings for various error indices. Moreover, the statistical evaluation method using a single error index cannot reflect the composite interactions between various error indices. It is also questionable how reasonably the ranges of error indices are defined and how they can represent the modeling performance (Donigian et al., 1983; Ramanarayanan et al., 1997; Gupta et al., 2009; Singh et al., 2005).

As the quantity and quality of hydrologic data increase, data-driven models can be alternatives to overcome the shortcomings of general evaluation methods. Data-driven models with different features can be combined for effective data analysis; these are called hybrid frameworks of data-driven models. There are several studies that use the concept of hybrid frameworks to combine two or more models (Hsieh, 2005; Tsai and Chen, 2010; Tsai et al., 2014). These studies used the hybrid framework to combine classification and clustering data-driven techniques for various objectives. It was concluded that the hybrid framework is suitable for various applications. It can complement the limitations of a single model and shows improved outcomes. Thus, the hybrid framework is considered an attractive approach for

hydrologic evaluation using various error indices. Moreover, it can be a reliable performance assessment tool by employing big data and has an advantage of determining a composite rating metric.

There are limitations to the previous studies that this research will overcome. They are as follows:

1) The evaluation of hydrologic model results may be subjective.

2) Single error indices cannot accurately represent the performance of the model.

3) Most of the evaluation methods disregard specific components of time-series data (e.g., the rising or recession limbs of hydrographs).

4) It is sometimes difficult for users of the model to understand the evaluation results.

2.2 Improvement of Modeling Performance Using Data-Driven Model

Many studies have used data-driven approaches to analyze and reduce the errors of hydrologic models for improving their performance. Moreover, various studies applied complementary modeling by using data-driven models to improve the accuracy of hydrologic models. Abebe and Price (2003; 2004) presented a complementary model to manage uncertainties in hydrologic models using an ANN model. They focused on the relationship between precipitation data and error in output (i.e., runoff) of the model. They used the ANN to determine the relationship between precipitation with various time steps and output error to forecast new residuals of the hydrologic model. They concluded that the use of ANN models to predict errors of hydrologic models can significantly improve the model performance. Wu et al. (2018) proposed a complementary model to predict the error and improve the performance of a hydrologic model. They used a random forest (RF) model as a machine learning technique to

predict the error using the relationships between the input variables (e.g., precipitation and temperature) and output (e.g., runoff) errors. They found that the machine learning technique is capable of improving the performance of the original model. In addition, some studies used the machine learning–based methods to estimate the uncertainties in the model. Shrestha and Solomatine (2009) used a machine learning approach to estimate the probability distribution of error in a hydrologic model. They applied machine learning to estimate the prediction intervals of the model outputs. The study showed that machine learning can estimate the uncertainties in the model reasonably compared to existing methods.

To improve the performance of groundwater models (e.g., MODFLOW), Xu et al. (2014) applied machine learning techniques to predict the error in groundwater head. They used several machine learning techniques to predict model errors and found that machine learning can reduce the error of spatiotemporal predictions of groundwater head in the models. Demissie et al. (2009) also presented a machine learning error-correcting method to improve the performance of groundwater models. They used four machine learning techniques (i.e., ANN, support vector machine (SVM), decision tree, and instance-based weighting) to demonstrate how machine learning methods can reduce model errors compared to typical calibration methods. Moreover, other studies applied a deep learning–based data-driven model to develop a post-processing method for improving the performance of hydrologic models (Frame et al., 2020; Nearing et al., 2020). These studies found that the data-driven approaches can be effective for improving the performance of the model.

Previous studies have focused on the relationship between input variables and output errors used in the hydrologic models. However, it is difficult to deal with external influences

because the models only consider model-related errors. Thus, this study performed an error analysis considering external errors originating from upstream regions.

2.3 Hourly Runoff Prediction Using Data-Driven Models

Data-driven models are gaining popularity in hydrology, and several studies have applied them for modeling hydrologic processes. Specifically, these models have been effective approaches for predicting hydrologic variables, including runoff, precipitation, ground-water level, and soil moisture, as alternatives to physically-based hydrologic models (Adamowski and Chan, 2011; Partal and Cigizoglu, 2008; Rajaee et al., 2011; Adnan et al., 2012; Sahoo et al., 2017; Choi et al., 2020; Xiang et al., 2020). These studies showed that data-driven models can provide satisfactory performance in hydrologic forecasting, and they can overcome the limitations of physically-based models.

One commonly used data-driven model for hydrologic prediction is the ANN model. Elsafi (2014) used an ANN model for one-day streamflow forecasting in the Nile River basin using upstream flow data. They found that the ANN is suitable for runoff forecasting for short lead times. Hidayat et al. (2014) forecasted discharge in a tidal river (Mahakam River, Indonesia) using an ANN model, and they reported that the ANN model shows good performance for discharge forecasting with a lead time of 2 days. In addition, various data-driven models, such as SVM, multilayer perceptron, and recurrent neural network (RNN), have been applied for runoff forecasting (Tian et al., 2018; Wu et al., 2019).

Recently, a data-driven approach known as deep learning has received increasing attention and has been applied in various fields. The deep learning technique has been used for forecasting dependent variables. Particularly, the long short-term memory (LSTM) model, one of

the state-of-the-art approaches of deep neural networks, has been successfully applied in various studies that involve time series datasets (Yan et al., 2019).

An LSTM technique has been applied in hydrologic studies to evaluate variables, such as precipitation (Akbari Asanjan et al., 2018), runoff (Boyraz and Engin, 2018; Krazert et al., 2018; Tian et al., 2018; Ayzel, 2019; Couta et al., 2019; Mehdizadeh et al., 2019; Le et al., 2019; Yan et al., 2019), groundwater level (Zhang et al., 2018b; Hrnjica and Bonacci, 2019), and soil moisture (Fang et al., 2019), as well as in decision making for optimal reservoir operation (Zhang et al., 2018a; Singh and Sharif, 2019) and for drought prediction (Xu et al., 2018; Poornima and Pushpalatha, 2019). These studies found that deep learning–based LSTM models have good performance for hydrologic forecasting in various areas. In addition, some studies reported that LSTM models can provide better performance than physically-based hydrologic models (Fan et al., 2020; Frame et al., 2020).

Le et al. (2019) demonstrated the use of LSTM models for daily streamflow forecasting in the Da River basin, Vietman with lead times of 1 to 3 days. They constructed forecasting models using two observation datasets (i.e., precipitation and streamflow) as input data and they found that the model exhibited good performance for streamflow forecasting for 1, 2, and 3 days. Furthermore, they suggested the potential of applying LSTM models in the field of hydrology for managing real-time flood warning systems. Tian et al. (2018) applied four RNNs including an LSTM model for runoff forecasting. They found that two models, including the LSTM model, demonstrated good performance for runoff forecasting, and these two models could improve physically-based hydrologic models by reducing uncertainty intervals by more than 50% of the flows. Finally, Yan et al. (2019) forecasted runoff with lead times of 1–6 h using an LSTM

model. They compared the results from the LSTM model with SVM learning and showed that the LSTM forecasting model has a better prediction accuracy, especially for flood peak flows.

The abovementioned studies performed runoff prediction with various time scales using many data-driven models. The predictive performances of the data-driven models were acceptable compared with physically-based hydrologic models, and their applicability was also confirmed. Nevertheless, the previous studies have the following limitations that will be overcome in this research:

1) The relative performance of common data-driven models using small temporal resolutions is still unclear. Most of the studies focused on daily runoff simulation instead of hourly or sub-hourly time scales. The applicable fields of simulated runoff depend on the temporal resolution. For instance, accurate simulation of hourly runoff is an important task for developing flood warning systems. Thus, this study aims to develop an hourly runoff forecasting model using data-driven models.

2) In previous studies, ground-based observations were mainly used as the forcing data for data-driven models; thus, the modeling performances were affected by the spatial resolution of the observations. Moreover, previous works have not tested data-driven models in mountainous basins that contain limited ground-based data. To address these limitations, this study aims to use distributed forcing datasets and apply data-driven models for runoff predictions.

Chapter 3

Data-Driven Models

This chapter introduces an overview of the data-driven models used in this research. The data-driven models are RF, K-means clustering, SVM, ANN, LSTM, and LSTM with sequence-to-sequence (LSTM-s2s) learning models.

3.1 Introduction

Recently, with the advances in computational and hardware systems, physically-based hydrologic models have been used for more accurate rainfall–runoff analyses. These models have been widely applied for analyzing the rainfall–runoff relationship based on many factors, mathematical equations, model parameters, and multiple datasets. However, different results may be obtained from the models owing to the influences of various variables. Thus, effective alternatives to physically-based models are required for rainfall–runoff analyses with fewer parameters (Solomatine and Ostfeld, 2008; Mosavi et al., 2018).

A data-driven model, which is considered an empirical model or a black box approach, is based on mathematical functions that are derived not from physical processes but from analyses of the concurrent input and output time series (Shrestha, 2009). While physically-based models are founded on well-established mathematical or physical theories, data-driven models utilize relationships between massive amounts of variables without requiring physical laws, using statistical or machine (deep) learning techniques. The main purpose of data-driven models is to find relationships between the system state variables (i.e., input and output) without explicitly understanding the physical behavior of the system (Solomatine et al., 2008). A simple example of a data-driven model is a linear regression model, which builds a relationship between input and output variables. It can be used to understand the relationships between various variables and can be applied to predict some variables.

Data-driven modeling is a multidisciplinary method for improving performance in many fields such as engineering, statistics, and information technology. Data-driven models aim to provide high performance in engineering processes, replacing processes that are more time consuming. With the improvement of computational power and the development of available datasets, data-driven models have been applied in various studies in the last decade. Recently, they have significantly contributed to the analyses of hydrologic processes and prediction of hydrologic variables. In this research, various types of data-driven models were applied to develop an integrated runoff analysis system.

3.2 Data-Driven Model Types

Data-driven modeling, including machine learning or deep learning techniques, is based on independent and dependent variables. It is divided into supervised learning and unsupervised

learning techniques based on whether it has the target variable (Bishop, 2006). The typical supervised learning techniques include ANN (McCulloch and Pitts, 1943), RF (Breiman, 2001), and SVM (Vapnik, 1995). The unsupervised learning techniques include K-means clustering (MacQueen, 1967), DBSCAN (Ester et al., 1996), hierarchical clustering (Johnson, 1967), and self-organizing map (Kohonen, 1982). In the past, it was difficult to create data-driven models because of the limitations in computing systems, but the improvement of technology has allowed the use data-driven models for various purposes. Recently, these models have been used for hydrologic applications with large amount of data and information.

Supervised learning aims to detect a pattern between the independent and dependent variables. It has been widely used for various fields that require data classification and regression. Generally, supervised learning techniques are applied in the fields of statistics and engineering for classifying and predicting the target variables according to the given input variables. There are two main types of supervised learning problems: classification problems that involve predicting class labels (categorical data type) and regression problems that involve predicting numerical labels (numerical data type). Table 3.1 presents the popular types of supervised learning techniques.

Table 3.1: Supervised learning techniques.

Types	Features	Advantages	Disadvantages
Artificial Neural Network	-Finds the minimum errors by adjusting the weights	-Ability to model nonlinear and complex relationships	-Presence of a black box -Architecture may be sensitive
Support Vector Machine	-Finds a decision boundary that maximizes the distance between support vectors	-Can be applied to nonlinear data using many kernels	-Robust against overfitting -Selection of a correct kernel is complicated
Decision Trees	-Decision support algorithm using a tree-like model of decisions	-Easy to understand and operate -Support advanced ensemble methods such as random forest	-Can be unstable -Relatively inaccurate compared to other models
Random Forest	-Ensemble learning method based on many decision trees	-High accuracy for classification and regression problems	-Requires much computational power and resources

In contrast to supervised learning, unsupervised learning techniques are based on complex relationships between independent variables with no determined dependent variable. The unsupervised learning technique is mainly used for clustering, dimension reduction, and anomaly detection (Kim et al., 2019). The clustering technique aims to detect similarities in groups of datasets and cluster similar data points into one group. It is also used to identify similarities between datasets in a cluster or differences with other objects in another cluster (Tsai and Chen, 2010). One of the main methods of unsupervised learning includes clustering analysis, which intends to group data points that have not been labeled, or categorize and detect anomalous data points that are not attached to any group. Table 3.2 lists the typical unsupervised learning techniques.

Table 3.2: Unsupervised learning techniques.

Types	Features	Advantages	Disadvantages
K-means	-Aims to partition datasets into k clusters with the nearest mean distance	-Relatively simple to implement -Easy to adapt to new datasets	-Choosing k manually -Sometimes clustering outliers exist -Being dependent on the initial value of parameters
Hierarchical	-Cluster analysis that intends to build a hierarchy of clusters	-Easy to implement and has a high performance	-Difficulty in identifying the correct number of clusters
DBSCAN	-Density-based clustering non-parametric algorithm	-Does not need to specify the number of groups	-Difficult to find the cluster datasets well with large differences in density

3.3 Supervised Learning–Based Models

In this research, three supervised learning based models, namely, ANN, RF, and SVM, were used for classification and regression. The RF model, which is a part of the HAT described in Chapter 4, was used for classification. The ANN and SVM models were used for regression for hourly runoff forecasting, as discussed in Chapter 6. The details of each model are presented in the following sections.

3.3.1 Artificial Neural Network

The ANN algorithm, proposed by McCulloch and Pitts (1943), is one of the representative data-driven models based on the human brain structure. ANN modeling is an effective approach for analyzing nonlinear relationships between independent and dependent variables. Different from the physically-based modeling, which is based on complex equations, the ANN model is used for prediction and classification of specific factors using only undefined

19

mathematical relationships between given datasets (Hu et al., 2018). Figure 3.1 depicts the conceptual diagram of the ANN model.
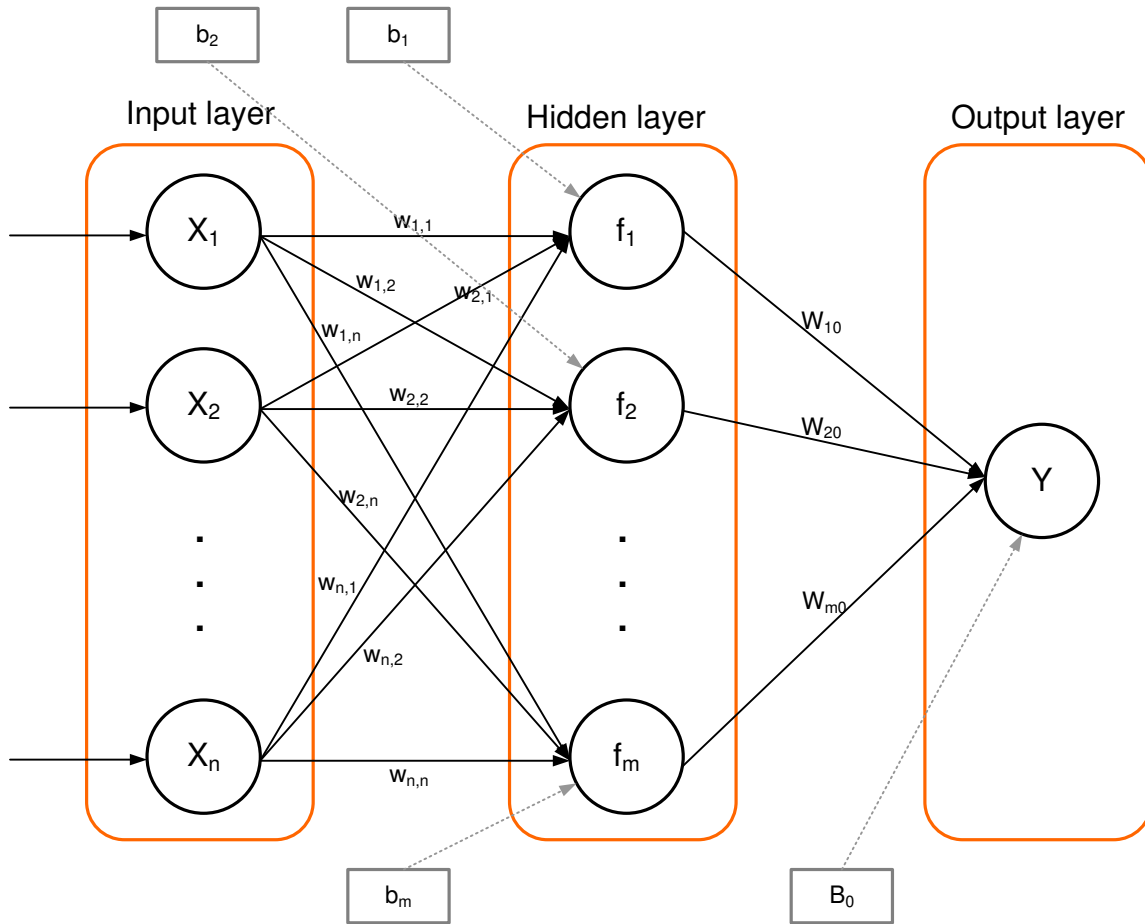
Figure 3.1: Conceptual diagram of the artificial neural network model.

The basic structure of the ANN model consists of three layers, that is, input, hidden, and output layers, and each layer has different weight values (*w*). The algorithms of ANN models aim to minimize the residuals between the target value and predictions by modifying the weights using the backward propagation process. Here, back propagation is used to effectively train a neural network. It performs a backward pass while adjusting the parameters (i.e., weights *w* and

biases *b*). Back propagation is a process of fine-tuning the parameters of a neural network based on the loss obtained in the previous iteration. Proper tuning of the parameters ensures a lower loss (i.e., error rate), making the model reliable by increasing its generalization. The ANN model can be mathematically formulated (Eq. 3.1).

$$f_1 = f(b_1 + w_{11}X_1 + w_{21}X_2 + \cdots + w_{n1}X_n)$$
$$f_2 = f(b_2 + w_{12}X_1 + w_{22}X_2 + \cdots + w_{n2}X_n)$$
$$\vdots$$
$$f_m = f(b_m + w_{1m}X_1 + w_{2m}X_2 + \cdots + w_{nm}X_n)$$
$$Y = f(B_0 + W_{10}f_1 + W_{20}f_2 + \cdots + W_{m0}f_m) \tag{3.1}$$

here, *X* denotes an input variable, *f* is an activation function for the hidden layer and output layer, *w* means the weight value between layers, and *b* and *B* indicate the biases in the hidden and output layers, respectively.

A linear combination is passed to the next node after the input *X* is multiplied by the weight value *w*. Then, the coupled value is converted based on the status of the activation function, and it is transmitted to the next layer as a signal. Through these processes, the final output value *Y* can be obtained. Representative activation functions used in ANN modeling include sigmoid, tanh, and ReLu functions.

3.3.2 Random Forest

The RF technique is highly suitable to various applications that require informed decision making based on numerous data with high accuracy. The RF combines prediction results from multiple trees and makes a decision by using a bootstrap of samples similar to the conventional bootstrap aggregating method (i.e., bagging method) and it can provide both predictability and

stability (Cutler et al., 2007; Wang et al., 2015; Kim et al., 2019). It applies randomness to both training sets and each decision tree's variable to reduce the overfit of the conventional decision tree method (da Silva Chagas et al., 2016).

The strengths of RF modeling include simplicity owing to the few parameters that need to be tuned, higher performance compared to other data-driven models for classification, and robustness as a result of the bagging process (Muñoz et al., 2018). The RF algorithms can be utilized by the scikit-learn package in Python.

The RF consists of multiple trees formed by several variables and typically, 500 different trees are produced to derive results. If the number of trees is extremely large, there is a high risk of overfitting. One of the features of RF is to determine the importance of variables by measuring the contribution of each variable to the prediction results. Figure 3.2 illustrates the conceptual diagram of the RF technique, whose algorithm can be described as follows.

1) Randomly select *n* sub-training sets (decision trees) from a given total training dataset using the bootstrap sampling method.

2) Obtain *n* classification results from each sub-training set.

3) Chose the final outcome based on majority voting determined from *n* decision trees.
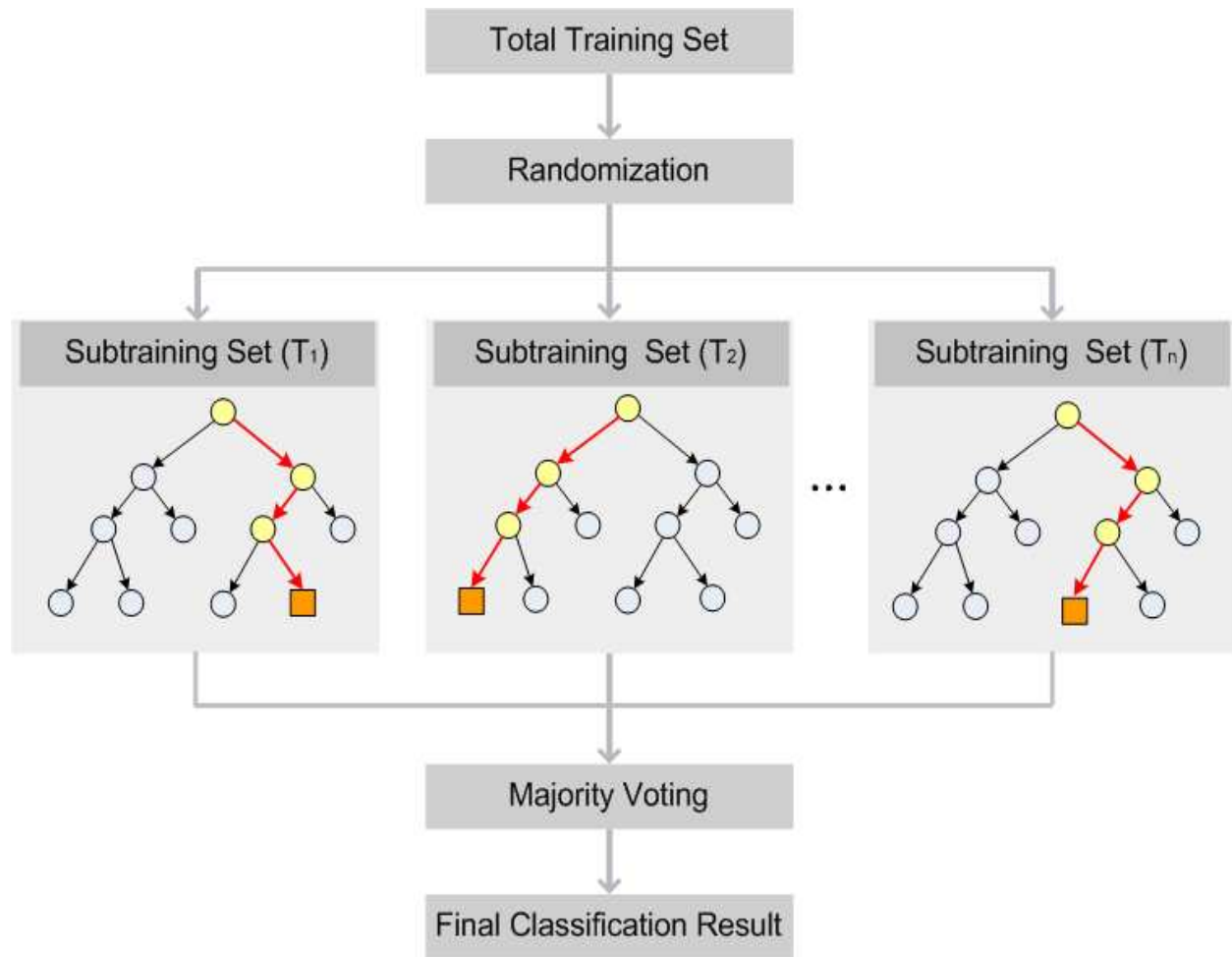
Figure 3.2: Conceptual diagram of the random forest model.

3.3.3 Support Vector Machine

The SVM model was introduced by Vapnik (1995) to deal with classification and regression issues. For dealing with the classification problem, the SVM model tries to classify vectors within different classes with maximum margin for the distance between vectors and to find an optimal hyperplane of support vectors for optimal classification results. Figure 3.3 displays the conceptual diagram of the SVM model.
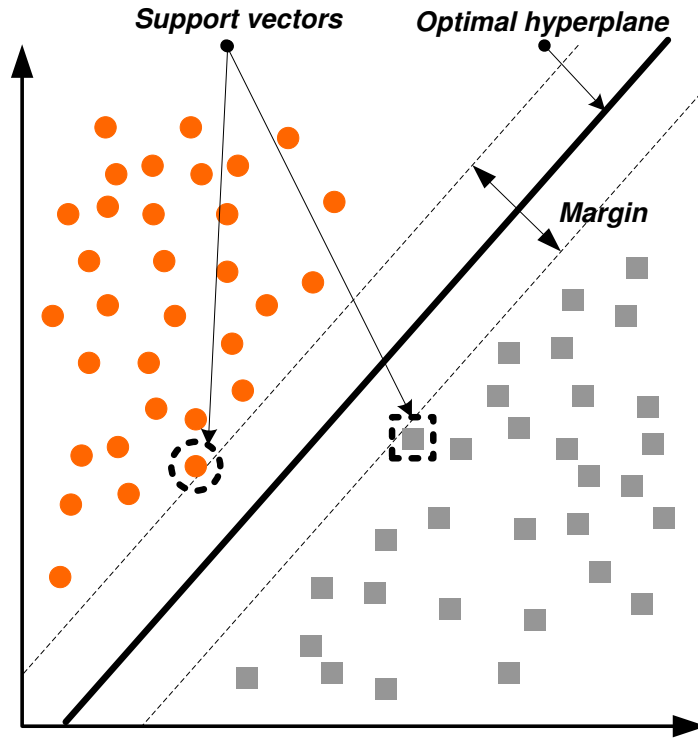
Figure 3.3: Conceptual diagram of the support vector machine model.

Data points that could not be linearly separated can be classified after being mapped into a high-dimensional space on a plane by using a kernel function. The types of kernel functions include the polynomial function, sigmoid function, and radial basis function (RBF).

The SVM model can be extended to solve regression problems by using an ε-insensitive loss function, which is called the support vector regression (SVR) model (Drucker et al., 1997). In this study, the SVR model was used to predict the hourly runoff, as described in Chapter 6, whereas the RBF, which shows excellent performance in solving classification and regression problems, was used as a kernel function (Choi et al., 2020).

The RBF is one of the most widely used kernel functions because of its similarity to the Gaussian distribution. It is also known as the most generalized form of a kernel function. For

example, the RBF kernel function for two data points X_1 and X_2 determines the similarity of the two points using a mathematical equation as follows:

$$K(X_1, X_2) = exp\left(-\frac{\|X_1 - X_2\|^2}{2\sigma^2}\right) \tag{3.2}$$

where σ denotes the variance and $\|X_1 - X_2\|$ is the distance between the two data points based on Euclidean distance.

The SVR model aims to find the flattest regression function $f(x)$, which is indicated in Eq (3.3), so that the target variable of the given learning data is within the given deviation ε. The regression function $f(x)$ aims to minimize errors, and the optimization equation and constraints for finding the flattest function are indicated in Eqs. (3.3)–(3.5).

$$f(x) = <w, x> +b \tag{3.3}$$

$$minimize \quad \frac{1}{2}\|w\|^2 + C\sum(\xi_i + \xi_i^*) \tag{3.4}$$

$$subject\ to \quad \begin{cases} y_i -<w, x_i> -b \leq \varepsilon + \xi_i \\ <w, x_i> +b - y_i \leq \varepsilon + \xi_i^* \end{cases}, \quad \xi_i, \xi_i^* \geq 0 \tag{3.5}$$

where C is a penalty value that is greater than zero, which can estimate how many data points have a deviation greater than ε. A high value of C can reduce the points exceeding the deviation, while increasing the possibility of overfitting. Thus, finding the optimal C value is essential for developing an SVR model with good performance. The optimization problem to find the optimal function can be solved through the Lagrange function from Eqs. (3.4) and (3.5).

3.4 Unsupervised Learning–Based Model

In this research, one unsupervised learning–based technique, the K-means model, was used for clustering datasets. The K-means clustering model was applied to find the similarity of given datasets and separate the points into given groups (i.e., clusters). The model was used as a part of the HAT in Chapter 4. The details of the model are presented in the following section.

3.4.1 K-means Clustering Model

K-means clustering is a popular unsupervised learning method that is based on a non-hierarchical clustering technique and aims to find the similarity of datasets partitioned into groups. The K-means technique is effective in detecting clusters from extensive large datasets (Hartigan and Wong, 1979; Everitt et al., 2001; Olden et al., 2012). Here, clusters refer to a collection of data points aggregated together with similarity. The strengths of the K-means technique are that the algorithm is simple and it can be used in several applications that involve a large amount of datasets (Kim et al., 2019). Figure 3.4 shows the conceptual diagram of the K-means technique. The algorithm of the K-means technique is as follows.

1) Specify the number of clusters K as a parameter is determined.
2) Initialize centroid points in the given dataset and then randomly select data points for each centroid point without replacement.
3) Change centroids repeatedly until the sum of the squared distances between each centroid and data points reaches the minimum.

$$distance = \sum_{i=1}^{c}\sum_{j=1}^{v}(\|x_i - y_j\|)^2 \tag{3.6}$$

Here, $\|x_i - y_i\|$ is the Euclidean distance between two data points, c denotes the number of clusters, v represents the number of data points in the ith cluster, and x and y are the centroid and data points in each cluster, respectively.

4) Determine the centroids that have the minimum sum of distances for each cluster.

The K-means technique has advantages, including rapid processing and simplicity compared to other approaches, and it is able to provide the best result when datasets are separated well from each other. However, some of its disadvantages are that the number of clusters (k) should be determined manually and the approach is unable to deal with noisy data and outliers.
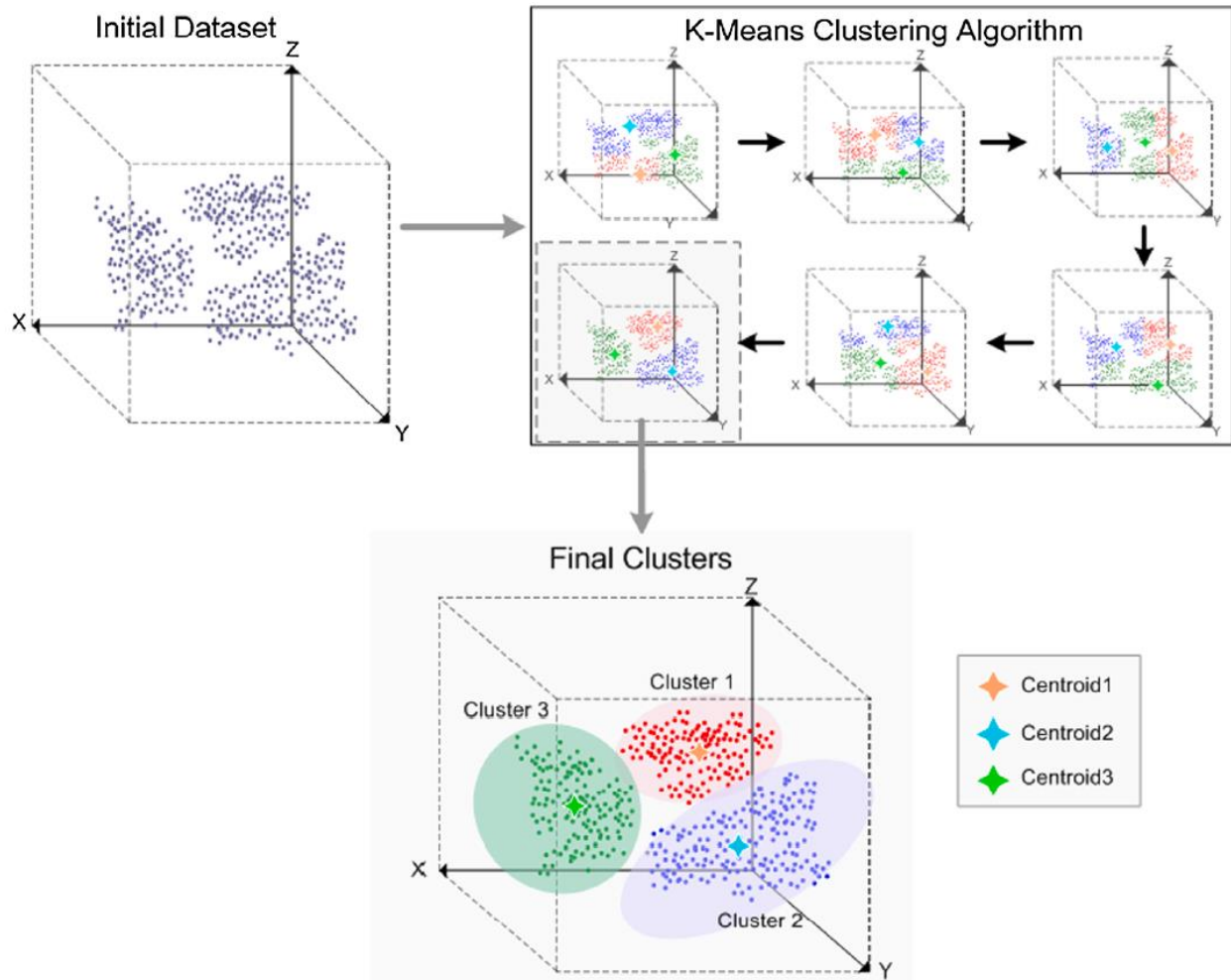
Figure 3.4: Conceptual diagram of the K-means clustering model.

3.5 Deep Learning–Based Model

In this research, a deep learning–based data-driven model, LSTM, was applied for hydrologic analysis and prediction. The LSTM network model shows high performance in analysis and prediction in time-series data. This model was used as part of the error correction tool presented in Chapter 5 and the runoff forecasting tool proposed in Chapter 6. The details of the model are described in the following sections.

3.5.1 Long Short-Term Memory

The LSTM model, introduced by Hochreiter and Schmidhuber (1997), is one of the deep learning based data-driven models that have been widely used for analysis and prediction of sequence-based datasets. The LSTM model is based on an RNN model. It was improved to solve the problems of gradient vanishing or gradient explosion of errors in the RNN model when analyzing long-term time series data. LSTM models can be used for learning continuously composed data, mainly for purposes such as language translation and speech pattern recognition. Recently, in the field of hydrology, the LSTM model has been used for prediction through learning the hydrologic time-series data, such as rainfall-runoff simulations (Hu et al., 2018; Fan et al., 2020; Xiang et al., 2020) and water-level prediction (Zhang et al., 2018b). Figure 3.5 indicates the structure and conceptual diagram of the LSTM.
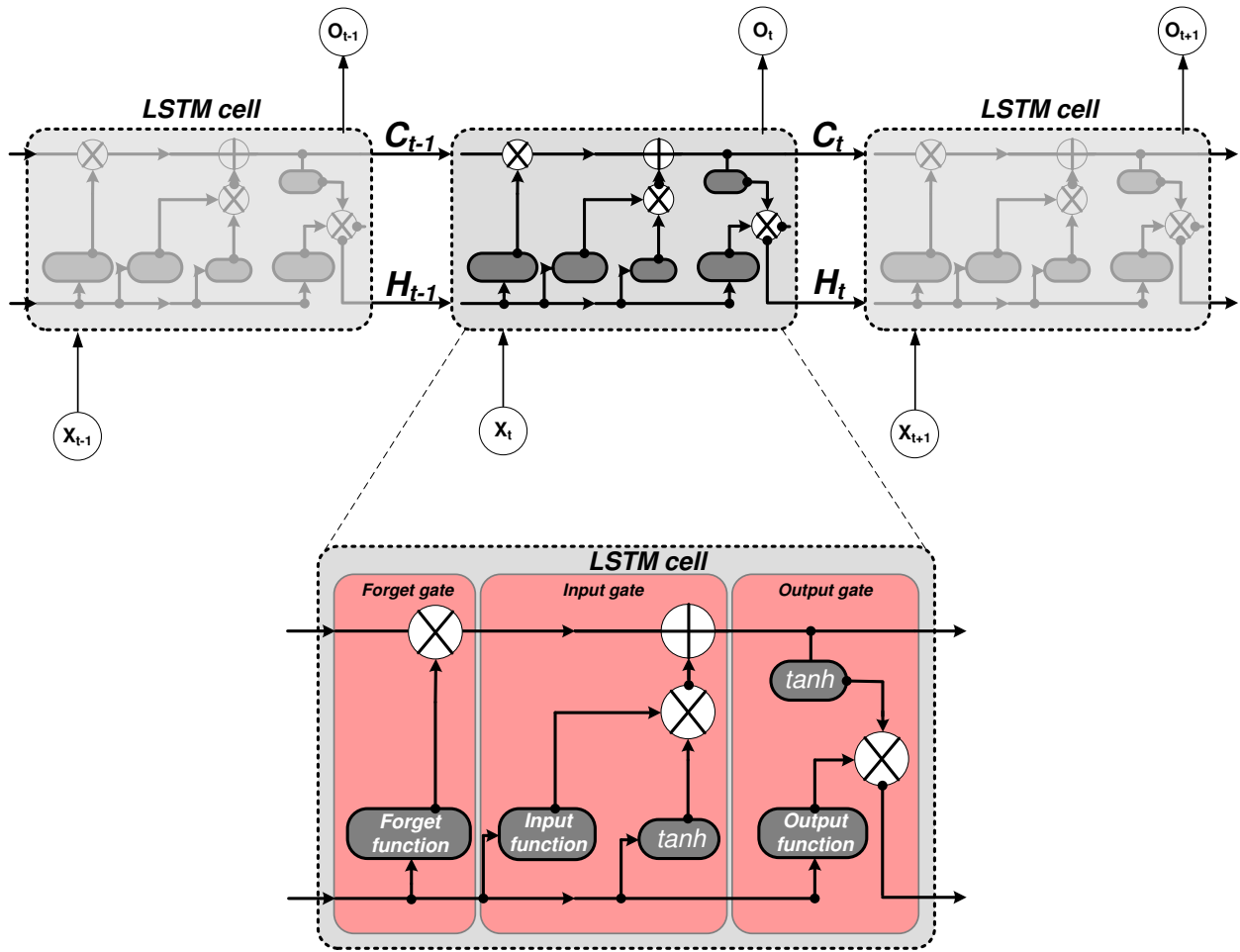
Figure 3.5: Conceptual diagram of the long short-term memory (LSTM) model.

The structure of LSTM models can be used to forget and retain the state information through the gates and memory cells (Fan et al., 2020). LSTM models are composed of multiple cells, each of which comprises cells that can maintain their state with time and three nonlinear gates that control the data flow (Figure 3.5). The three nonlinear gates are the forget gate (f_t), input gate (i_t), and output gate (o_t). The forget gate (Eq. (3.7)) determines how much of the information from the previous block should be retained. For this purpose, the forget gate uses the value obtained by applying the output data of the previous cell (h_{t-1}) and the current input data (x_t) to the activation function.

$$f_t = \sigma\big(W_f \cdot [h_{t-1}, x_t] + b_f\big) \tag{3.7}$$

where σ is the activation function, W_f is the weighting of the gate, h_{t-1} is the output data of the previous cell, x_t is the input data of the current stage, and b_f is the bias value.

The purpose of the input gate (Eq. (3.8)) is to determine which of the new information is stored in the cell, which is achieved through two steps. The first step determines the information to be updated, using the activation function. Then, the hypertangent function (i.e., tanh), as shown in Eq. (3.9), is used to generate a random cell ($\tilde{C}_t$)) for updating the state of the new cell.

$$i_t = \sigma(W_i \cdot [h_{t-1}, x_t] + b_i) \tag{3.8}$$

$$\tilde{C}_t = \tanh(W_C \cdot [h_{t-1}, x_t] + b_C) \tag{3.9}$$

where $\tilde{C}_t$ is the state of any cell generated from the activation function, and W_i and W_C are the weightings of the input gate and the cell, respectively.

A random cell state ($\tilde{C}_t$) is applied to Eq. (3.10), together with the previous cell state (C_{t-1}), to update the current cell state.

$$C_t = f_t \times C_{t-1} + i_t \times \tilde{C}_t \tag{3.10}$$

The output gate (Eq. (3.11)) determines the final output value among the information stored in the cell. Similar to the previous gate, it updates the state (h_t; Eq. (3.12)) at a specific point in time by multiplying the information, whose output is determined using the weighting and activation function, with the previously calculated current cell state.

$$o_t = \sigma(W_o \cdot [h_{t-1}, x_t] + b_o) \tag{3.11}$$

$$h_t = o_t \times \tanh(C_t) \tag{3.12}$$

where W_o is the weight of the output gate and h_t is the final output value.

As the calculation process of LSTM is based on multiple parameters, it is somewhat more complicated and time-consuming than the other models, but it presents a high-performance result. In addition, unlike other models, it is very useful for learning the relation of long-term data because it uses the concept of a cell to store and update information selectively according to the previous state and current input (Tran and Song, 2017; Lee et al., 2018). Selecting optimal parameters is important to obtain a result with high accuracy.

3.5.2 LSTM-s2s Learning

A conventional LSTM model is limited because it requires a fixed length of time steps for the input and output variables, as shown in Figure 3.6. However, it is necessary to know the input variables at previous time steps other than the time steps that need to be predicted (Xiang et al., 2020). To solve this limitation of the conventional LSTM model, the LSTM-s2s or encoder–decoder model was proposed by Cho et al. (2014), which can solve this limitation using a sequence-to-sequence structure based on different time steps of input and output variables. Generally, LSTM-s2s models have been applied in such fields as text translation, speech recognition, and image analysis, which are based on sequential datasets (Xiang et al., 2020). Similar to these study fields, LSTM-s2s models can be considered for use in hydrologic time series predictions. In the field of hydrology, the LSTM-s2s model can be an effective approach for hydrologic predictions using relationships between variables. Figure 3.6 illustrates the conceptual diagram of the LSTM-s2s model.
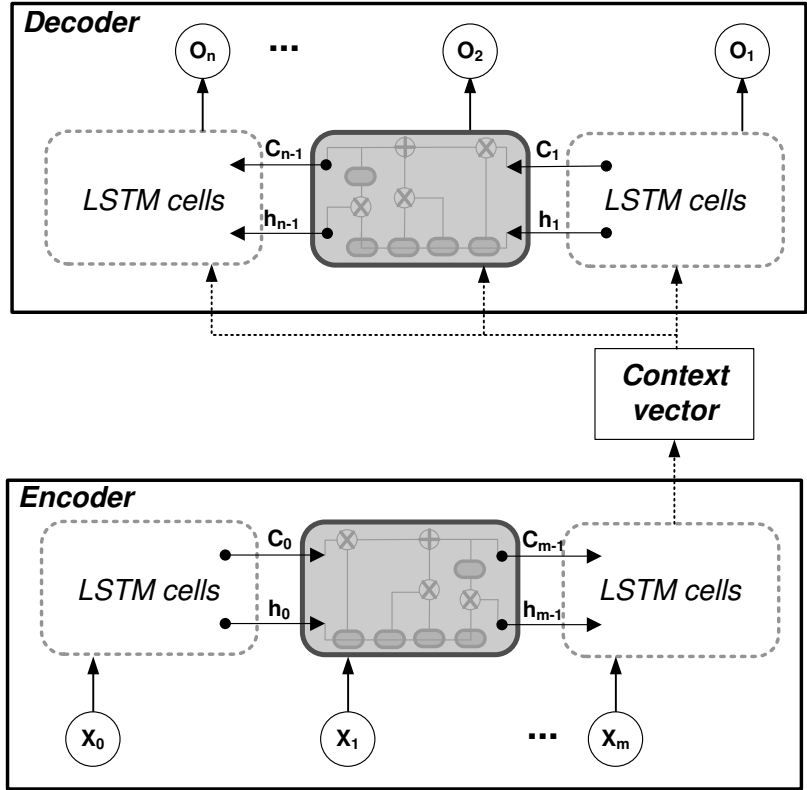
Figure 3.6: Conceptual diagram of the LSTM-s2s model. Details of each LSTM cell (gray box) are presented in Figure 3.5.

The LSTM-s2s model process is similar to that of the conventional LSTM model, but the LSTM-s2s has two stages, called encoder and decoder. The encoder stage uses the information of given datasets as input variables and then outputs from the encoder with m time steps can be stored in one cell, which is called context vector. Subsequently, the information is used as input for the decoder LSTM stage to predict output variables with n time steps. Here, time steps m and n can be determined by users. One of the features of LSTM-s2s models is that the time steps of the encoder and decoder stages can be decided differently. In this study, X_t represents the historical input variables and O_t denotes the predicted outcomes. The data-driven models are available as standard packages in various software programs and the Keras framework in Python 3.4 was used to operate the models in this research.

Chapter 4

Development of the HAT Using Data-Driven Models

This chapter introduces a novel HAT based on a hybrid framework of data-driven models. The framework combines two data-driven models, namely, unsupervised clustering and supervised classification techniques, to build a practical assessment tool and provide reasonable evaluation ratings for hydrologic models. The HAT was applied to evaluate the performance of the NWM in San Francisco Bay area.

4.1 Introduction

Accurate simulation of the water cycle and hydrologic processes using hydrologic models is very important to reduce the magnitude of damages from natural disasters such as floods and droughts (Abbott et al., 1986; Dutta et al., 2003; Rozalis et al., 2010; Kim et al., 2019). Generally, hydrologic models have been used to simulate various water-related factors that impact the water

cycle, such as runoff, soil moisture, evapotranspiration, and ground water. In addition, as the observation systems of hydrologic variables are developed, the products obtained from the model are widely used in various fields such as agriculture, environmental studies, and hydrology. Several hydrologic models have advanced from lumped models, which use the characteristics across the entire watershed, to distributed models, which account for spatially varying characteristics of the watershed (Liang et al., 1994; Arnold et al., 1998; Singh and Woolhiser, 2002; Kim et al., 2019). While hydrologic models are developing and evolving, their evaluation methods have not improved significantly. Most of the methods depend on a few error indices (Kim et al., 2019). The current hydrologic assessment methods should be improved and a new hydrologic evaluation tool, which can provide objective evaluation indices that are easy-to-understand, is necessary.

The evaluation of a hydrologic model can be used for calibration and improvement of the model performance, communication with decision makers for operating water-related systems. The hydrologic model, which is based on a complicated structure and various parameters, requires a calibration process that depends on the output quality. The evaluation of model results determines the necessity, strategy, and extent of calibration (Moriasi et al., 2007; Kim et al., 2019). Thus, an improved hydrologic evaluation method can contribute to enhance the model performance. Moreover, the evaluation method can serve as a guideline on the model's reliability to operators using the hydrologic model for decision-making, especially on flood warning and mitigation (Al-Sabhan et al., 2003; Kim et al., 2019).

Generally, graphical and statistical methods are used to evaluate hydrologic models (Green and Stephenson, 1986; Legates and McCabe, 1999; Coffey et al., 2004). The graphical method is used for a qualitative evaluation by comparing observed and simulated hydrographs,

whereas the statistical method is for a quantitative evaluation based on various error indices (ASCE, 1993; Kim et al., 2019). One of the limitations of the current evaluation methods is that it is difficult to provide standardized ratings based on multiple error indices. More importantly, the evaluation framework based on a single error index cannot reflect the complementary interactions between different error indices. It is also questionable how reasonably the error index range defined statistically can represent the performance of a hydrologic model (Donigian et al., 1983; Ramanarayanan et al., 1997; Gupta et al., 2009; Singh et al., 2005; Kim et al., 2019).

Some requirements are necessary to develop a HAT. First, the evaluation framework should include objectivity of statistical error indices. Second, a combination of multiple error indices must be considered instead of using single error index (Green and Stephenson, 1986; Coffey et al., 2004). In addition, the evaluation should be performed according to the purpose of the hydrologic model. For example, when evaluating a flood forecasting model, a long-term runoff time-series that has multiple hydrographs should be separated into single hydrograph events because some periods with no rainfall can influence the evaluation results due to inadequate error indices (Ramirez, 2000).

It is also important to consider the effects of the hydrograph components, i.e., the rising and recession limbs, as each component has different important effects on the hydrologic process. For example, the rising limb is mainly formed by the concentration of direct runoff, which determines the peak and time-to-peak flows. Since the recession limb is formed by all types of runoff, it is dominant over the rising limb in determining the total runoff volume related to the water budget (Boyle et al., 2000; Kim et al., 2019).

The data-driven approach can be used to overcome the limitations of the general evaluation method. The approach uses an algorithm that detects patterns and analyzes the

relationships inherent to inputs and outputs. It is used across many fields with advanced resources and algorithms and more powerful computational systems (Hong, 2008; Sahoo et al., 2017; Choi et al., 2020; Xiang et al., 2020). In hydrology, as the quality and quantity of available datasets are improved, the usage of the data-driven approach is increasing. Moreover, the approach is expected to serve as a supplementary method in physically-based hydrologic models to simulate various hydrologic factors such as surface runoff, groundwater, and soil moisture (Coulibaly and Anctil, 1999; Tokar and Johnson, 1999; Shortridge et al., 2016).

The data-driven models can be combined for effective data analysis. This is referred to as a hybrid framework of data-driven models. Two or more models with different strengths and features can be combined to complement the limitations of a single model and provide a better performance. In general, hybrid frameworks of models have been used in financial applications. Hsieh (2005) combined the K-means clustering technique and neural network technique to develop a credit scoring model. Huysmans et al. (2006) used a framework that combines a self-organizing map technique and a multi-layered perceptron technique to improve a credit scoring method. In addition, Tsai and Chen (2010) reviewed various combinations of data-driven models and reported that the hybrid framework can improve the performance of a credit rating system.

Previous studies have coupled the two techniques of unsupervised clustering and supervised classification to establish a hybrid framework of data-driven models (Tsai and Chen, 2010). The framework is considered an attractive approach for hydrologic evaluation using various error indices. Furthermore, it is expected to secure a stable performance assessment by employing big data and has the advantage of providing composite performance ratings.

This study aims to develop a new HAT using a hybrid framework of data-driven models, which is a combination of clustering and classification techniques. The new HAT is designed to

provide four performance ratings (very good: VG; good: G; satisfactory: S; and unsatisfactory: US) based on a combination of error indices for evaluating hydrologic models. In this research, the NWM of the NOAA was evaluated by the HAT. The performance evaluation was conducted on rising and recession limbs in a single hydrograph as well as on the entire hydrograph. For designing, training, and validating the model, streamflow data modeled from the NWM from October 2013 to February 2017 were used at selected United States Geological Survey (USGS) gages across the San Francisco Bay area.

4.2 Materials and Methods

4.2.1 Study Area and Data

The HAT was developed for the San Francisco Bay area, California. The six counties (San Mateo, Santa Clara, Alameda, Marina, Sonoma, and Napa) in this area were considered as study sites. This area is a flood-prone region due to orographic precipitation, which is generated from moisture plumes known as atmospheric rivers (Ralph et al., 2012; Cifelli et al., 2018; Han et al., 2019). Figure 4.1 presents the location of the study area and the USGS streamflow gages used in this study. There are 91 USGS stream gages in the region and available data of observed runoff from 57 gages were used to evaluate the NWM performance. The gages providing low-quality observed data were excluded in this study. The sizes of the watersheds for these 57 gages vary from 11.5 to 3425.3 km^2. This study used the retrospective streamflow data from the NWM (Cosgrove et al., 2003) as input variables of the HAT. The period for training and testing the HAT was from October 2013 to February 2017. The performance of the NWM for the San Francisco Bay area was assessed based on the USGS streamflow data.
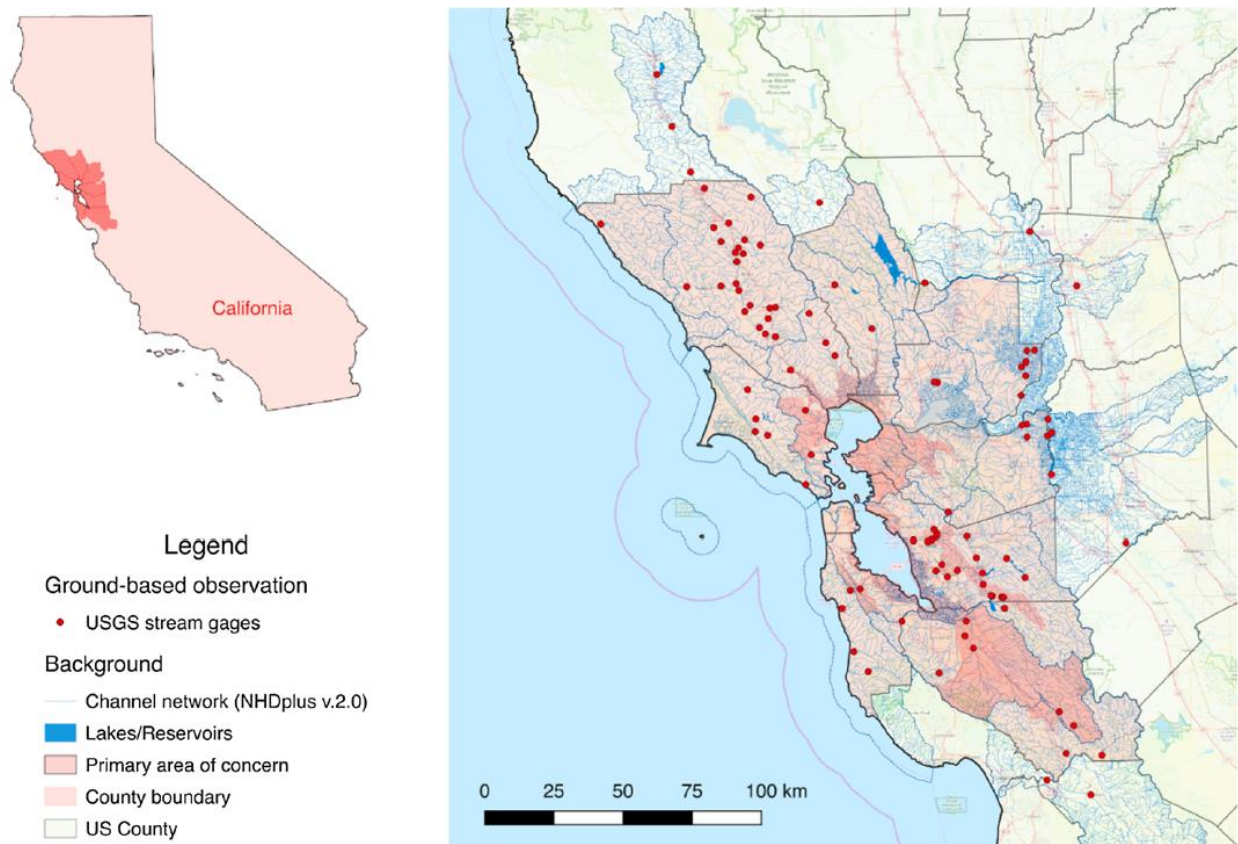
Figure 4.1: Study area and USGS streamflow gages used in this research.

4.2.2 National Water Model

The NWM is a fully distributed hydrologic modeling framework, which was developed by the NOAA in 2016. It aims to simulate observed and forecast streamflows over the entire CONUS. The core system of the NWM is the National Center for Atmospheric Research (NCAR)-supported community WRF-Hydro. The NWM provides products of streamflow forecasting on the 2.7 million river reaches of the USGS National Hydrography Dataset (NHDPlusV2), as well as gridded analyses of a host of other hydrologic variables such as soil

water contents at various depths, accumulated evapotranspiration, snow temperature, snow depth, and ponded water depth (Han et al., 2019).

The NWM analyzes and simulates the hydrologic cycle using mathematical representations of physical processes and interactions between various hydrologic variables. The framework is able to show how the processes distribute water at the surface and subsurface. These processes include precipitation, snowmelt, infiltration, movement of water through various soil depths, and vegetation types (Cosgrove et al., 2018; Han et al., 2019). Figure 4.2 shows the conceptual diagram of the NWM indicating how it works and provides the forecast products.
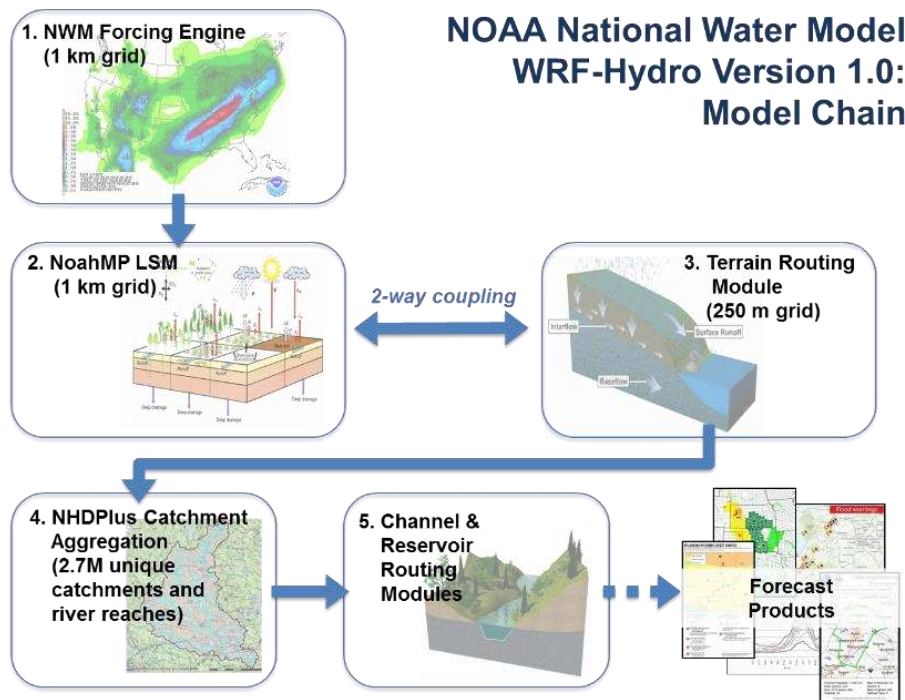
Figure 4.2: Diagram of hydrological process of National Water Model (NWM) (https://ral.ucar.edu/projects/supporting-the-noaa-national-water-model).

The forcing engine of the NWM is provided by various sources, namely, the Multi-Radar/Multi-Sensor System and Stage IV Multi-Sensor Precipitation Estimator radar-gauge observed precipitation data as well as the High-Resolution Rapid Refresh, Rapid Refresh, North American Mesoscale Nest, Global Forecast System, and Climate Forecast System Numerical Weather Prediction forecast data (https://water.noaa.gov/about/nwm). From these forcing systems, the WRF-Hydro is configured to use the Noah-MP Land Surface Model to simulate land surface processes and provide various hydrologic forecasts.

Water routing modules perform diffusive wave surface routing and saturated subsurface flow routing on a 250 m grid as well as Muskingum–Cunge channel routing down NHDPlusV2 stream reaches. River analyses and forecasts are provided across a domain encompassing the CONUS and hydrologically contributing areas, while the land surface output is available for a larger domain extending beyond the CONUS into Canada and Mexico (https://water.noaa.gov/about/nwm; Han et al., 2019). For a detailed methodology background, readers can refer to the WRF-Hydro technical description and user's guide provided by NCAR (https://ral.ucar.edu/projects/wrf_hydro/overview).

Many hydrologic variables, including soil water content, streamflow, depth to soil saturation, water velocity, reservoir inflow/outflow, and snow depth, are provided by the NWM framework. These hydrologic products are available at Environmental Data Commons (http://edc.occ-data.org/nwm/getdata/#archive-data-access), which provides hourly streamflow, lake and reservoir-related products, land surface model outputs (three-hour time steps and 1 km resolution), and ponded water depth and soil saturation outputs (three-hour time steps and 0.25 km resolution). These products are available for 25 years (January 1, 1993 to December 31, 2017). Table 4.1 indicates the hydrologic products obtained from the NWM. The 1 km gridded

product data include volumetric soil water content, evapotranspiration, and snow-related variables. The soil water content is provided for four soil layers (layer-1: 0–100 mm; layer-2: 100–400 mm; layer-3: 400–1000 mm; and layer-4: 1000–2000 mm), making it possible to examine the flux between the top and bottom soil layers. The 250 m gridded products include ponded water depth, which represents the direct runoff, and depth to soil saturation, which represents the saturation state of the soil (Han et al., 2019).

Table 4.1: Hydrologic products provided by NWM.

Type	Resolution	Variable	Unit
Grid	1 km	Soil moisture saturation for four layers	Fraction (m^3/m^3)
		Soil temperature	K
		Accumulated evapotranspiration	mm
		Average snow temperature	K
		Snow water equivalent	km/m^2
		Snow depth	m
	250 m	Ponded water depth	mm
		Water table depth	m
Point	-	Streamflow	m^3/s
		Velocity	m/s
		Lake inflow/outflow	m^3/s
		Water surface elevation	m

*(https://water.noaa.gov/about/output_file_contents)

42

The NWM has three forecast configurations, which differ in duration, time step, and frequency (Souffront Alcantara et al., 2018). Table 4.2 shows the features of the configurations. The NWM provides short-, medium-, and long-term forecast products. The short-term configuration produces hourly deterministic forecasts of streamflow and hydrologic state up to 18 hours. The medium-term configuration produces deterministic outputs every 3 hours and the long-term generates streamflow every 6 hours and daily land surface outputs. In this study, short-term products were used for comparison with forecasted results.

Table 4.2: Features of NWM configurations for prediction.

Configurations	Frequency	Forecast duration	Forecast step
Short range	Hourly	0–18 hours	1 hour
Medium range	Daily	0–10 days	3 hour
Long range	Daily	0–30 days	6 hour

*(https://water.noaa.gov/about/output_file_contents)

4.2.3 Evaluation Metrics

In this study, five metrics were used for evaluating the performance of the HAT and NWM: correlation coefficient (CC), percent bias (PBIAS), Nash-Sutcliffe efficiency (NSE), root mean square error observation standard deviation ratio (RSR), error in peak runoff (PE), and error in time to peak (PTE).

$$CC = \frac{\sum(y_e - \overline{y_e})(y_o - \overline{y_o})}{\sqrt{\sum(y_e - \overline{y_e})^2}\sqrt{\sum(y_o - \overline{y_o})^2}} \tag{4.1}$$

Here, y_e and y_o indicate the simulated and observed runoff, respectively, and $\overline{y_e}$ and $\overline{y_o}$ denote the average simulated and observed runoff, respectively. The CC ranges from 0 to 1 and describes

43

the strength of the relationship between two variables. A CC value of 1 indicates that there is a strong positive relationship between the observed and simulated runoff values.

$$\text{NSE} = 1 - \frac{\Sigma(y_e - y_o)^2}{\Sigma(y_o - \overline{y_o})^2} \qquad (4.2)$$

The NSE denotes the predictive power of the model. It ranges from $-\infty$ to 1 and the closer the value to 1, the better the performance of the model. In contrast, a value less than zero means that the average observed value is better than the simulated one.

$$\text{PBIAS} = \frac{|\Sigma y_o - \Sigma y_e|}{\Sigma y_o} \times 100 \ (\%) \qquad (4.3)$$

The PBIAS represents the ratio of the difference between the sums of the simulated and observed values to the sum of the simulated and observed values. It measures the error in the volume of the simulated runoff compared to the observed value.

$$\text{RSR} = \frac{\sqrt{\Sigma(y_o - y_e)^2}}{\Sigma(y_o - \overline{y_o})} \qquad (4.4)$$

The RSR represents the ratio of the root mean square error and standard deviation of the measured data. The RSR ranges from the optimal value of 0 to a large positive value and a lower value of RSR indicates a better performance of the simulated results.

$$\text{PE} = \frac{y_{e,peak} - y_{o,peak}}{y_{o,peak}} \times 100 \ (\%) \qquad (4.5)$$

Here, $y_{e,peak}$ and $y_{o,peak}$ are the peak values of the simulated and observed runoff event, respectively. The PE shows the accuracy of the predicted peak value of the runoff event obtained from the model.

$$\text{PTE} = |T_{e,peak} - T_{o,peak}| \qquad (4.6)$$

where $T_{e,peak}$ and $T_{o,peak}$ denote the time to peak of the simulated and observed runoff, respectively. The PTE measures the difference between the time to peak of the simulated and observed runoff.

4.2.4 Hybrid Framework of Data-Driven Models

A hybrid framework of data-driven models is a combination of two or more data-driven models (Tsai and Chen, 2010; Kim et al., 2019). Various hybrid frameworks can be designed depending on the sequence and type of techniques. Generally, the techniques used for building hybrid frameworks include combinations of 1) multiple unsupervised learning techniques, 2) multiple supervised learning techniques, and 3) unsupervised and supervised learning techniques. In the case of combining unsupervised and supervised learning techniques, the unsupervised learning technique defines the Y label based on a pattern of independent variables, and the framework shares it with the supervised learning technique for the training model.

Figure 4.3 displays the conceptual diagram of a hybrid framework consisting of two data-driven models, i.e., unsupervised clustering technique and supervised classification technique. The algorithm of the hybrid framework is as follows.

1) The unsupervised clustering technique creates groups using X datasets and provides groups (i.e., clusters) as Y labels to the supervised classification technique for the training model.

2) The classification technique can be trained using X datasets and Y labels provided from the clustering technique in step 1).

3) Before testing the model, the trained hybrid framework is verified to confirm the applicability of the models.

4) In the test process, the hybrid framework estimates and predicts the new Y labels for new X datasets. In this study, the Y labels denote the four performance ratings (i.e., VG, G, S, and US) for hydrologic assessment, whereas the X datasets refer to error indices (i.e., CC, NSE, PBIAS, PE, and PTE).
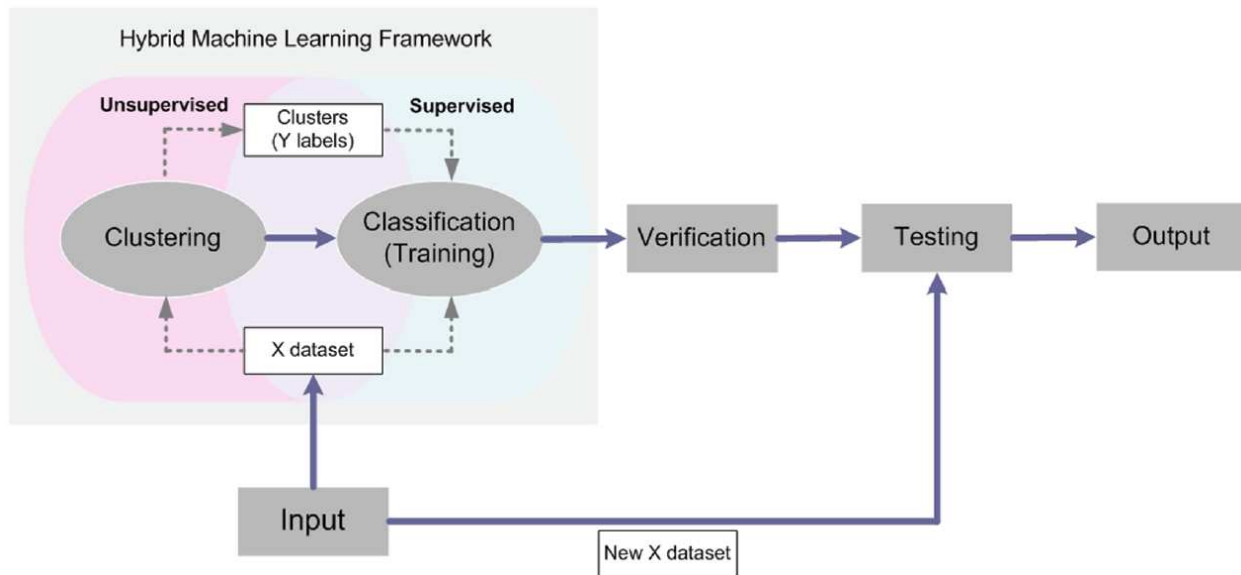
Figure 4.3: Conceptual diagram of a hybrid framework of two data-driven models: unsupervised clustering technique and supervised classification technique.

4.2.5 Development of the HAT

The novel HAT was developed using a hybrid framework of data-driven models described in Section 4.2.4. In this study, a combination of the K-means clustering and RF classification techniques was used for the hybrid framework. The main purpose of the HAT is to evaluate the accuracy of the simulated streamflow from the hydrologic model (i.e., NWM). The hydrologic assessment focuses on two hydrograph components, i.e., the rising and recession

limbs, and the entire hydrograph. Figure 4.4 illustrates a conceptual diagram of the HAT processes.
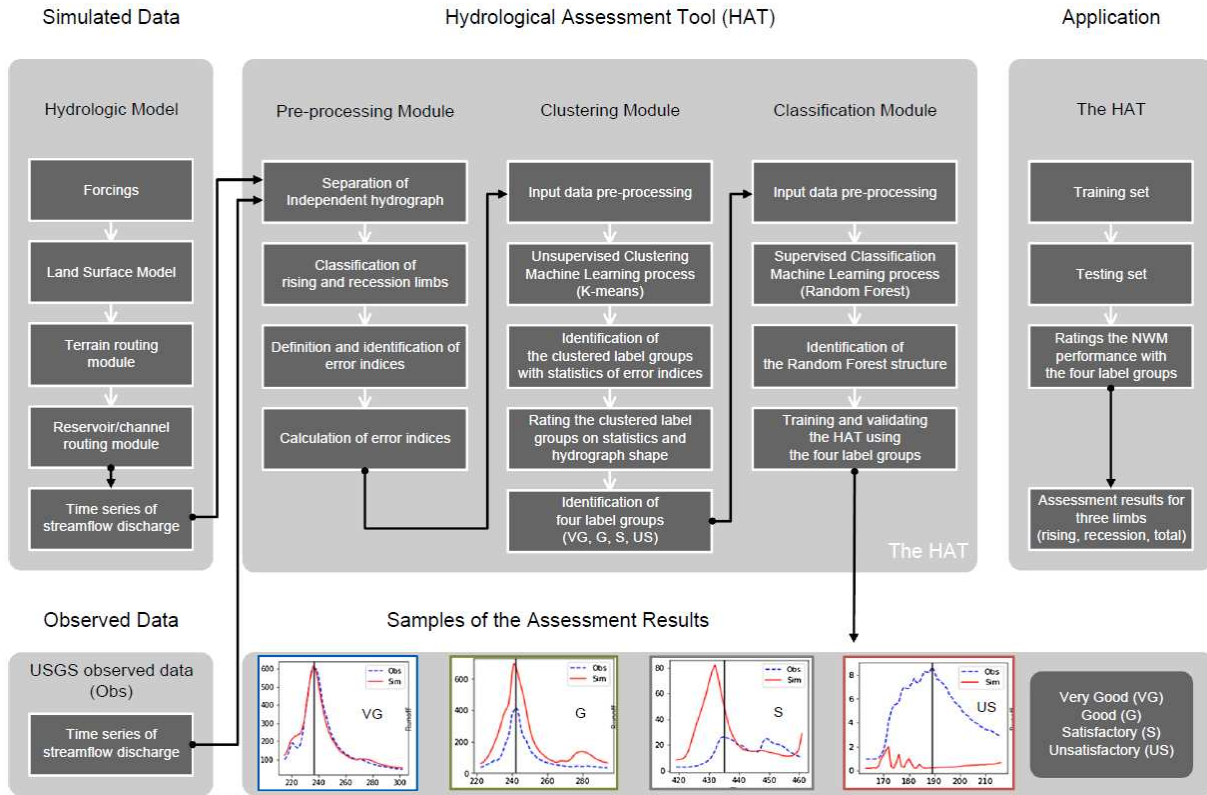
Figure 4.4: Flowchart of the hydrologic assessment tool.

For evaluating the performance of hydrologic models, the HAT provides four ratings, namely, VG, G, S, and US, which are easy-to-understand by users. The HAT can evaluate hourly or daily streamflow hydrographs estimated from any hydrologic model. Moreover, the number of evaluation ratings can be adjusted by users. Since the HAT has a relatively simple structure, it can be applied not only for hydrologic modeling but also for other geophysical models. The HAT comprises three modules, i.e., pre-processing module, clustering module, and classification module.

The pre-processing module aims to separate the entire streamflow into a single hydrograph with rising and recession limbs and calculate the error indices for each component. In this study, five error indices (CC, NSE, PBIAS, PE, and PTE) were used to evaluate the performance of the NWM, as described in Section 4.2.2. Each error index has a different role in determining the clusters in the second module. For example, the CC indicates the trend of the runoff, whereas the NSE shows the variance of simulated errors against observed values. The PBIAS considers the runoff volume errors between the simulated and observed runoff data. The PE and PTE represent the errors in the peak value of runoff and peak time. These estimated error indices for the components are used as the X dataset in the clustering and classification modules.

The second module of the HAT is the clustering module, which aims to determine ratings that represent the accuracy of the outcomes of the hydrologic model using three or five error indices estimated by the previous module. This module provides the Y label, which is required for the training process in the next step, i.e., the classification module. For evaluating the rising and recession limbs, three indices, namely CC, NSE, and PBIAS, are used, whereas the five indices are used to evaluate the entire hydrograph. The four clusters from VG to US are determined in this module.

The third module is the classification module, which is the main part for training and testing the HAT. The classification module uses the error indices for each event as the X dataset and the four ratings given by the clustering module are used as Y labels for the training model. In the classification module, the relationships between the X dataset and Y labels are used for training. After that, the trained HAT can test the performance of the hydrologic model for simulating streamflow by providing an evaluation rating for each hydrograph component (rising and recession limbs), as well as for the entire hydrograph. Moreover, in the classification module,

the weights of each error index can be provided to analyze the contribution of the index to the evaluation.

4.3 Results

4.3.1 Creating Rating Labels Using the Clustering Module

In the pre-processing module, the observed and simulated time-series runoff values were separated into independent hydrographs, including rising and recession limbs, and the five error indices were estimated for each component. The indices were used for the clustering module as input data to the group based on the similarity of datasets. The four ratings, i.e., VG, G, S, and US, were determined by the clustering module. Figures 4.5 to 4.7 depict the probability distribution of the error indices for each component, i.e., the rising and recession limbs, and for the entire hydrograph. For the two components and the entire hydrograph, the probability distributions of each rating provided by the clustering module clearly reflect the characteristics of each error index. For example, VG has a higher probability near the ideal value (i.e., 1.0) for CC and NSE than for the other ratings, while US is mostly distributed at values below zero. These results are demonstrated in all error indices and in the rising and recession limbs as well as in the entire hydrograph.
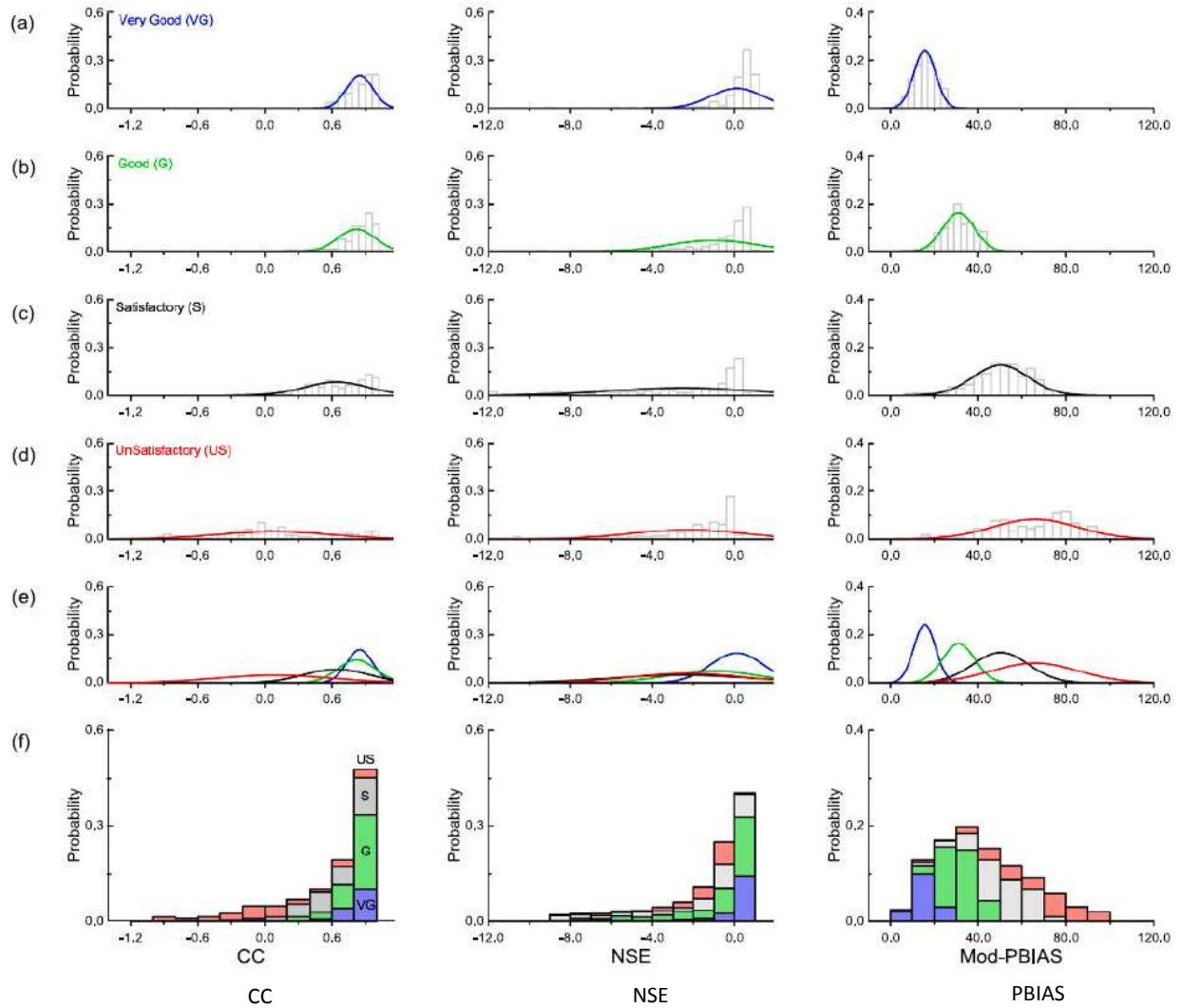
Figure 4.5: Probability distribution of error indices for the rising limb. In this figure, (a)–(d) indicate the probability distributions of each rating label, i.e., VG, G, S, and US; (e) shows a comparison of the probability distributions for the four ratings, while (f) displays a fraction of the probability distributions of each rating.
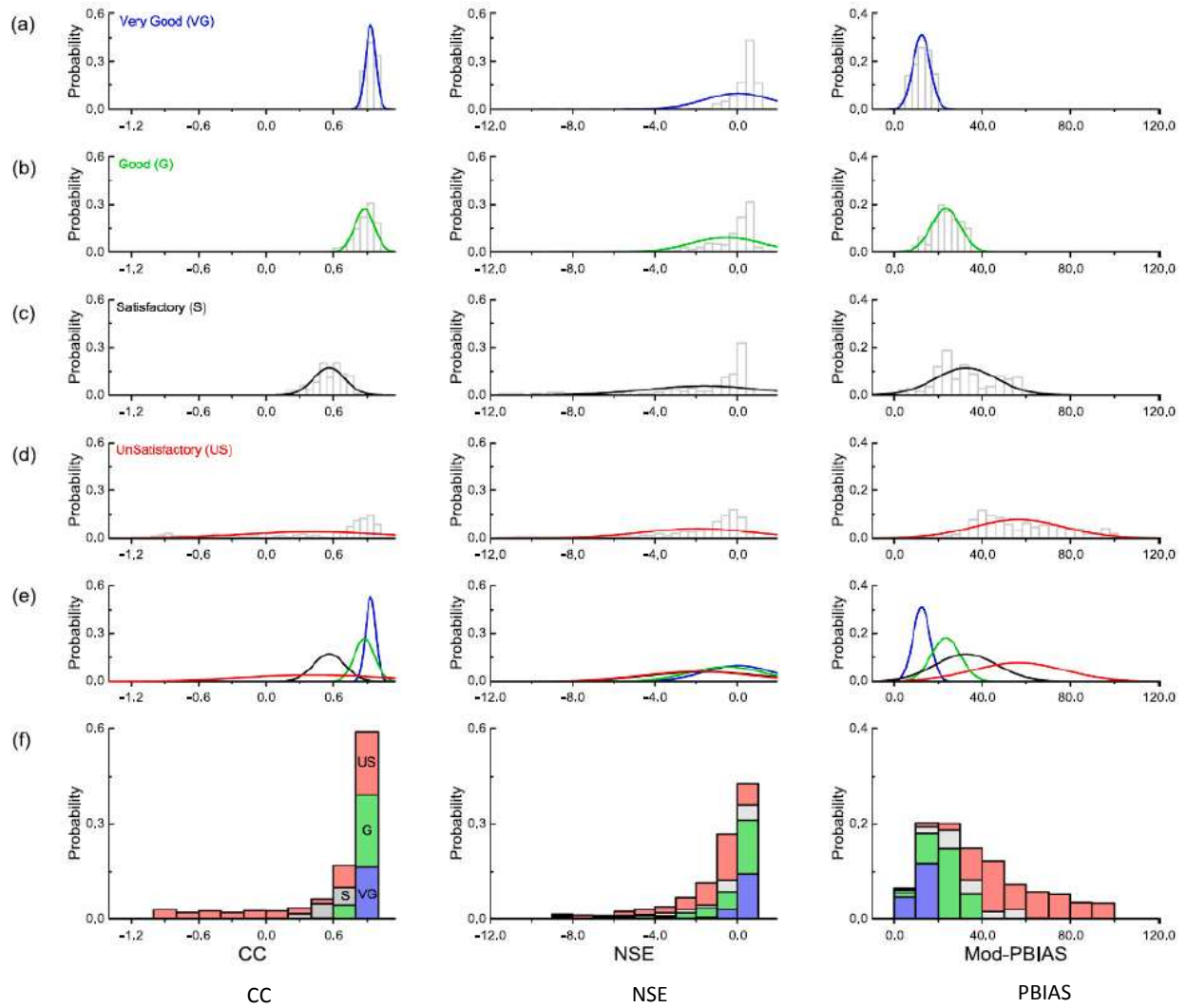
Figure 4.6: Probability distribution of error indices for the recession limb. (a)–(f) have the same descriptions as in Figure 4.5.
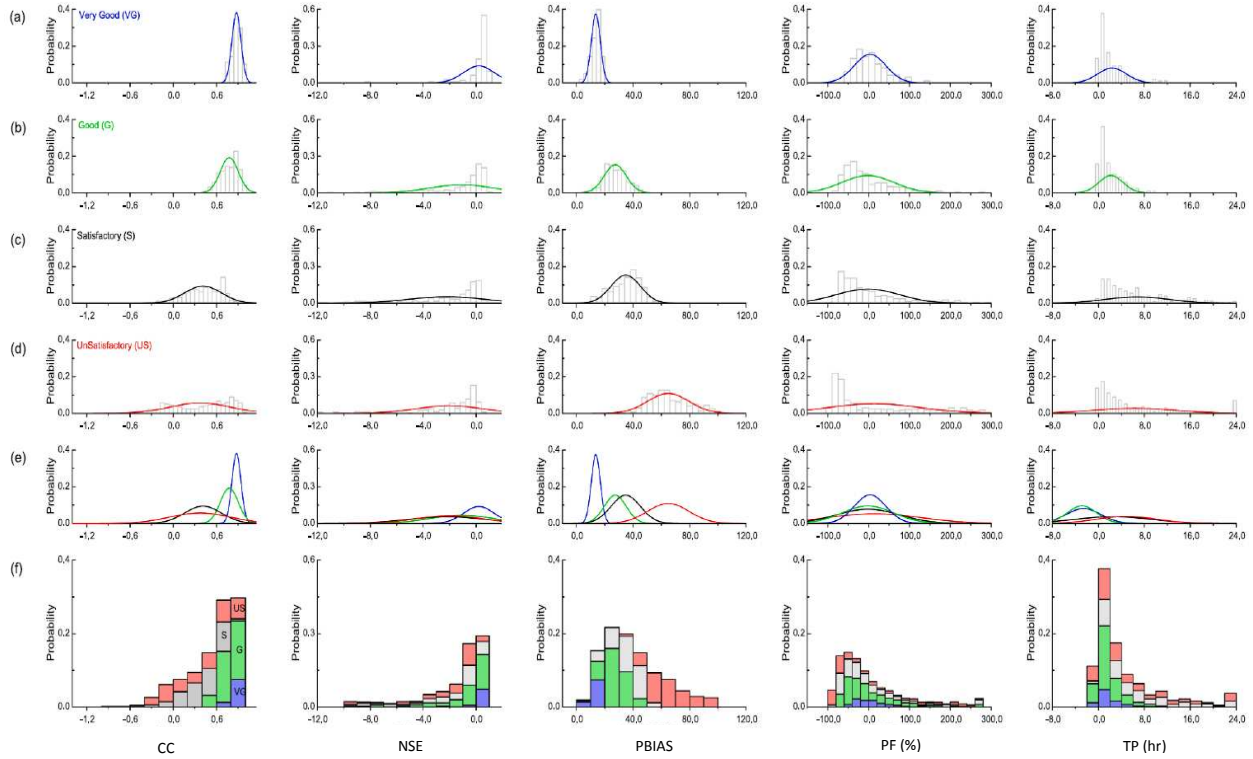
Figure 4.7: Probability distribution of error indices for the entire hydrograph. (a)–(f) have the same descriptions as in Figure 4.5.

Table 4.3 indicates the statistics of three error indices of each performance rating for the case of the entire hydrograph. From the results listed in the table, it can be observed that the statistical ranges (minimum to maximum) of the three indices are overlapping because the ratings have clustered with a composite of the error indices. For example, CC in VG ranges from 0.74 to 1.0 and from 0.44 to 0.98 in G. These results indicate that the clustered ratings are reasonable, as there is no absolute range for the performance rating. In contrast, the ranges from Q^1 to Q^3 of the error indices rarely overlap in the ratings. The mean and variance values in the table are distinct for each rating, which can support the results exhibited in Figure 4.7. All clustered ratings with error indices are listed in Appendix A.

Table 4.3: Statistics of three error indices of each performance rating for the case of the entire hydrograph.

Ratings	Statistics	CC	NSE	PBIAS
Very good	Min/Max	0.74/1.00	−8.16/1.00	0.00/18.50
	Q^1/Q^3	0.84/0.92	0.25/0.72	11.31/15.74
	Mean (variance)	0.88 (0.004)	0.22 (1.342)	13.63 (10.148)
Good	Min/Max	0.44/0.98	−54.34/0.87	5.64/45.44
	Q^1/Q^3	0.68/0.88	−1.79/0.34	21.81/32.89
	Mean (variance)	0.78 (0.015)	−2.23 (33.984)	27.36 (60.616)
Satisfactory	Min/Max	−0.41/0.89	−165.40/0.72	8.63/55.74
	Q^1/Q^3	0.24/0.65	−5.62/−0.13	27.69/42.26
	Mean (variance)	0.41 (0.065)	−5.13 (161.571)	34.78 (108.115)
Unsatisfactory	Min/Max	−0.92/0.98	−534.44/0.60	25.36/99.38
	Q^1/Q^3	0.01/0.76	−13.22/−0.44	53.92/74.89
	Mean (variance)	0.37 (0.176)	−21.74 (3713.448)	64.89 (214.739)

* Q^1 and Q^3 denote the lower (25%) and upper (75%) quartiles.

Based on the results presented in Figures 4.5 to 4.7 and Table 4.3, it is evident that the error indices are reasonably categorized in each rating. For the next step, the overall quality of the simulated hydrologic model (i.e., NWM) for each rating was evaluated. For this, the observed and simulated single hydrographs of runoff from the USGS and NWM were collected for evaluation. Figure 4.8 shows the scatter density plots between the observed and simulated runoff data for the four ratings. The runoff data were normalized by the peak flow to remove the variability of different scales due to various watershed areas. The range of the data is from 0 to 1. The distribution shapes of the scatter points shown Figure 4.8 reflect the characteristics of each rating reasonably, indicating that the clustering module can effectively determine the quality of the simulated runoff through the four ratings. In addition, the R-squared values of each plot

confirm the performance of each rating determined from the clustering module. For example, the R-squared values of VG, G, S, and US range from 0.83–0.86, 0.65–0.71, 0.33–0.49, and 0.01–0.16, respectively. Moreover, for the VG rating, the data points fit the $X = Y$ line, whereas many data points are located near the X and Y axes for the US rating, indicating that the simulated runoff values are largely underestimated or overestimated compared with the observed streamflow.
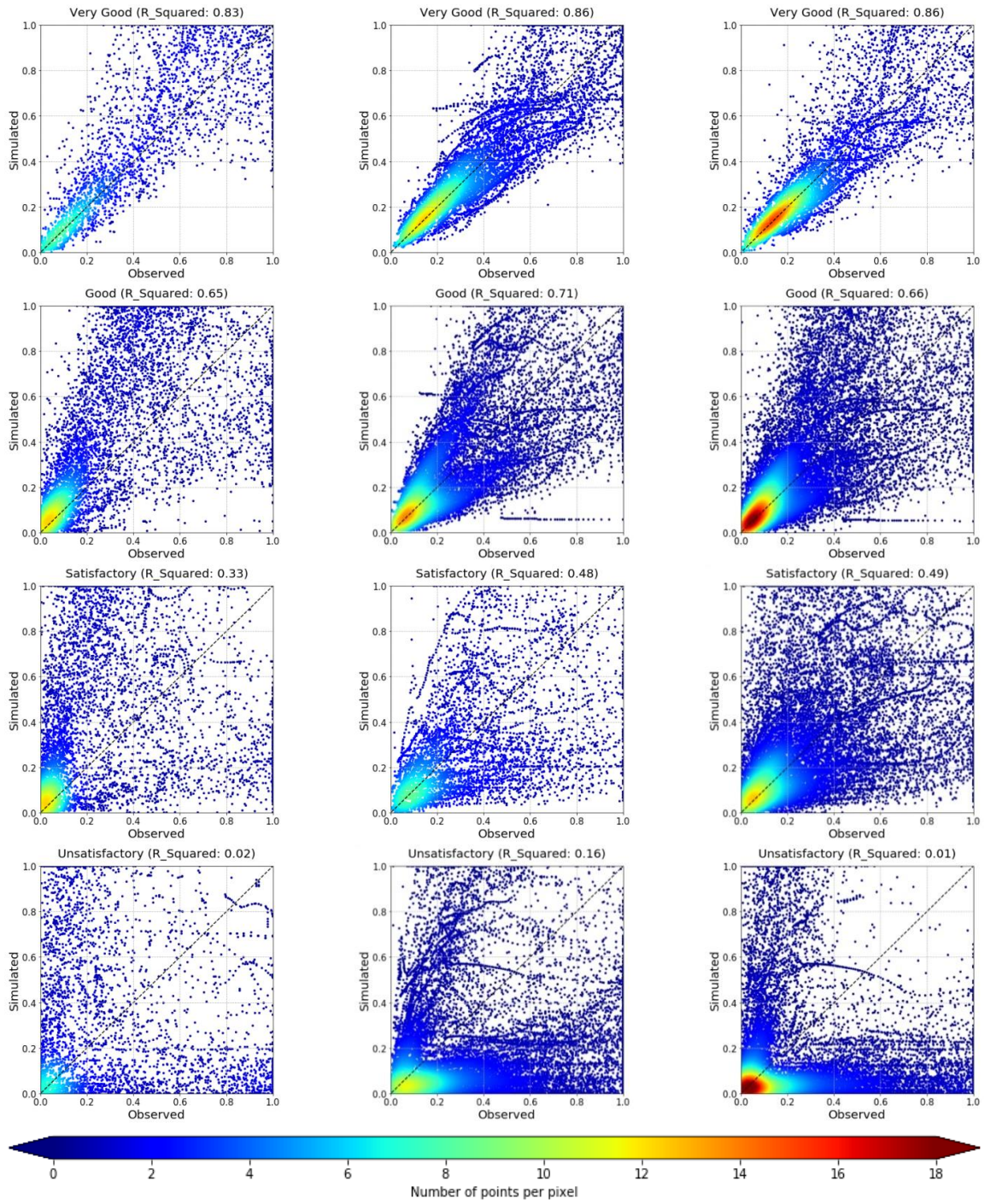
(a) Rising limb (b) Recession limb (c) Entire hydrograph

Figure 4.8: Density scatter plots of observed and simulated runoff data of NWM for the four ratings, i.e., VG to US. The results are for the two components, i.e., the rising and recession limbs, and for the entire hydrograph.

55

Figure 4.9 shows multiple samples of two single hydrographs from the simulated and observed runoff data for the four ratings and the two components, as well as for the entire hydrograph. The runoff values were normalized by the maximum value (i.e., from 0 to 1). It is evident that each rating reflects the performance of the simulated hydrograph reasonably compared with the observations. In addition, these plots can graphically indicate the reliability of the clustering module in the HAT. From the results presented, it is clear that the clustering module can provide reasonable ratings both statistically and graphically. The categorized ratings from this module were then used as the Y label in the classification module and served as the link between the two data-driven models.
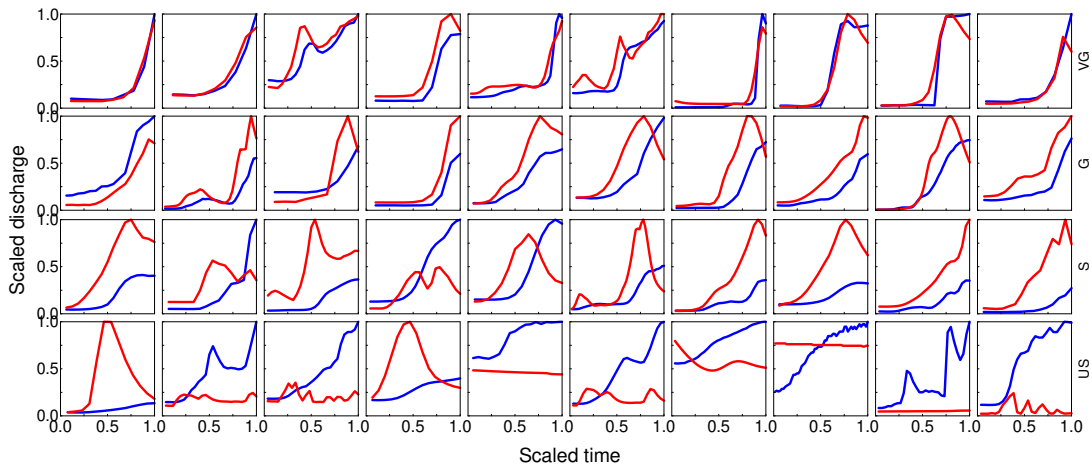
(a) Rising limb
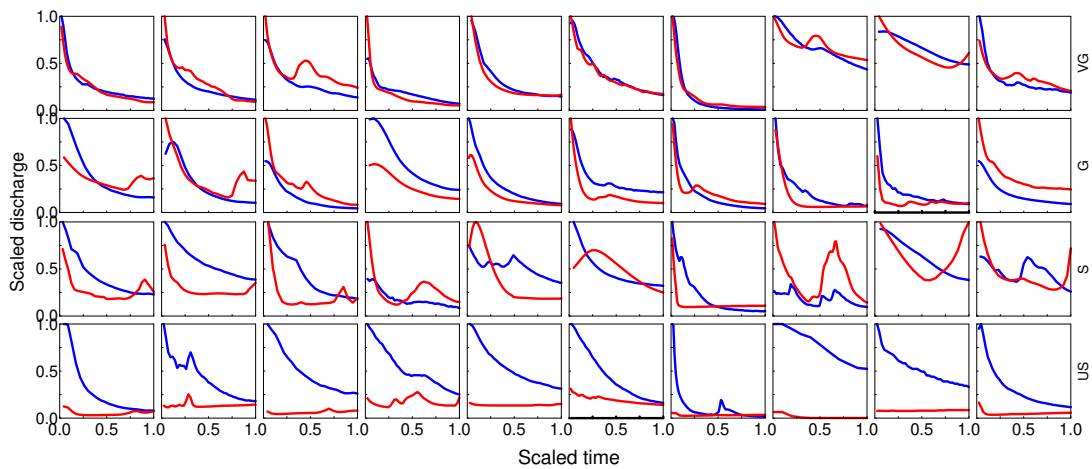
(b) Recession limb
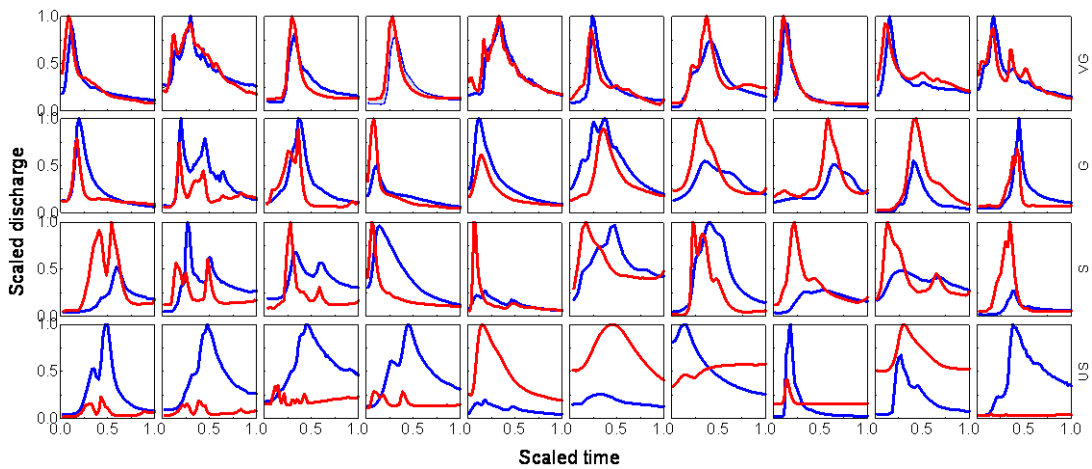
(c) Entire hydrograph

Figure 4.9: Examples of comparison results between observed and simulated single hydrographs from the NWM for the four ratings. The red and blue lines denote the simulated and observed hydrographs.

57

4.3.2 Training the HAT Using the Classification Module

The classification module is the third module of the HAT and is based on the RF technique. It is designed to detect hidden patterns between a combination of error indices and one of the performance ratings. After determining the performance ratings in the clustering module, the classification module was trained using the ratings and error indices for building the HAT. The trained classification module was used to evaluate the performance of the hydrologic model. Table 4.4 presents the verification results for the trained classification module. The classification module was verified by comparing the ratings previously determined by the clustering module and the ratings determined through the HAT. The results in Table 4.4 show that the mean concordance rates of the four ratings are approximately 98, 99, and 97%, respectively, for the rising limb, recession limb, and the entire hydrograph. This demonstrates that the HAT can provide a hydrologic assessment with high performance.

Table 4.4: Verification results for the two components and the entire hydrograph.

Ratings	Rising limb		Recession limb		Entire hydrograph	
	Match	No match	Match	No match	Match	No match
Very good	96.8	3.2	100.0	0.0	100.0	0.0
Good	97.7	2.3	96.7	3.3	96.8	3.2
Satisfactory	98.4	1.6	100.0	0.0	92.8	7.2
Unsatisfactory	97.8	2.2	100.0	0.0	100.0	0.0
Mean	97.7	2.3	99.2	0.8	97.4	2.6

In addition, the classification module of the HAT can indicate the contribution of each index to the performance ratings, as described in Section 4.2.5. Table 4.5 lists the weight values

of each error index determined by the classification module. For the two components and the entire hydrograph, the PBIAS has largest contribution for determining the ratings. The CC and NSE also affect the rating performance. In the case of the entire hydrograph, the PE and PTE have similar weight values with the NSE.

Table 4.5: Weight values of each error index.

Error indices	Rising limb	Recession limb	Entire hydrograph
PBIAS	0.55	0.56	0.52
CC	0.30	0.29	0.26
NSE	0.15	0.15	0.07
PTE	-	-	0.08
PE	-	-	0.07
Sum	1.00	1.00	1.00

4.3.3 Hydrologic Assessment Results

The trained HAT was used to test the performance of the NWM for runoff simulations in 57 streamflow stations in the San Francisco Bay area. The evaluation results were analyzed by drainage size. Figure 4.10 shows the percentage of the performance ratings of the NWM for three drainage sizes. In categorizing the drainage size, the ranges of small, medium, and large sizes are 0–63 mi^2 (mean: 28.3 mi^2), 63–390 mi^2 (mean: 150.7 mi^2), and over 390 mi^2 (mean: 742.6 mi^2), respectively.

(a) Rising limb
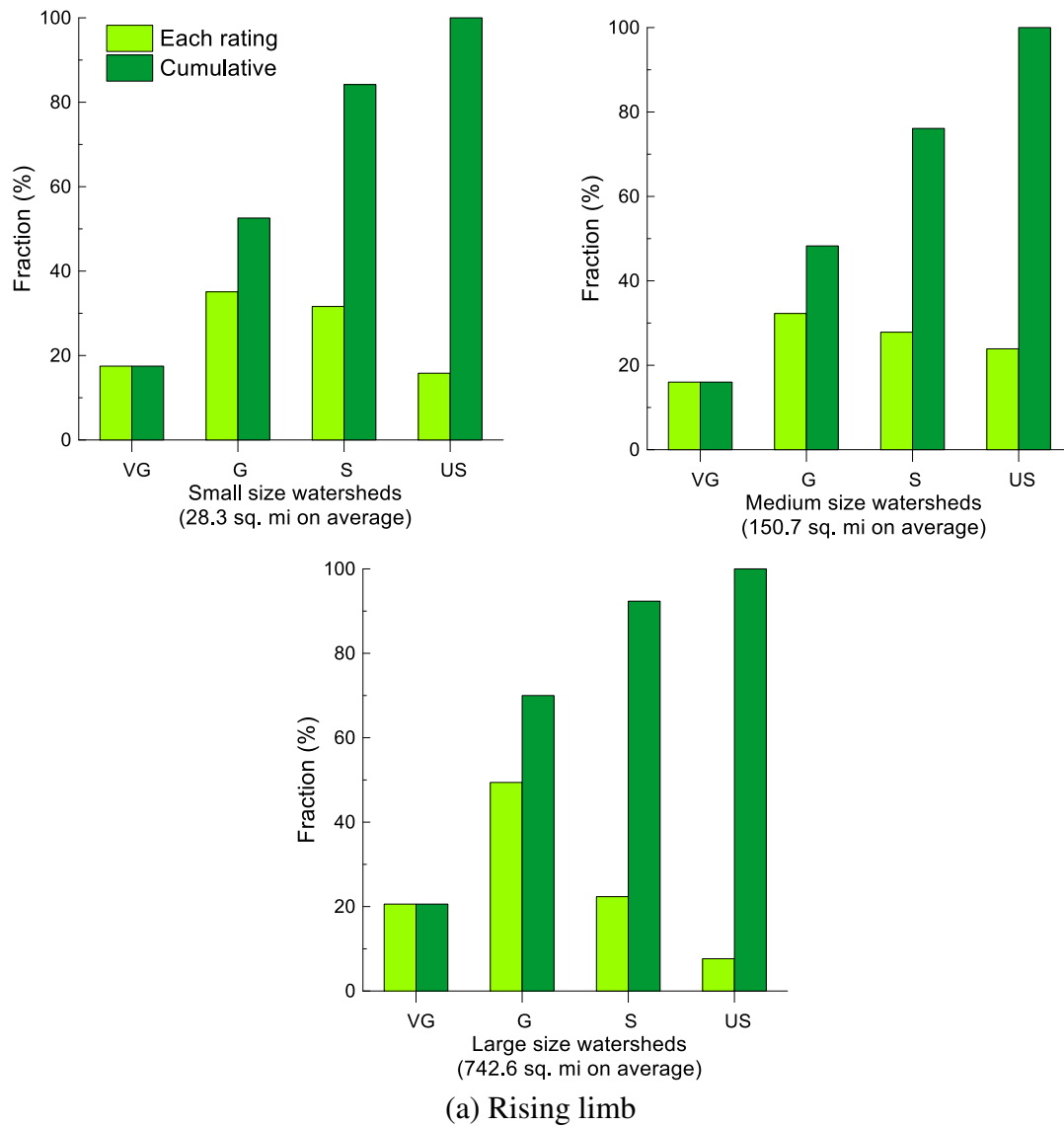
Figure 4.10: Fraction of the performance ratings of the NWM for three drainage sizes. (a) − (c) indicate results of rising, recession limbs, and entire event.
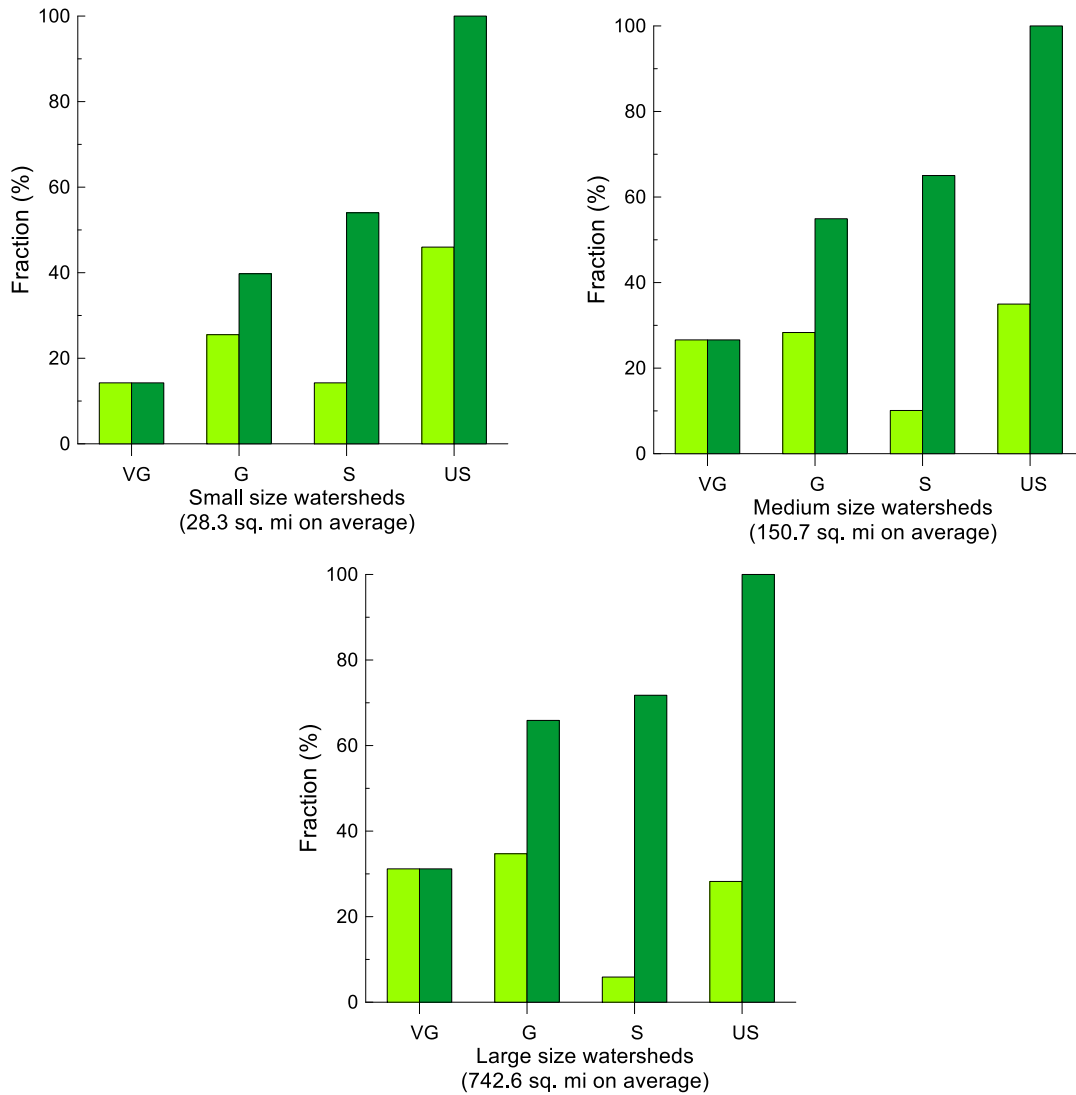
(b) Recession limb

Figure 4.10: Continued
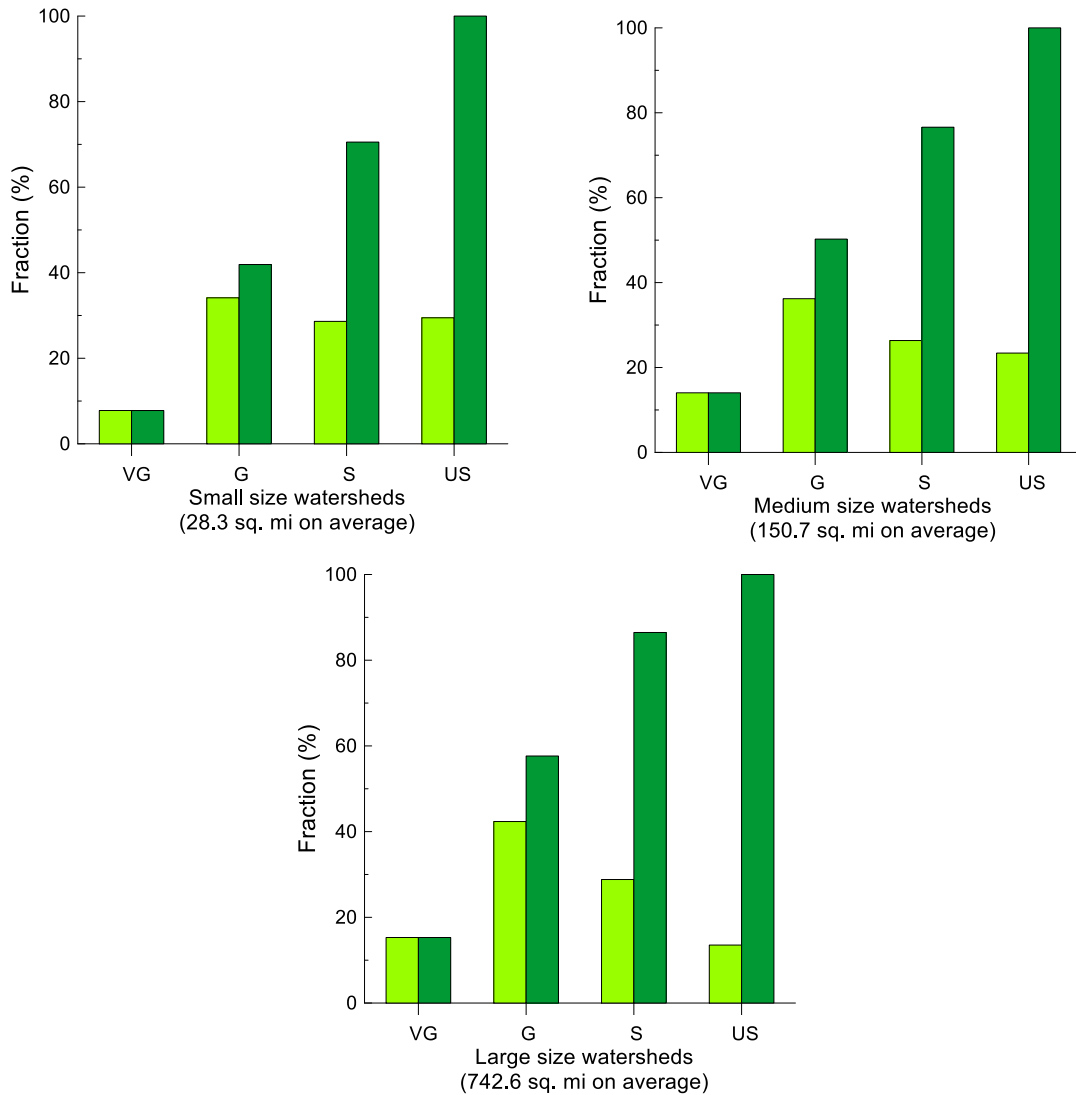
(c) Entire hydrograph

Figure 4.10: Continued

The evaluation result using the HAT showed that 46% of the simulated hydrographs were rated as VG and G. As shown in Figure 4.10, the percentages of VG and G ratings increase with drainage size. In contrast, the percentages of S and US decrease with drainage size. For example, for the entire hydrograph case, the VG and G ratings are approximately 42, 50, and 58% for small, medium, and large sizes, respectively. This trend is similar for the two components, i.e.,

the rising and recession limbs. These results indicate that the NWM provides a better performance for large drainage sizes than small ones.

There is a difference in the performance rating percentages between components. For example, the US rating in the rising limb is approximately 5% while it is 28% for the recession limb, which is approximately 5 times higher. Moreover, the S rating in the entire hydrograph is approximately 27% while it is only 13% for the recession limb, which is approximately half of the percentage in the entire hydrograph.

Figure 4.11 depicts the assessment results mapping of the performance ratings on the San Francisco Bay area for each county. On the map, the arithmetically averaged score for each station is indicated. A score of 0.0 denotes the lowest score (i.e., US) whereas 3.0 represents the highest score (i.e., VG). As exhibited in Figure 4.11, the NWM provides the lowest performance at six stations located in Marin County with an average score of 0.62. In Marin County, the VG and G ratings are less than 19%. Moreover, Napa County shows the second lowest performance with an average score of 1.11. It has 78% for S and US ratings and 22% for VG and G. In contrast, the NWM has a better performance in the Alameda and Santa Clara counties. These counties have 67, 70, 33, and 30% for VG, G, S, and US ratings, respectively. In addition, the NWM provides a better performance for simulating the streamflow for the Southern San Francisco Bay area (San Mateo, Santa Clara, and Alameda counties) than for the Northern area (Marina, Sonoma, and Napa counties).
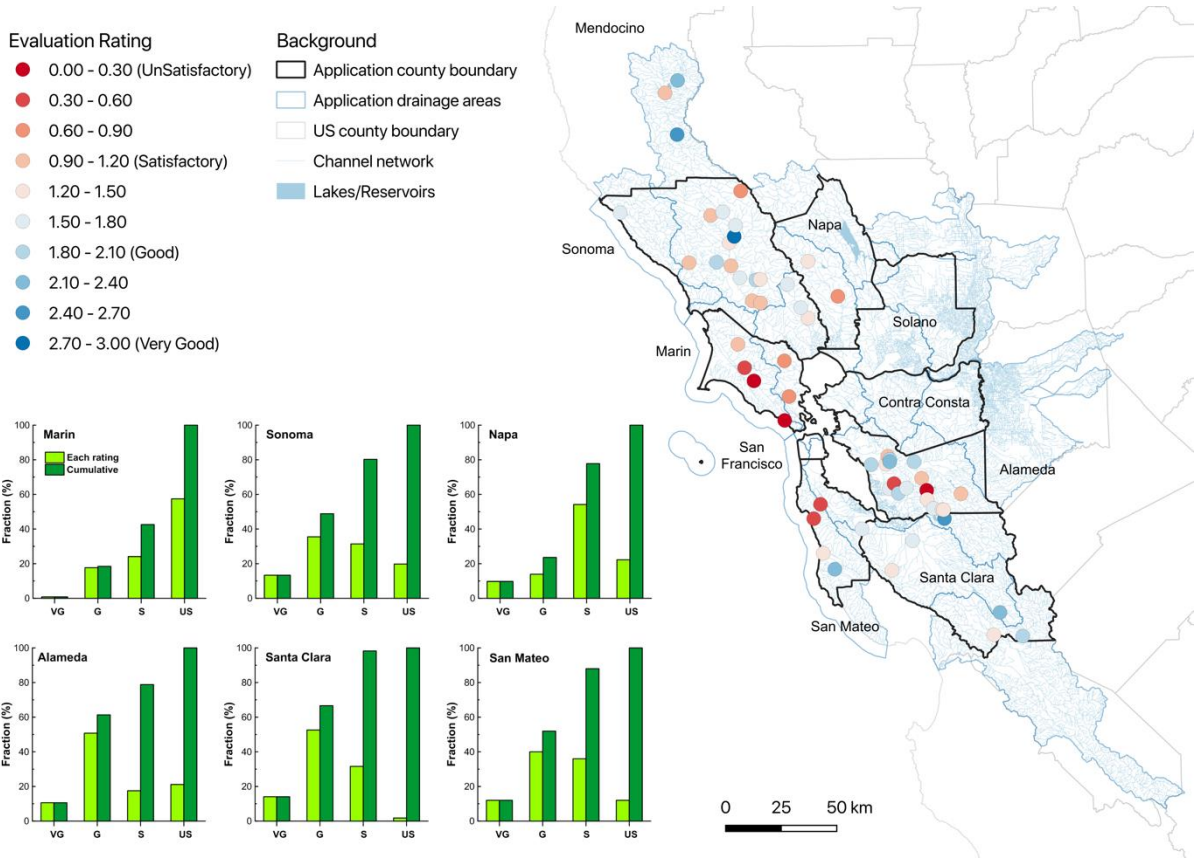
Figure 4.11: Assessment results mapping of the performance ratings on the San Francisco Bay area for six counties (Southern area: San Mateo, Santa Clara, and Alameda counties; Northern area: Marina, Sonoma, and Napa counties).

It is also necessary to determine how the performance ratings are affected by several factors, such as features of precipitation and watershed, because such factors can affect the streamflow. Figure 4.12 illustrates the contributions of four factors, namely, number of peaks in the hydrograph, runoff duration, drainage size, and regulations, to the performance ratings. From the results in Figure 4.12 (a), there is no significant difference between the four performance ratings in the case of the number of peaks. The performance of the NWM for storm events with complex hydrographs is reliable and comparable to simulations for single-storm events. In the case of runoff duration, the performance ratings do not show significant differences by duration

features. In addition, the drainage size affects the performance of the NWM. Higher performance ratings are shown in watersheds with larger drainage sizes. The percentages of VG and G ratings are the highest in large drainage sizes and the lowest in small sizes. These results can be because the performance ratings were based on the entire runoff flow, which is a combination of base flow and direct flow, and areas with large drainage can be affected by the base flow. Furthermore, as presented in Table 4.5, the PBIAS has the highest influence in determining the performance ratings. As for the regulation features, the performance ratings do not show significant differences.

(a) Hydrograph   (b) Runoff duration   (c) Drainage size   (d) Regulation
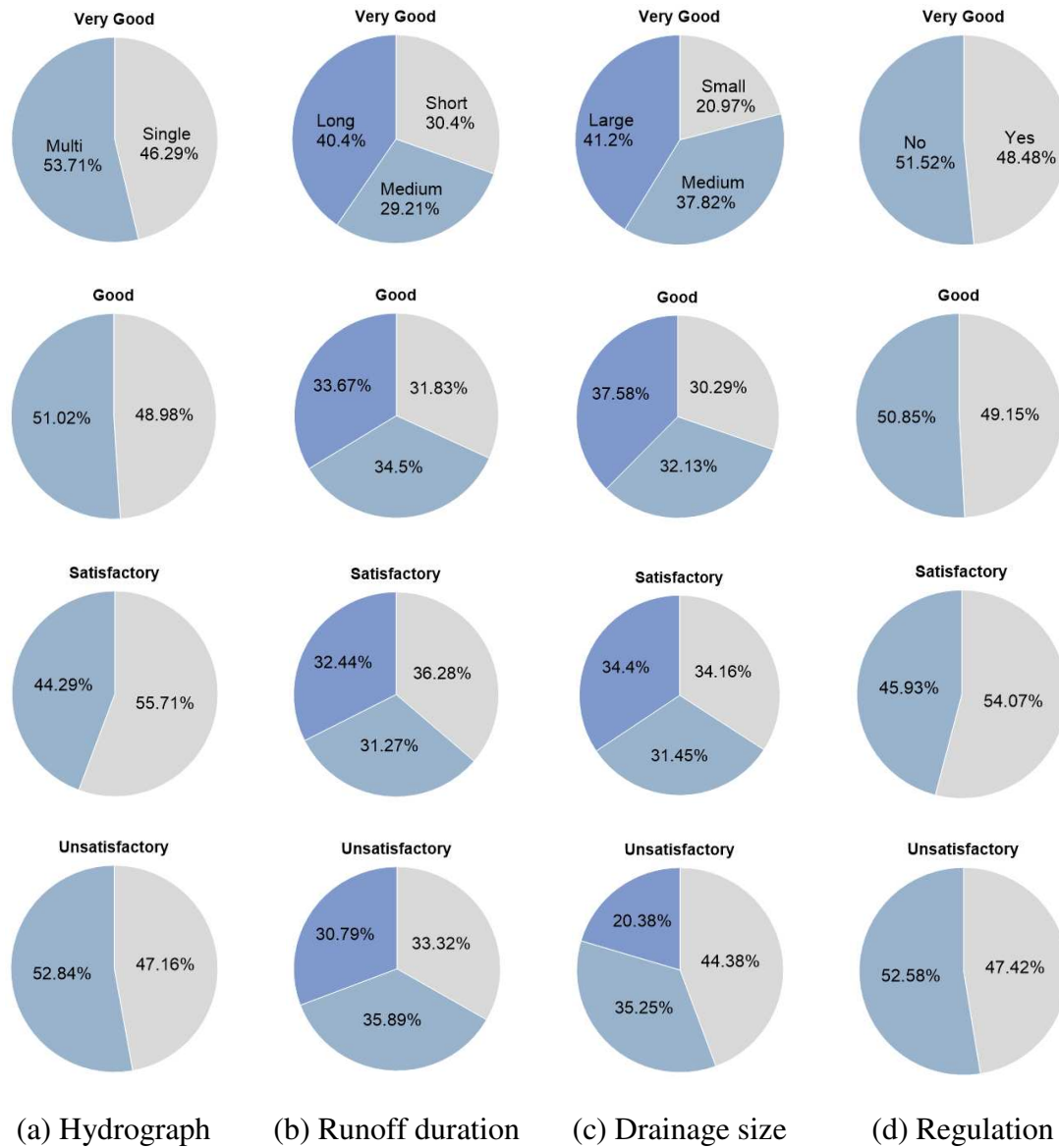
Figure 4.12: Contributions of four factors, i.e., number of peaks in the hydrograph, runoff duration, drainage size, and regulation, to the performance ratings: (a) indicates the number of peaks in the entire hydrograph; (b) shows the time interval between the beginning and end points of the hydrograph consisting of short term (< 36 h), medium term (36 < duration < 72 h), and long term (> 72 h); (c) shows the drainage size comprising small (< 63 mi^2), medium (63 < drainage size < 390 mi^2), and large (> 390 mi^2) areas; and (d) represents regulation conditions which means whether the streamflow is controlled by other factors such as infrastructure, reservoirs or not.

4.4 Discussion

In this study, a new HAT was developed using a hybrid framework of two data-driven models for a composite and easy-to-understand hydrologic assessment. To evaluate the performance of the HAT, this study compared it with another hydrologic evaluation framework proposed by Moriasi et al. (2007). They used a classification criterion for the error index through a basic framework of decision trees and tested the performance of the hydrologic model based on the basic framework. However, one of the limitations of their framework is the use of only one error index, which makes it difficult to evaluate the model performance comprehensively.

Figure 4.13 indicates a comparison of the two frameworks, i.e., the HAT framework proposed in this study and the basic framework by Moriasi et al. (2007). For a graphical comparison, three indices, namely NSE, PBIAS, and RSR, were used. As shown in Figure 4.13, the distributions of data points from the HAT are separated well according to the four ratings, whereas the distributions from the basic framework are difficult to interpret in terms of the performance rating results. For instance, the three ratings, i.e., VG, G, and S, have very similar distributions and it is difficult to find a trend in the scatter plot distribution of the US rating. In addition, the R-squared values (R^2) indicate that there are no significant differences between the distributions of VG, G, and S ratings. For the PBIAS, the values of R^2 of VG, G, and S ratings range from 0.75 to 0.7, and the R^2 of the G rating is higher than that of the VG rating. In the case of the NSE and RSR, the ranges of R^2 values are 0.85–0.92 and 0.84–0.92, respectively, which are similar to the results of the PBIAS. Even though the R^2 values of the US rating are lower than the other ratings, it is difficult to conclude that the simulated results of the US rating are evaluated well because the scatter distribution has no trend. From the comparison results with the basic framework, it is evident that the new HAT can provide reliable and objective assessment

results for hydrologic models and it can be an effective alternative to the conventional evaluation

method.
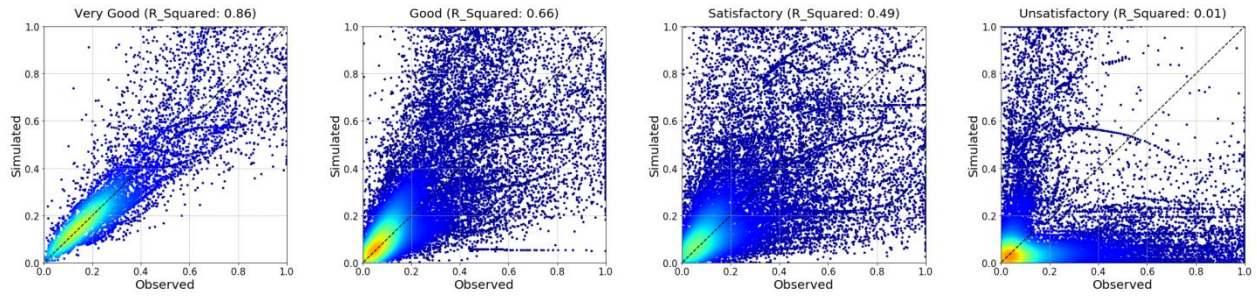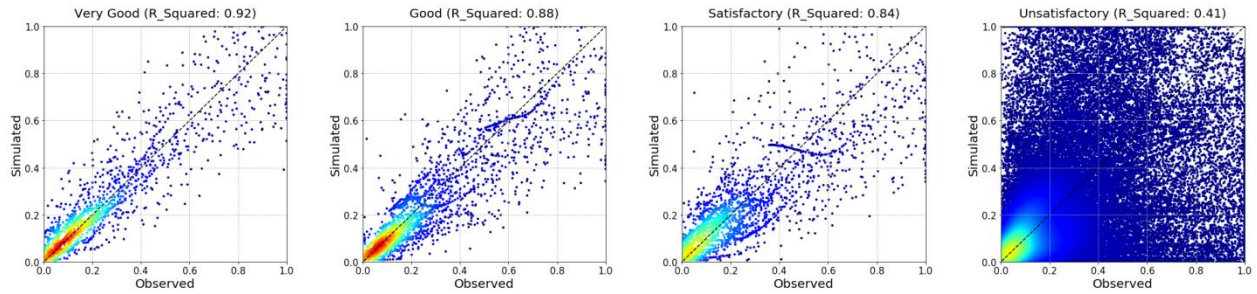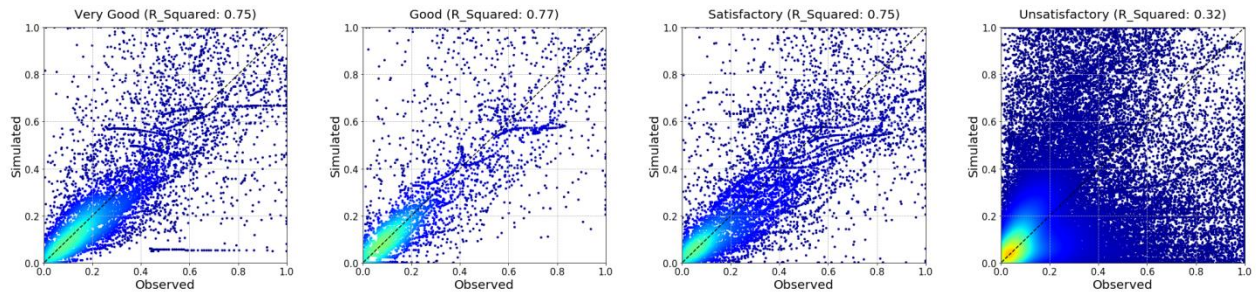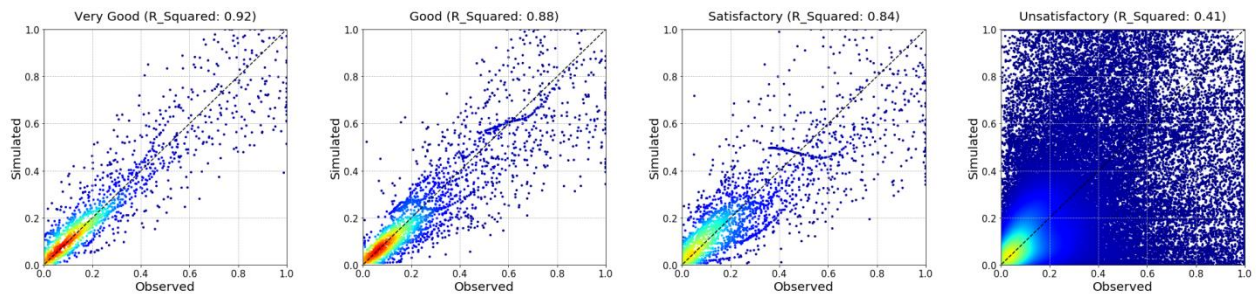
Figure 4.13: Comparison results of density scatter plots generated from the (a) proposed HAT and (b)–(d) basic framework by Moriasi et al. (2007).

Chapter 5

Improvement of Predictive Performance Using Data-Driven Model as Post-Processor

This chapter applied a deep learning based data-driven model to predict errors in forecasted runoff provided from NWM in Russian River basin, California. The proposed model was used to predict errors in hourly runoff with lead time between 1 to 18 hours using observed precipitation and errors that come from upstream regions. The forecasted errors were applied to improve the predictive performance of the NWM.

5.1 Introduction

Accurate simulation of rainfall-runoff relationship is necessary for various water-related purposes, including flood forecasting (Shrestha and Solomatine, 2008; Neitsch et al., 2011; Hu et al., 2018; Fan et al., 2020; Xiang et al., 2020). Generally, physically-based numerical hydrologic

models are often used to simulate the nonlinear relationships between rainfall and runoff, and these models are applied in many hydrologic applications such as short-term simulations for flood prediction and long-term simulations for drought analysis and water resources management (Ott et al., 1991; Lee et al., 2005; Wu et al., 2011; Kang and Sridhar, 2017; Wang et al., 2017). Several hydrologic models have multiple parameters used to calibrate modeling processes and to reduce output errors or residuals.

When using hydrologic models, errors inherent in the runoff prediction results can lead to inaccurate hydrological analysis results. In particularly, decision makers operating water-related infrastructures for flood forecasting, irrigation control, drought prediction, and other water management purposes require reliable hydrologic modeling outcomes considering uncertainties inherent in the results (Shrestha and Solomatine, 2008). Appropriate error estimates can enhance the reliability and credibility of hydrologic modeling results for water management and improve the understanding of error propagations within modeling frameworks (Krzysztofowicz, 2001).

Differences between simulated runoff estimates and observed data can caused by four sources within a hydrologic model: (a) uncertainties or inaccuracies in modeling input data; (b) uncertainties or inaccuracies in modeled outputs used for calibration; (c) uncertainties or inaccuracies in modeling parameters; and (d) uncertainties caused by imperfect model structures (Refsgaard and Storm, 1990; Shrestha and Solomatine, 2008). A major contributor to errors caused by any of these types of uncertainties is the difficulty in accurately measuring the spatial and temporal variability in hydrologic modeling inputs across large modeling domains (Shrestha and Solomatine, 2008).

According to Shrestha and Solomatine (2008), there are many methods have been used to analyze uncertainties in hydrologic models. These methods are analytical and approximation

methods (Rosenblueth, 1975; Harr, 1989; Melching, 1992; Maskey et al., 2004; Montanari, 2007; Tung, 2011), Monte Carlo-based methods (Kuczera and Parent, 1998; Hong et al., 2006; Vrugt et al., 2008), Bayesian methods and generalized likelihood uncertainty estimation (GLUE) methods (Krzysztofowicz, 1999; Jin et al., 2010; Li et al., 2010), and Fuzzy theory-based methods (Maskey and Guinot, 2003; Huang et al., 2010). However, the majority of these uncertainty analysis methods consider only with a single source of uncertainty, and most methods assume that the model structure is accurate, and input data is free from uncertainty. These limitations make it difficult to consider the inherent uncertainties of input variables and numerical approaches for limiting the effects of input errors on model results. In addition, according to Abebe and Price (2003), uncertainties associated with the quality of input data that come from upstream affect the calibration of the model parameters, and input uncertainty translate through the model to its outcomes. As long as there are unaccounted uncertainties that come from upstream, it is difficult to expect accurate rainfall-runoff simulations through hydrologic models.

In the case of short-term hydrologic model, which may predict the streamflow for a flood warning system, accurate runoff prediction is necessary. Maintaining high model accuracy is crucial because the flood warning level is determine based on the forecasted results from the hydrologic model. In addition, it is essential to deal with the errors in real time because the short-term hydrologic model provides predicted runoff every hour or minutes. Ideally, it is possible to minimize the errors in the predicted runoff by predicting the errors that can be generated from various sources in advance.

Numerous studies have investigated how uncertainty that come from upstream sources affect the errors in model results (Kobold and Sušelj, 2005; Haydon and Deletic, 2009; Arnaud et al., 2011; McMillan et al., 2011). For example, Muñoz et al. (2014) used Monte Carlo method to

examine how the uncertainty in rainfall data affects the errors in runoff simulated by a hydrologic model, and they resulted that the uncertainty in the rainfall estimation process had a significant effect on the error in modeling outcome. Also, uncertainty in the rainfall data during a rainy period had a larger impact on output errors compared to periods with less precipitation. Another study, led by Datta and Bolisetti (2016), investigated the impacts of precipitation uncertainty on error in model output using the precipitation multiplier method. They found that residuals between estimated precipitation and measured value have crucial effects on the errors in prediction results of hydrologic model. In particular, the model errors in runoff prediction resulted in underestimated runoff for high-flow events and overestimated for low-flow events. Thus, it is necessary to consider the impact of uncertainty in upstream data sources when minimizing the output errors of hydrologic models.

Recently, data-driven models been applied for various purposes in the field of hydrology. Data-driven models generally require massive amount of datasets to analyze non-linear relationships between data components, such as rainfall-runoff relationships. With advances in computational resources and technology, such models have significantly contributed to the advancement of hydrological analyses since they produce high-quality and cost-effect modeling results (Mosavi et al., 2018). In addition, the data-driven models have shown predictive powers with fewer parameters compared to the physically-based models (Solomatine and Ostfeld, 2008; Castelletti et al., 2010).

Data-driven models can adequately simulate highly non-linear complex systems and widely used in forecasting applications, including predictions of precipitation (Lin et al., 2013; Agrawal et al., 2019; Sønderby et al., 2020), runoff (Yilmaz and Muttil, 2014; Hu et al., 2018; Fan et al., 2020; Xiang et al., 2020), soil properties (Feng et al., 2019), groundwater levels

(Sahoo et al., 2017), and river stages (Choi et al., 2020). In addition, data-driven models can be used in combination with two or more models (Kim et al., 2019) and can be used to improve the performance of physically-based models as they are used complementarily (Abebe and Price, 2003).

Data-driven models are not only effective in predicting hydrological variables as mentioned above, but they are also be used to predict how errors in model outputs are affected by multiple sources of uncertainty. Numerous studies have used data-driven models to improve the performance of hydrologic models by predicting and minimizing the uncertainty of hydrologic models. For instance, Abebe and Price (2003) presented a complementary framework to analyze uncertainty in hydrologic models using ANN model. Their study analyzed the relationships between precipitation and error in runoff of the model, and they found that application of data-driven model (e.g., ANN model) for error estimation in hydrologic models can significantly contribute to improve the models` performance. In addition, Wu et al. (2018) successfully applied RF model to predict the errors using relationships between input data such as precipitation and temperature and error in runoff, and, similarly, Shrestha and Solomatine (2009) applied multiple data-driven models to estimate the prediction intervals of outputs and resulted that application of data-driven models on error prediction is effective method for improving model`s ability. Recently, various data-driven models have been applied as a post-processor for minimizing runoff errors and improving the modeling performance (Frame et al., 2020; Nearing et al., 2020).

Previous studies only used error sources related to uncertainties within the hydrologic model, such as input variables, parameters, and model structure, so it may difficult to account for the influences of uncertainties that come from upstream on errors in model output. By building

74

upon previous data-driven modeling studies, this study aims to evaluate a deep learning-based data-driven approach to reduce hydrologic modeling errors by explicitly considering uncertainties in upstream runoff data. The LSTM model, which is a deep learning-based data-driven model, was combined with a sequence to sequence learning structure (hereafter referred to as LSTM-s2s) to predict the errors in the forecasted runoff from a hydrologic model (e.g., NWM). The specific objectives of this are as follows: (i) analyze errors in forecasted runoff from the physically-based hydrologic model, (ii) develop an error correction tool using a data-driven model as a post-processor tool, and (iii) investigate how the developed post-processing tool improves the predictive performance of hydrologic model.

5.2 Materials and Methods

5.2.1 Study Area and Data

This study focuses on the Russian River basin located in California, USA as study area. Figure 5.1 shows location observation stations for streamflow and precipitation located in the Russian River basin and the stream channel network on a digital elevation model. The basin has a drainage area of approximately 3,850 km^2 with elevations ranging from 50 m to nearly 800 m. In this area, two reservoirs, Mendocino and Sonoma, which are regulated by the Coyote Valley and Warm Springs dams. The Russian River basin is located on the west coast of the United States with an average annual precipitation of 925 mm, and more than 80% of the annual precipitation has been observed from November to March. In this area, not only heavy precipitation is generated from extratropical cyclones or jet streams from the Pacific ocean, but atmospheric rivers cause flood damages during the wet season (Ralph et al., 2006; Han et al., 2019). The Russian river is one of the most flood-prone rivers in California because of the

75

unique geography and its proximity to the west coast, which produce climatologically heavy precipitation. This implies the need for an accurate runoff forecasting system, as the area has more than three flood events every year (Johnson et al., 2016).
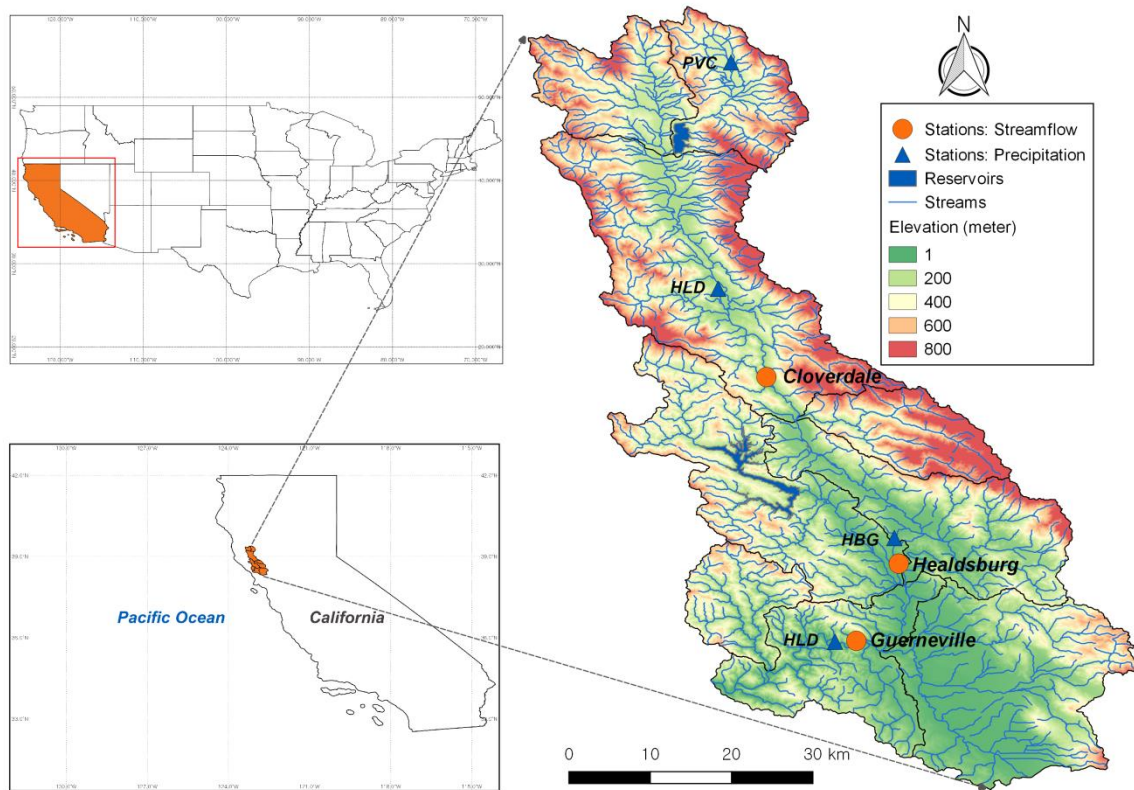
Figure 5.1: Application area of this study. Location observation stations for streamflow and precipitation located in the Russian River basin, CA.

Datasets for this study include forecasted runoff data with a lead time of 1 to 18 hours from the NWM and observed runoff at three USGS stations located in the Russian River basin: USGS 11463000 at the Russian River basin near Cloverdale (Cloverdale station), USGS 11464000 at the Russian River near Healdsburg (Healdsburg station), and USGS 11467000 at the Russian River near Guerneville (Guerneville station). The Guerneville station is located at

the outlet point of the watershed. Additional data is hourly precipitation data from NOAA Physical Sciences Laboratory (https://www.psl.noaa.gov/data/) at the Potter Valley Central (PVC), Hopland (HLD), Rio Nido (ROD), and Healdsburg (HBG) stations. In this study, datasets from 2019 to 2020 were collected and the data for 2019 was used for training and the remaining data was used for test of the model. Table 5.1 describes the various datasets used in this study.

Table 5.1: Information for observed datasets (streamflow and precipitation) used in this study.

Datasets (Source)	Stations (USGS)	Location		Time-step
		Latitude	Longitude	
Streamflow (waterdata.usgs.gov)	Cloverdale (11463000)	38.8794	-123.0525	Hourly
	Healdsburg (11464000)	38.6133	-122.8352	Hourly
	Guerneville (11467000)	38.5086	-122.9266	Hourly
Precipitation (https://psl.noaa.gov/data/)	PVC	39.3209	-123.1027	Hourly
	HLD	39.0030	-123.1209	Hourly
	ROD	38.5073	-122.9565	Hourly
	HBG	38.6529	-122.8732	Hourly

5.2.2 Evaluation Metrics

In this study, four statistical metrics for evaluating the performance of different data-driven models are CC, NSE, PBIAS, which are described in Chapter 4.2.3 and root mean square error (RMSE).

$$RMSE = \sqrt{\frac{\Sigma(y_o - y_e)^2}{m}} \tag{5.1}$$

where, y_e and y_o indicate the simulated and observed runoff, m denotes the number of data point. Value of RMSE range from 0 to $+\infty$ and describes how well the simulated value matches to the observed value. The zero value of RMSE means modelled value is perfect.

5.2.3 Model Development

This study used a LSTM-s2s model to improve the predictive performance of a physically-based hydrologic model (i.e., NWM) by forecasting errors in advance. The LSTM-s2s model was used to predict errors between 1 and 18 hours using errors in runoff that come from upstream and observed precipitation as input datasets. Figure 5.2 shows the flow chart of this study, which includes the following five components: 1) collecting forecasted and observed runoff time series data; 2) calculating errors between forecasted and observed datasets; 3) training the LSTM-s2s model using the calculated errors and observed data; 4) predicting future model errors using the LSTM-s2s model; 5) improving the forecasted runoff and evaluating the forecast performance. Error is estimated using Eq (5.2) for each time steps between 1 and 18 hours.

$$error\ (\%) = \frac{(Runoff_{obs} - Runoff_{sim})}{Runoff_{obs}} \times 100 \tag{5.2}$$

Where, *Runoff*$_{obs}$ and *Runoff*$_{sim}$ denote the observed and forecasted runoff from the NWM. Estimated errors in each time step are used as input variables of the LSTM-s2s model for training and error predictions. The overall model design can be formulated as follows:

$$error_{t+m} = f(error_{upstream,t-1,t-2,...t-n}, precipitation_{t-1,t-2,...t-n}) \tag{5.3}$$

In this model algorithm, time series input, including errors in forecasted runoff at three stations (two upstream stations and the outlet point) and precipitation data at four ground-based gauges were used to predict the error for each time steps from $1 - 18$ hours. The final forecast error for each time-step between 1 to 18 hours will be the output of the LSTM-s2s model and used to improve modeling performance.
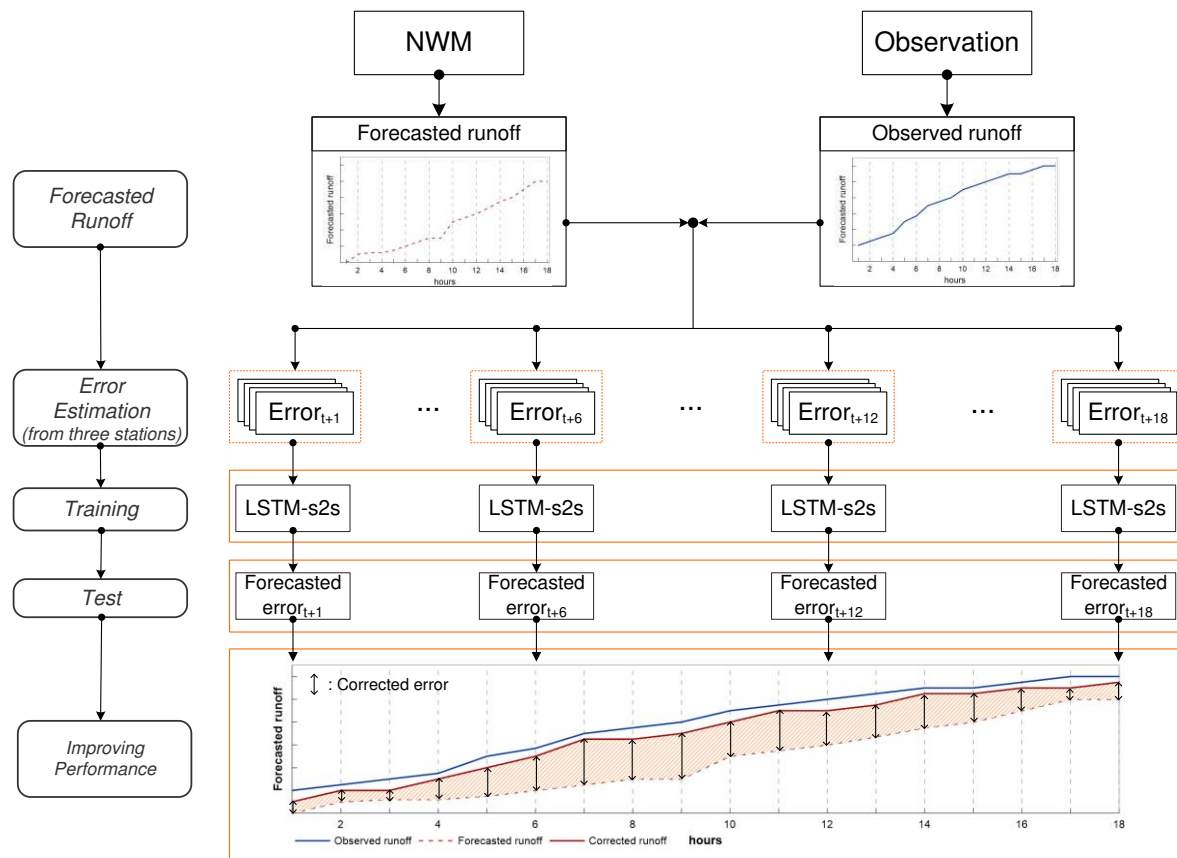
Figure 5.2: Flowchart of this study which is representing five steps from estimating errors in forecasted runoff to the improvement of forecasting performance.

5.3 Results

5.3.1 Performance of NWM for Runoff Forecasting

Firstly, it was necessary to evaluate the performance of the NWM for runoff predictions before testing prediction improvements using LSTM-s2s model. In this study, the ability of NWM for prediction of runoff between 1 to 18 hours was evaluated. A total of 11,647 values of predicted runoff from the NWM were compared with observed runoff data collected at the USGS stations. Four evaluation metrics of CC, NSE, PBIAS, and RSME were used to compare runoff

predicted by the NWM and observed runoff at each of the three USGS gages, and the cumulative distributions of each metric were plotted to assess the NWM predictive performance (Figure 5.3).

As shown in the Figure 5.3, the predictive performance of NWM was similar at three points, and Healdsburg has relatively better performance than other two stations. Overall, according to PBIAS values, the NWM runoff predictions at each USGS station tended to overestimate actual runoff, indicating that a post-process is necessary to improve the prediction performance of the NWM model.
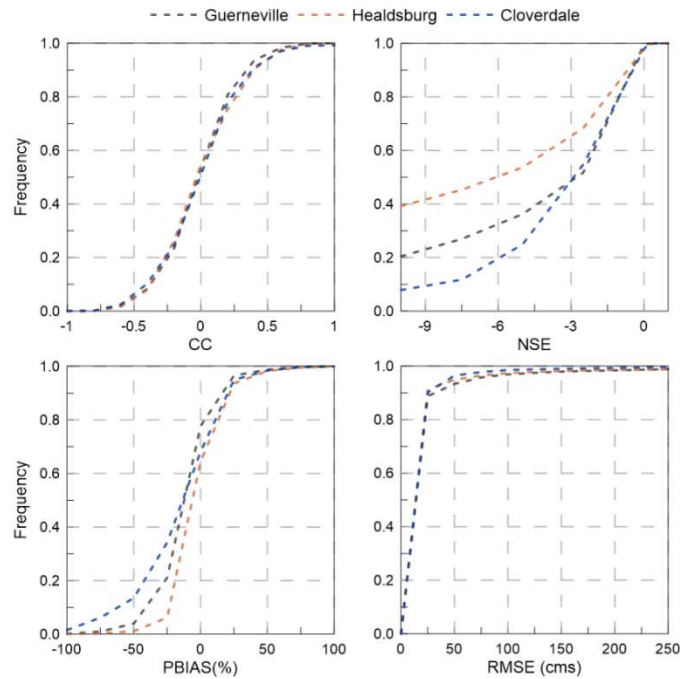
Figure 5.3: Cumulative distributions of model performance estimated as CC, NSE, PBIAS, and RMSE for three stations (Cloverdale, Healdsburg, and Guerneville).

The forecasting performance of NWM for each 1-hour time step between 1 and 18 hours was evaluated using four metrics (Figure 5.4). As shown in Figure 5.4, the predictive performance of the NWM at the Guerneville station tends to decrease with growing lead times

until the performance stabilizes for lead times greater than approximately 12 hours (CC ≈ 0.66, NSE ≈ 0.55, PBIAS ≈ 10%, and RMSE ≈ 40 cms). These results show the necessity of improving the predictive performance of NWM for effective flood forecasting, especially at longer lead times.
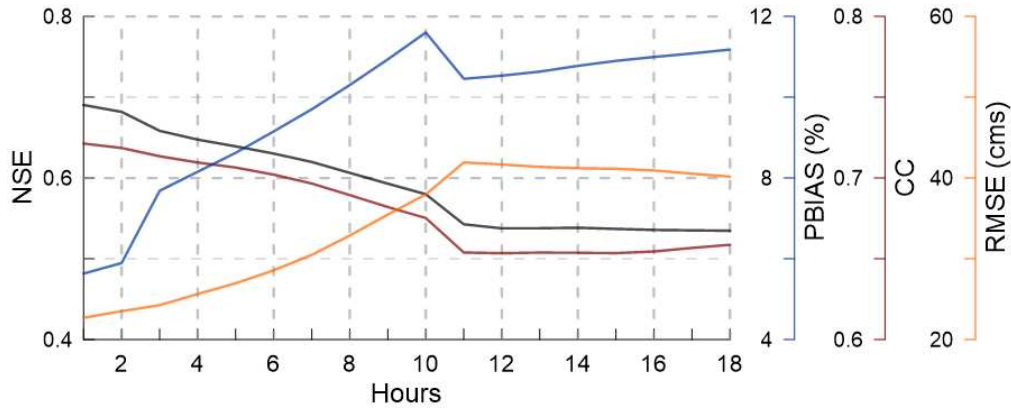
Figure 5.4: Evaluation results of predictive performance using four error indices for 1 to 18 hours of lead time at Guerneville station.

5.3.2 Model Optimization

Optimization of model parameters is significant task for data-driven model training and validation. The parameters in LSTM-s2s model can be adjustable to improve the model performance and these parameters include input time-steps, batch sizes, and number of cells in each layer (Xiang et al., 2020). This study used three parameters, time-steps of input, number of layers, and batch size, for model optimization. Previous studies have also focused on adjusting these parameters during the LSTM model training period (Fan et al., 2020; Xiang et al., 2020).

In this study, two variables, hourly observed precipitation at four stations (PVC, HLD, ROD, and HBG) and residuals in runoff at two upstream USGS stations (Cloverdale and

Healdsburg), were used as input data of the model. In addition, three parameters, sequence length (i.e., input time-step), number of layers, and batch size, were used as in the LSTM-s2s model. To evaluate the sensitivity of the model to variations in sequence length of input data, the observation time-steps n for historical input variables were tested from 6 to 24 hours at upstream stations and model performance was evaluated at the most downstream USGS station (Guerneville). Figure 5.5 (a) shows the three metrics (i.e., NSE, PBIAS, and CC) for each time-step. The result indicates that the model with 6 hours of observations shows the highest performance with 0.95 for NSE, 0.97 for CC, and 47% for PBIAS. The models with time-steps from 6 to 12 hours have similar performance with CC and NSE above 0.9, but PBIAS values also increased as time-step increased. The models with time-steps from 12 to 18 hours have relatively low performance, although the time to concentration between upstream stations and outlet is ranged from 10 to 18 hours. This shows that other hydrologic factors, including soil moisture and evapotranspiration, are also important for predicting runoff with longer time-steps (Xiang et al., 2020), though not considered in this study.

Figure 5.5 (b) and (c) show the evaluation metrics for different values of parameters of the models (i.e., number of layers, batch size). These two parameters were adjusted from 32 to 256 and tested at Guerneville station. The model with number layers of 32 and batch size of 128 has the best performance with 0.96, 0.75 for CC, 0.91, 0.71 for NSE, 59.4%, 63.9% for PBIAS, and 1.4 cms, 2.4 cms for RMSE, respectively. The model with batch size of 32 also showed acceptable performance with high values of CC and NSE, but it has larger PBIAS than other models which is important element in runoff simulation. From the optimization results, this study used that input time-steps of 6 hours, number of layers of 32, and batch size of 128 as parameters of LSTM-s2s model.
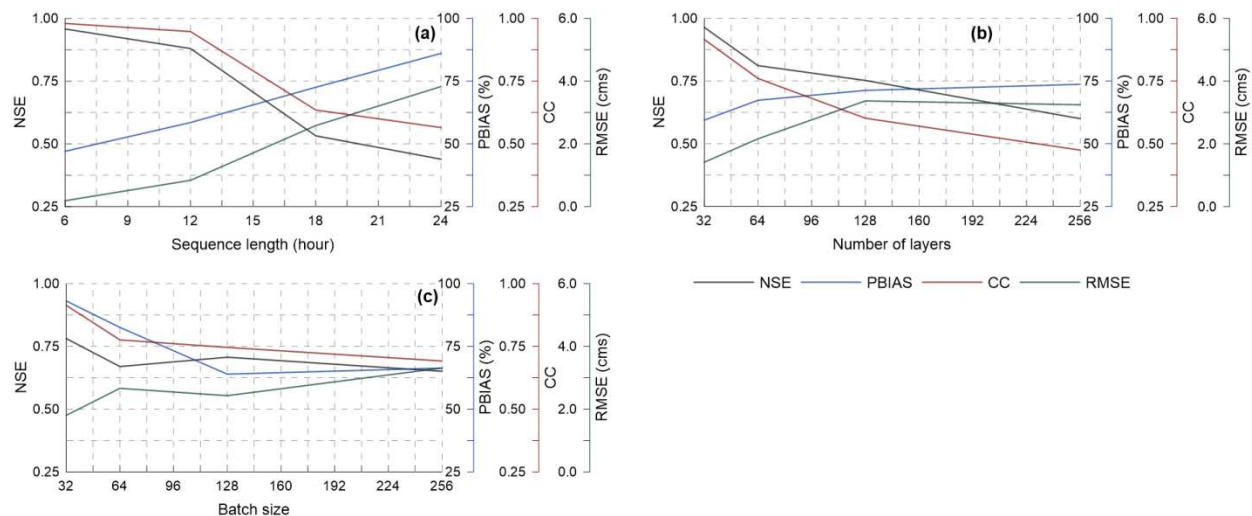
Figure 5.5: Model optimization results based on three parameters including input time steps, number of layers and batch size using four evaluation metrics (NSE; black line, PBIAS; blue line, CC; red line, and RMSE; green line).

5.3.3 Performance of LSTM-s2s for Error Prediction

The trained LSTM-s2s model was used to predict runoff errors at the Guerneville station with forecasting lead times of 1 to 18 hours in 1-hour increments. The measured and simulated errors with lead time of 1 to 18 hours from the LSTM-s2s model are shown in Figure 5.6. As shown in Figure 5.6 (a)-(e), two error datasets seems to fit the 1:1 line with average R^2 values of 0.97. Distribution of error is ranged from -100% to 100% for 12-18 hours lead times, and from -50% to 100% for 1-6 hours lead times, and a high density (red point in Figure 5.6) was between -20% and 0%. In addition, as a lead time increases, the distribution range of the errors tends to be wider. From these results, the applicability of the LSTM-s2s model for error prediction was confirmed to improve the predictive performance of NWM for runoff forecasting.

(a) 1hour   (b) 3hour   (c) 6hour

(d) 12hour   (e) 15hour   (f) 18hour
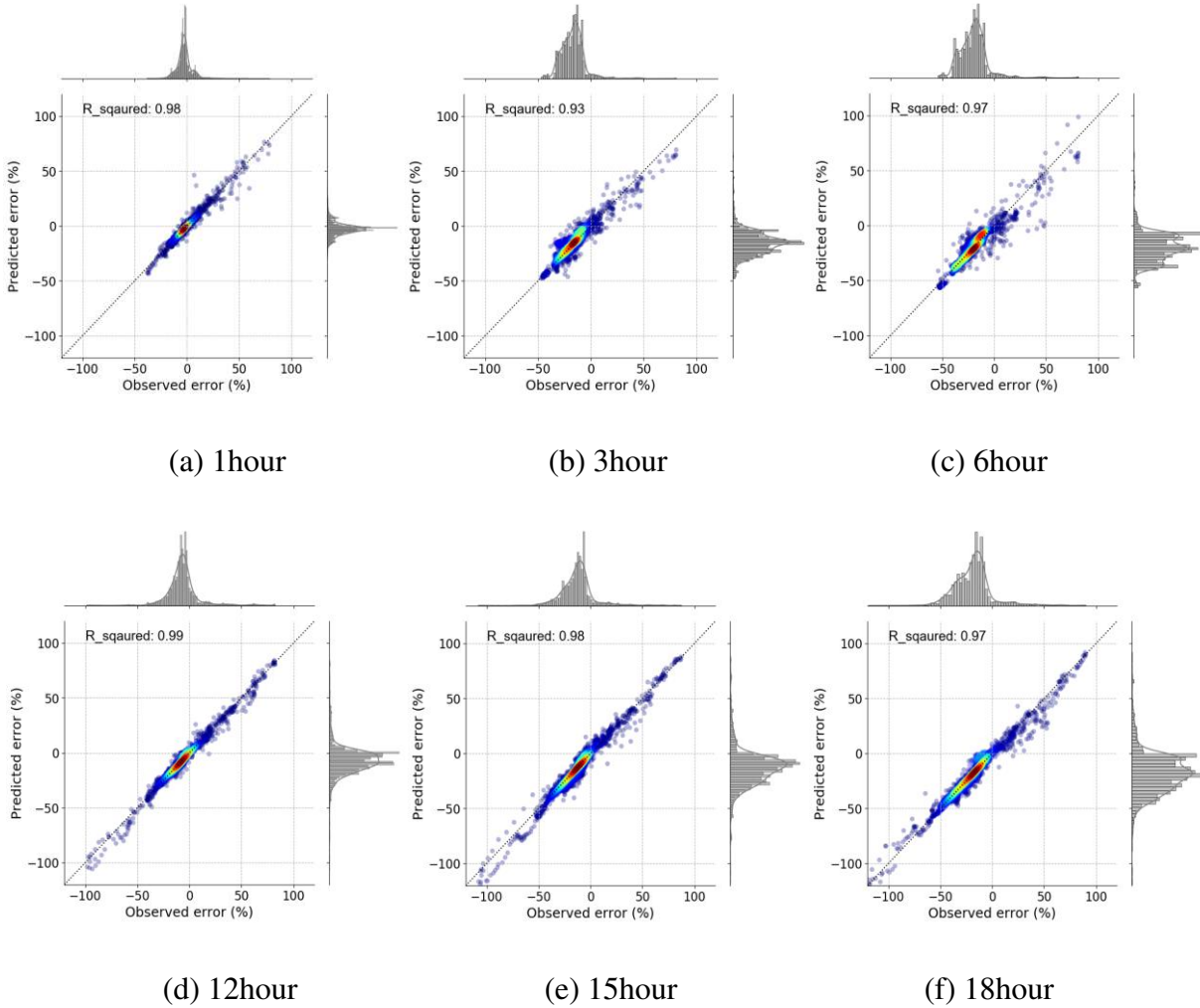
Figure 5.6: Comparison results of predicted errors with actual values.

The statistical results for the overall predictive performance of LSTM-s2s for lead times between 1 to 18 hours listed in Table 5.2. As shown in Table 5.2, LSTM-s2s model provided high performance for error prediction with average CC of 0.95, NSE of 0.86, RMSE of 5.31, and PBIAS of 2.11%, respectively. The PBIAS values were positive, indicating predicted errors were overestimated compared to the observations. According to the Xiang et al. (2020), Moriasi et al. (2007), prediction results with NSE > 0.5 can be acceptable. Thus, from the statistical results, the

LSTM-s2s model showed acceptable error prediction compared to the observed error, confirming

its applicability for improving model performance as a post-processor.

Table. 5.2: The statistical results for the overall predictive performance of LSTM-s2s for error prediction for lead time between 1 to 18 hours.

Lead time	CC	NSE	PBIAS (%)	RMSE	Lead time	CC	NSE	PBIAS (%)	RMSE
1	0.98	0.96	-11.83	2.05	10	0.89	0.72	-13.53	8.65
2	0.96	0.92	-30.75	3.03	11	0.99	0.98	-3.94	2.17
3	0.93	0.84	9.40	5.07	12	0.99	0.97	1.20	2.87
4	0.94	0.81	12.18	5.79	13	0.98	0.97	-4.63	3.24
5	0.85	0.53	30.71	9.59	14	0.98	0.95	-19.09	4.06
6	0.94	0.89	1.03	4.94	15	0.98	0.96	-4.94	4.06
7	0.87	0.68	16.82	8.51	16	0.95	0.84	32.91	7.92
8	0.94	0.87	-2.33	5.59	17	0.96	0.90	9.25	6.56
9	0.93	0.82	13.03	6.71	18	0.97	0.95	2.55	4.79

5.3.4 Improved Predictive Power by LSTM-s2s

Predicted errors for each lead time from the LSTM-s2s model, described in section 5.3.3, were used to improved accuracy of forecasted runoff. The LSTM-s2s model based post-processor significantly improved predictive power of NWM model at Guerneville station. Figure 5.7 shows the scatter plots comparing the performance of standalone NWM and NWM with LSTM-s2s models including R-squared values. The distributions of observed (grey marker) and corrected runoff (blue marker) were mainly between 0 to 50 cms. In addition, the R-squared values of NWM model were ranged from 0.75 to 0.95 and from 0.98 to 0.99 for improved runoff of NWM with LSTM-s2s model. Improvements in runoff predictions were shown in all lead times between 1 and 18 hours (Figure 5.7).

(a) 1hour   (b) 3hour   (c) 6hour

(d) 12hour   (e) 15hour   (f) 18hour
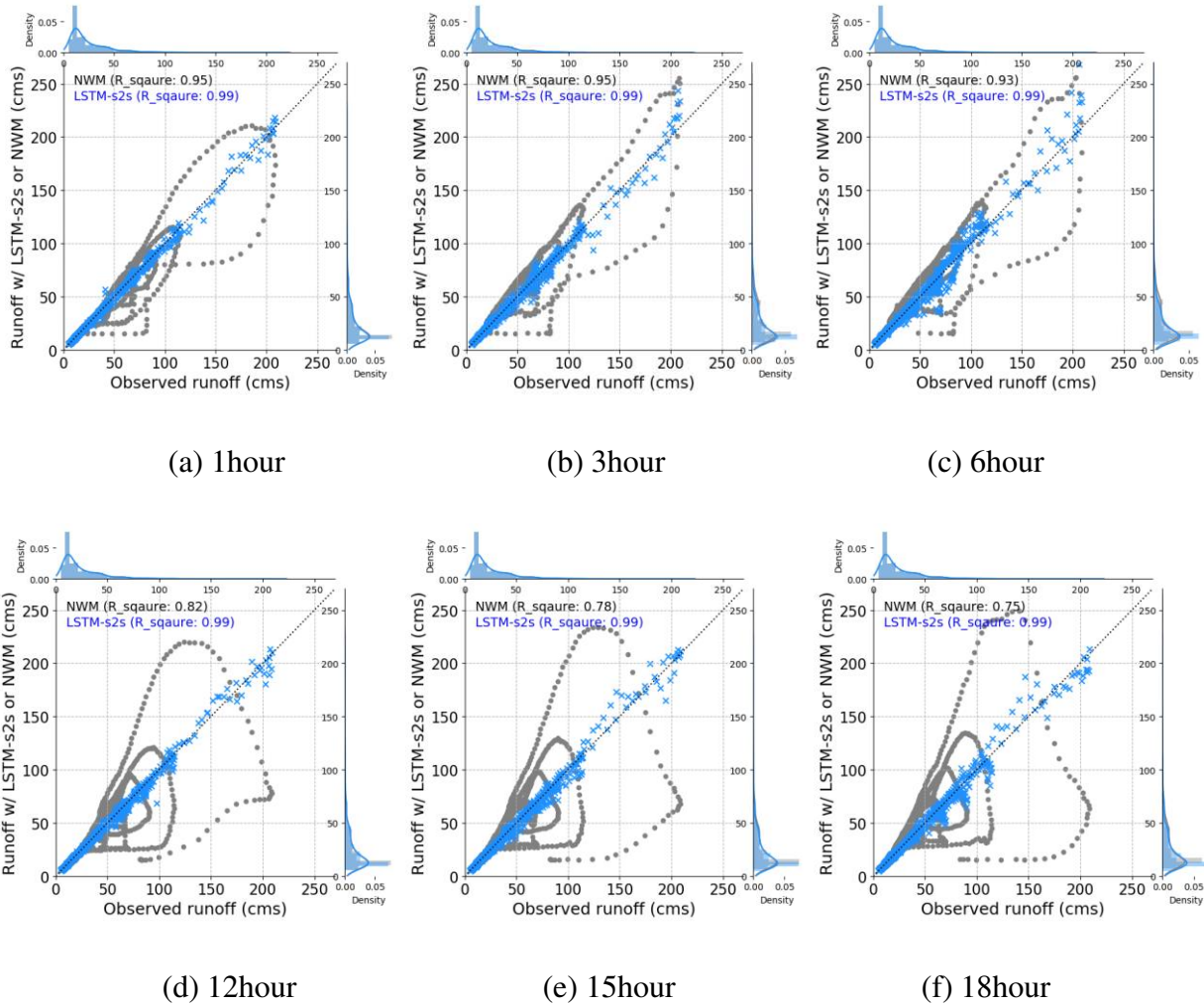
Figure 5.7: Scatter plots comparing the forecasted runoff from NWM and runoff corrected by LSTM-s2s based post-processor tool. (a)-(e) represent scatter plots for 1 to 18 hours.

Figure 5.8 also indicates scatter plots of three statistical metrics (i.e., CC, PBIAS, and RMSE) representing performance of NWM, NWM with LSTM-s2s models for runoff prediction of lead time for 1 to 18 hours. The LSTM-s2s based post-processor provided better runoff prediction performance compared to when NWM model was used alone. These results showed that the LSTM-s2s based post-processor improved predictive performance of the NWM according to the metrics, CC, PBIAS, and RMSE, respectively. As shown in Figure 5.8, the CC of post-processor was mainly ranged from 0 to 1, whereas the NWM has CC values between -0.5

to 0.5. The improved performance was obviously indicated in results of PBIAS and RMSE. The PBIAS and RMSE values of NWM ranged from -60% to 80% and 0 to 120 cms, whereas -15 to 10% and 0 to 20 cms for improved runoff from NWM with LSTM-s2s model. From the result of Figure 5.8, the LSTM-s2s based post-processor can contribute to improve the predictive performance of NWM in terms of not only temporal pattern of runoff, but also the volume of predicted runoff.

| (a) | (b) | (c) |
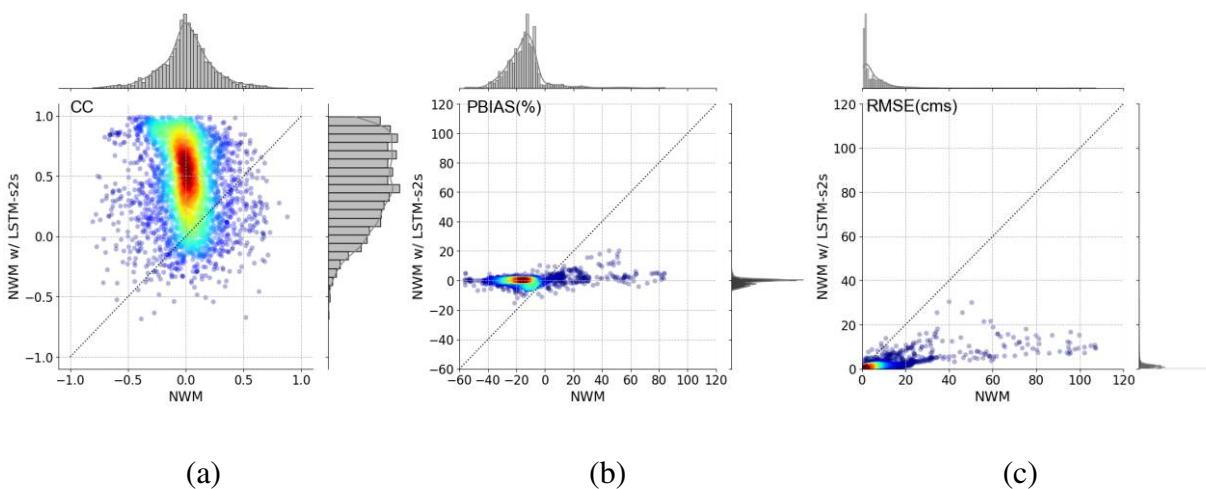
Figure 5.8: Density scatter plots showing performance of two models (NWM, NWM w/ LSTM) using three metrics (CC, PBIAS, and RMSE).

To highlight the effects of using the LSTM-s2s model to improve runoff forecasting, Figure 5.9 represents two observed runoff hydrographs and the forecasting results of the NWM with and without the addition of the LSTM-s2s model for lead times between 1 and 18 hours. From the comparison results with observation, the NWM improved by LSTM-s2s model provides much better predicted runoff than the result when the NWM was used alone for all lead times. The runoff from NWM model showed a large deviation compared to the observations, while the NWM with LSTM-s2s showed a result of significantly reducing the deviation. In

addition, the fluctuation and deviation of the improved runoff were significantly lower during the low-runoff periods than periods of high-runoff. As shown in both Figure 5.9 (a) and (b), the error in the predicted runoff compared to the observations was also larger in NWM than NWM with LSTM-s2s model. For example, in the case of Figure 5.9(a), the range of total errors (for 1-18 hours) in runoff predicted from NWM model was from -25% to 50%, whereas the range of errors in predicted runoff from NWM with LSTM-s2s model was from -3% to 3% for period from 2020-01-16 to 2020-01-20.
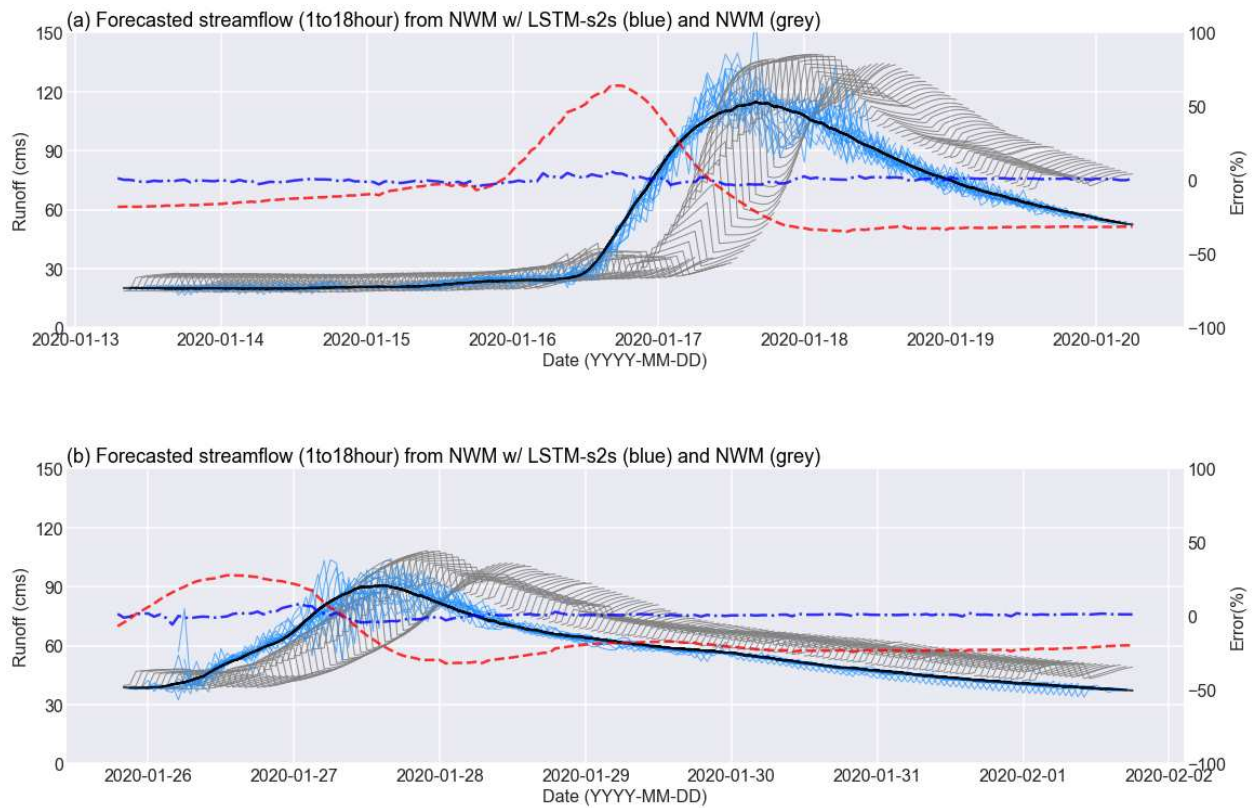
Figure 5.9: Time-series of improved runoff from NWM with LSTM-s2s model (blue line) and NWM alone (grey line) for lead time between 1 to 18 hours. Black line indicates observed runoff. Dark blue and red dot lines represent total errors in predicted runoff from NWM w/ LSTM-s2s and NWM models for 1-18 hours.

5.4 Discussion

This study demonstrates improvements in hydrologic runoff forecasting when a data-driven model is used to predict errors in hourly runoff data at various lead times. In particular, in the Russian River basin, CA, it was shown that a LSTM-s2s post-processor model has the potential to improve the predictive performance of the NWM with lead times between 1 and 18 hours at a Guerneville USGS station, located near the outlet of the basin. This study found that the errors are related to the errors that come from the upstream stations, and the data-driven model is able to use the error relationships between them to improve the modeling performance. In this study, a small basin was focused as a case study to show how the data-driven model works, but it is expected that the data-driven model can be applied in other basins (over 500 basins in United States) to improve the NWMs` forecasting performance. For instance, Frame et al. (2020) indicated that LSTM based post-processor (without the sequence-to-sequence structure) can be applied to improve the NWM simulation performance for daily runoff at 531 basins across the continental United States. They focused on predictions of daily runoff using NWM output data as input for a LSTM model. In addition, they directly predicted the runoff, which is different from the method of our study, which predicts the errors in forecasted runoff in advance. However, these two studies have a same purpose of improving NWM runoff prediction performance using an LSTM-based post-processor. Both studies show that an LSTM post-processor can be used to significantly improve the predictive ability of the NWM for daily and hourly runoff forecasting.

In this study, only observed precipitation and errors generated from upstream stations were considered as input variables, but further work needs to consider other variables such as water related infrastructure, reservoirs, and other regulations, can impact on errors in the runoff

89

prediction from NWM. For example, Frame et al. (2020) used other NWM variables, such as air temperature, radiation, vapor pressure, potential evapotranspiration, and snow fraction, as inputs of their data-driven model to improve the representation of streamflow patterns. They showed the data-driven model is able to improve prediction accuracy of NWM. Although they used output states of the NWM as input data for their LSTM model, further work can consider actual errors in input variables and their effects on forecasted runoff.

The proposed model used only precipitation and error datasets as input data. To apply the model to other areas with various meteorological characteristics, a new input selection process may be required to consider other hydrologic variables, such as snow accumulation, which is not observed for the Russian River basin. Thus, it is expected that several variables, including snow accumulation data, soil moisture data, and evapotranspiration data, can be considered to improve the predictive accuracy of the NWM model in other regions. Although soil and topography data such, as soil properties, land use, and slope, were not considered in this study, they can be used to make efficient prediction results in other regions. In addition, this study considered only short-term prediction period between 1 to 18 hours provided from NWM. The proposed model has the potential to be applied to medium- (to 10days) and long-term (to 30days) applications.

The error correction model proposed in this study can be applied to improve the performance of any hydrologic model, not limited to the NWM. Since the model works as a post-processor, it can predict new errors based on historic uncertainties that occur in the specific hydrologic models. In addition, as this study has shown, the various factors related to the uncertainties in the outcomes can be used together depending on the characteristics of the local observation systems. Although only hourly-based datasets such as precipitation and errors in

90

runoff were used in this study, the error correction tool can consider multiple time-steps, from

sub-hourly to monthly for forecasting error and improving models` performance.

Chapter 6

Application of Data-Driven Models for Runoff Prediction Using Distributed Data

This chapter presents an application of data-driven models using distributed datasets for runoff predictions. Three data-driven models, including the ANN, SVM, and LSTM, were used. Predicted results were compared with the forecasted runoff from NWM. In addition, the predicted results were evaluated in terms of seasonal and event-based performance using various statistical metrics.

6.1 Introduction

In hydrology, rainfall-runoff simulation plays critical role in various fields such as flood analyses and water resources planning. Thus, accurate rainfall-runoff modeling is significant to understand hydrological processes in various fields such as agriculture, hydrology, environmental studies (Xiang et al., 2020). Accurate runoff modeling can be used for predictive

flood warning systems during wet season and proper water resources management during dry season (Hu et al., 2018). In addition, the simulated runoff can be a reference for an assessment of available water resources regarding various scenarios of a future climate (Ayzel, 2019). There are the methods for simulating runoff.

Generally, two types of models for rainfall-runoff simulation are used: physically-based models and data-driven models (Wang, 2006). Physically-based hydrologic models use complex physical equations and parametric assumptions for physical interpretations of watershed system processes (Seo et al., 2018). However, understanding the rainfall-runoff process is often difficult because of temporal and spatial variability of datasets, topographic features, and meteorological complexities (Lin et al., 2013; Doycheva et al., 2017; Hu et al., 2018). Moreover, physically-based hydrologic model sometimes provide inadequate results due to uncertainty in the structure and parameters of the model (Fan et al., 2020; Choi et al., 2020). Thus, physically-based hydrologic model requires significant efforts for the calibration process. As the resolutions of the various forcing data have developed, the rainfall-runoff simulation using physically-based hydrologic models have become time and computationally intensive. Recently, in the hydrology filed, data-driven models are known as an effective alternative to reduce these limitations of physically-based model.

Data-driven models, which are based on the functional relationships between independent (e.g., input) and dependent (e.g., target) variables, have shown significant advancements in hydrological study by providing accurate quality and cost-effective solutions (Mosavi et al., 2018). In addition, data-driven models, using machine learning and deep learning algorithms, have been widely used in hydrology study and they have demonstrated very good prediction

performances with fewer parameters than physically-based hydrologic models (Solomatine and Ostfeld, 2008; Castelletti et al., 2010; Zia et al., 2015; Mosavi et al., 2018).

Several studies applied data-driven models for simulating various hydrological variables such as precipitation, runoff, soil properties, and water levels (Solomatine and Dulal, 2003; Jothiprakash and Magar, 2012; Lin et al., 2013; Ba et al., 2018; Chang and Tsai, 2016; Bui et al., 2020; Xiang et al., 2020). For example, Lin et al. (2013) developed a precipitation forecasting model with a 6-hour lead time using SVM and multi-objective genetic algorithms to improve the accuracy of hourly precipitation forecasting. This study used various meteorological factors, such as air pressure, air temperature, and wind speed, as input data of the data-driven model. They suggested that the proposed model can expand the range of predictive precipitation usage for a short-term hydrological analysis. In addition, the data-driven model could be used for analysis of soil property. Feng et al. (2019) estimated half-hourly and daily soil temperature using various meteorological factors data-driven models. The study showed that the data-driven models can be an effective alternative to the physically-based model for estimating soil temperature that is difficult to be observed because of many limitations.

In addition, many studies applied various types of data-driven approaches for runoff forecasting. In these studies, runoff forecasting can be performed on multiple time scales from hourly to monthly for predictive flood control and proper water resources management. For example, Hu et al. (2018) applied data-driven models with ANN and LSTM for runoff simulation and they concluded that both models are suitable for the runoff simulation and showed better performance than physically-based model. Young et al. (2017) developed a hybrid model that combines the outputs of physically-based model and data-driven model. The model was used to predict runoff with a 6-hour lead time and showed better performance than when the

94

physically-based model was solely used. Recently, Xiang et al. (2020) proposed LSTM based data-driven model for hourly runoff prediction with a 24-hour lead time. The study concluded that the proposed model outperforms various prediction models and has sufficient predictive power for improving forecast accuracy in short-term flood forecast application. Moreover, Fan et al. (2020) developed a runoff forecasting model using LSTM based data-driven model and compared the performance of LSTM SWAT for runoff simulations. The study used meteorological factors, such as precipitation, temperature, and relative humidity as input of the LSTM. They found that LSTM can provide higher accuracy to runoff simulation than SWAT model. These above studies demonstrated the capabilities to both predict runoff but also significantly outperform physically-based hydrologic models in some cases.

However, in previous studies, since ground-based observed datasets, including historic precipitation, runoff, soil moistures, air temperatures, were mainly used as the input variables for models for runoff forecasting, the modeling results were affected by the spatial resolution of the observations. In addition, just few studies have applied data-driven models in mountainous regions that contain limited observation system. Because of these limitations, it can be difficult to apply data-driven models requiring massive amount of datasets for runoff prediction and simulation in regions with low density of available observation systems. Recently, in the field of hydrology, data products with high spatial and temporal resolution that have been generated from remote sensing and data assimilation methods have been used to supplement ground-observations. To address these limitations, this study aims to use distributed forcing datasets provided from the assimilation system product of the North American Land Data Assimilation system (NLDAS) and to apply data-driven models to predict hourly runoff in the Russian River basin. Specifically, the main objectives of this study are as follow: (1) develop data-driven

models using ANN, SVM and LSTM for hourly runoff forecasting with distributed forcing datasets; (2) evaluate the performance of the data-driven models based on multiple time scales (hourly, seasonal, and event based); and (3) compare the results of data-driven models to predictions from the NWM, a fully distributed physically-based hydrologic model.

6.2 Materials and Methods

6.2.1 Study Area and Data

This study applied data-driven models to predict the runoff at USGS gage 11467000 as the modeling outlet point in the Russian River basin, California, USA (Figure 6.1). The size of the Russian River basin is approximately 3,850 km^2 with elevations ranging from 24 m to 800 m. The basin consists of eight sub-watersheds based on Hydrologic Unit Code 10 (HUC-10), and two reservoirs have been located in the basin, which are used for flood control and storage for downstream irrigation. Due to the unique geography and proximity to the coast, the Russian River Basin has challenges related to flood mitigation, water resources management, water quality and soil erosions (Johnson et al., 2016). The mean annual precipitation in this basin is approximately 1,180 mm, and more than 80% of the annual precipitation occurs between November and March (Johnson et al., 2016). The Russian River Basin is affected by various meteorological factors such as extratropical cyclones, jet streams, and atmospheric rivers from the Pacific oceans (Han et al., 2019).
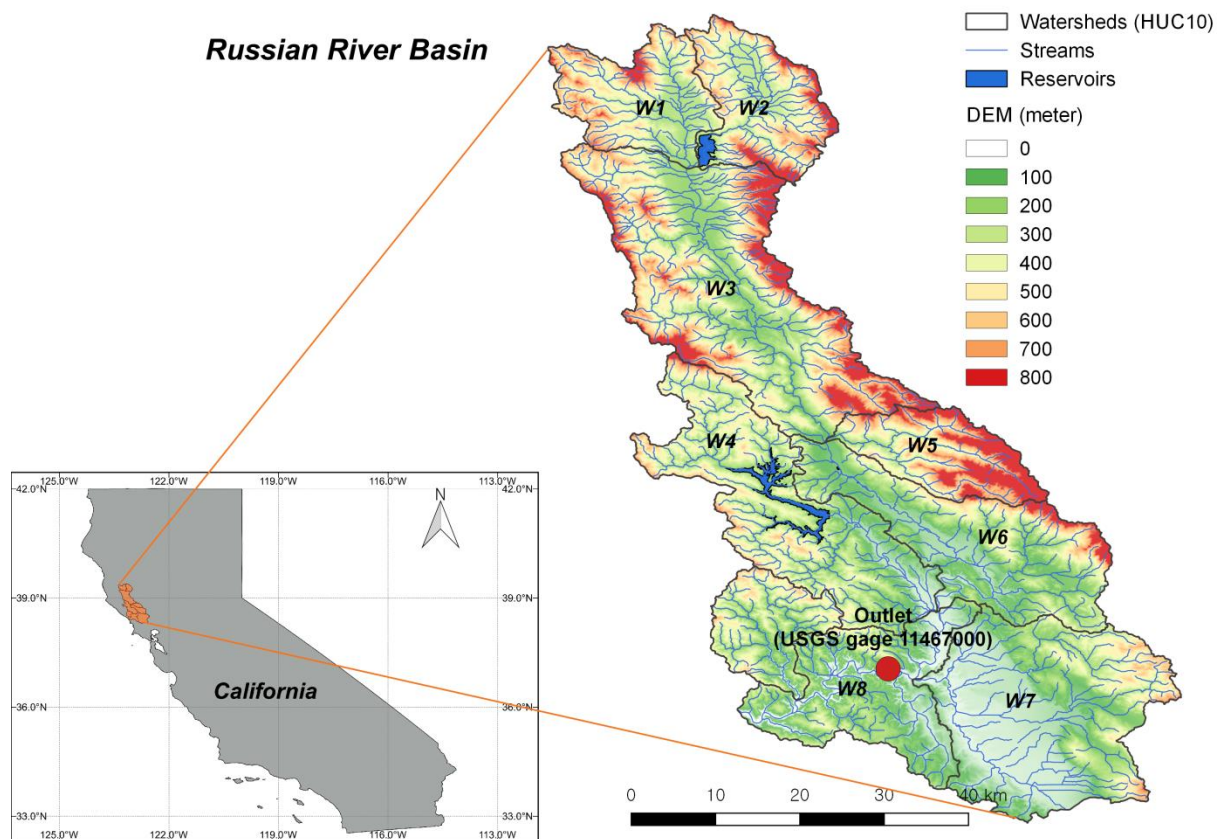
Figure 6.1: Study area, outlet point, and eight sub-watersheds in the Russian River basin, CA.

The NLDAS-2 system provides the broad features of the energy flux, water flux, and state variables (Xia et al., 2012; Hao et al., 2016). The atmospheric data from NLDAS-2 are as follows: precipitation, air temperature, specific humidity, surface air pressure, wind speed and solar radiation (Xia et al., 2012). The spatial and temporal resolutions of data are 1/8th-degree grid and hourly (and monthly). The data is available from 1979 to present. These forcing data are derived from North American Regional Reanalysis (NARR) data and combined with multiple sources of observations such as gauge data, satellite data and radar measurements to produce estimates of climatological properties near the surface. In addition, they are used as forcing data for land surface models (LSMs) such as the Noah, the Mosaic, the Sacramento Soil Moisture

Accounting model and the Variable Infiltration Capacity model. In this study, hydrological variables simulated from the Noah LSM are used as input data for data-driven models. Figure 6.2 shows the four forcing data derived from the NLDAS-2.

(a) Precipitation

(b) Land surface temperature

(c) Specific humidity

(d) Potential evaporation
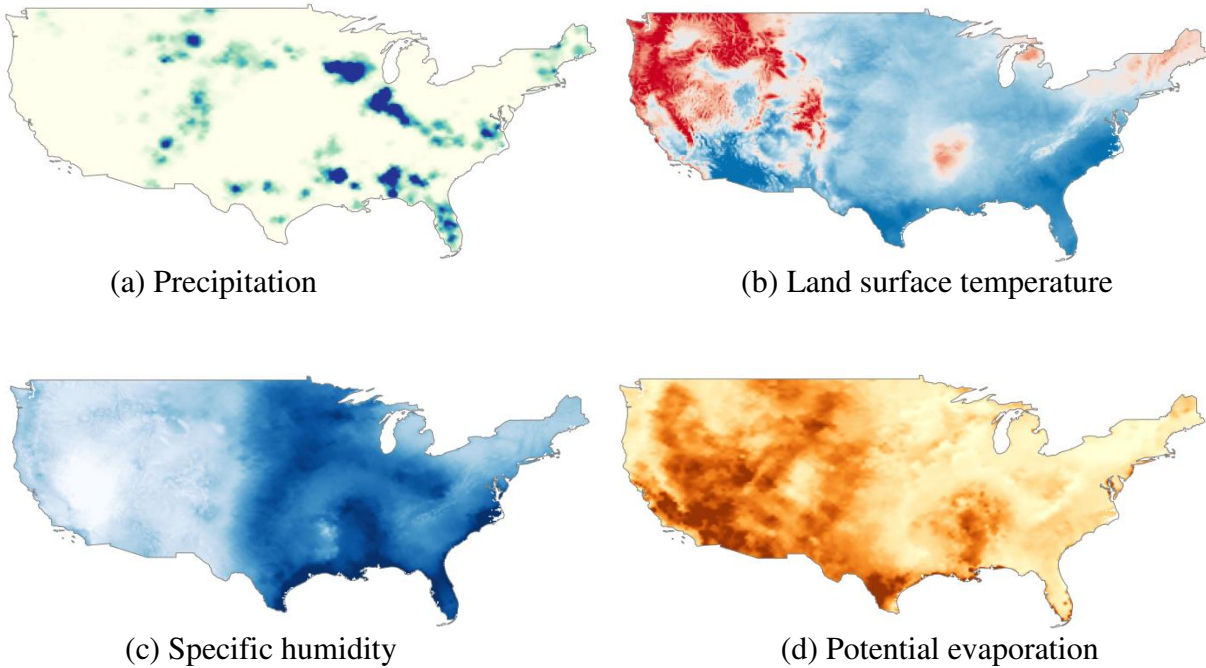
Figure 6.2: NLDAS-2 forcing datasets over United States.

In this study, meteorological and hydrological datasets for each of the eight sub-watersheds were collected from the NLDAS for a 10-year period between 2010 and 2019. As shown in the Table 6.1, the forcing data collected from the NLDAS included precipitation, land surface temperature, soil moisture, and baseflow. The temporal resolution of the data is hourly and the spatial resolution is 0.125-degree. To analyze the contribution of each sub-watershed on the runoff at the outlet, gridded-NLDAS data overlapping each sub-watershed was averaged and determined as a representative value of each sub-watershed. Generally, 70-80% of the available

datasets is allocated for training and remaining 20-30% data is partitioned for testing (Gholami et al., 2015). In this study, the training period used in each data-driven model was from January 2010 to December 2016, and the model testing period was from January 2017 to December 2019.

Table. 6.1: Input datasets provided from NLDAS.

Variable	Unit	Spatial resolution	Temporal resolution
Precipitation	kg/m^2	0.125°	Hourly
Land surface temperature	K	0.125°	Hourly
Soil moisture content	kg/m^2	0.125°	Hourly
Subsurface runoff (Base flow)	kg/m^2	0.125°	Hourly

6.2.2 Evaluation Metrics

In this study, six statistical metrics were used for evaluation of data-driven models for hourly runoff prediction. The CC, NSE, PBIAS, RMSE, PE, and PTE, which are described in Chapter 4.2.3 and 5.2.3, and BIAS were used in this study.

$$\text{BIAS} = \frac{\sum y_e}{\sum y_o} \tag{6.1}$$

6.2.3 Model Development

In this study, three data-driven models, ANN, SVM and LSTM, were applied for runoff prediction with lead time of 1 to 6 hours. The spatially distributed forcing products provided from NLDAS-2 assimilation system, including precipitation, land surface temperature, soil moisture and base flow, were used as input data of the models. The values of each input data associated with a 12-hour lag were used in the model design, such that:

$$Q_{t+leadT} = f[P_1(t), \cdots, P_1(t-12); P_2(t), \cdots, P_2(t-12); \cdots P_8(t), \cdots, P_8(t-12);$$

$$T_1(t), \cdots, T_1(t-12); T_2(t), \cdots, T_2(t-12); \cdots T_8(t), \cdots, T_8(t-12);$$

$$S_1(t), \cdots, S_1(t-12); S_2(t), \cdots, S_2(t-12); \cdots S_8(t), \cdots, S_8(t-12);$$

$$B_1(t), \cdots, B_1(t-12); B_2(t), \cdots, B_2(t-12); \cdots B_8(t), \cdots, B_8(t-12)] \qquad (6.2)$$

where, *P, T, S* and *B* are precipitation, land surface temperature, soil moisture and base flow, and *leadT* refers to the predicted time-steps between 1 to 6 hours.

Figure 6.3 shows how to design the models using NLDAS based distributed forcing datasets for eight sub-watersheds. Four variables of each sub-watershed were used as input data to the models to analyze the contributions of sub-watershed properties to runoff downstream outlet point. As shown in Figure 6.3, the input variables at previous times from t-1 to t-12 collected from each sub-watershed and the runoff with lead time from t to t+6 observed at the outlet of the basin are used as the input data and target values of the data-driven models. In this study, the time-steps for the historical input variables was tested between 3 hours and 24 hours, and the results showed that lag time of 6 hours and 12 hours produced the best performance. Since the average time of concentration between each sub-watersheds and outlet point is about from 12 - 18 hours, a lag of 12 hours was selected as the time-step in the models. The train period is from January 2010 to December 2016 and the test period is from January 2017 to December 2019.
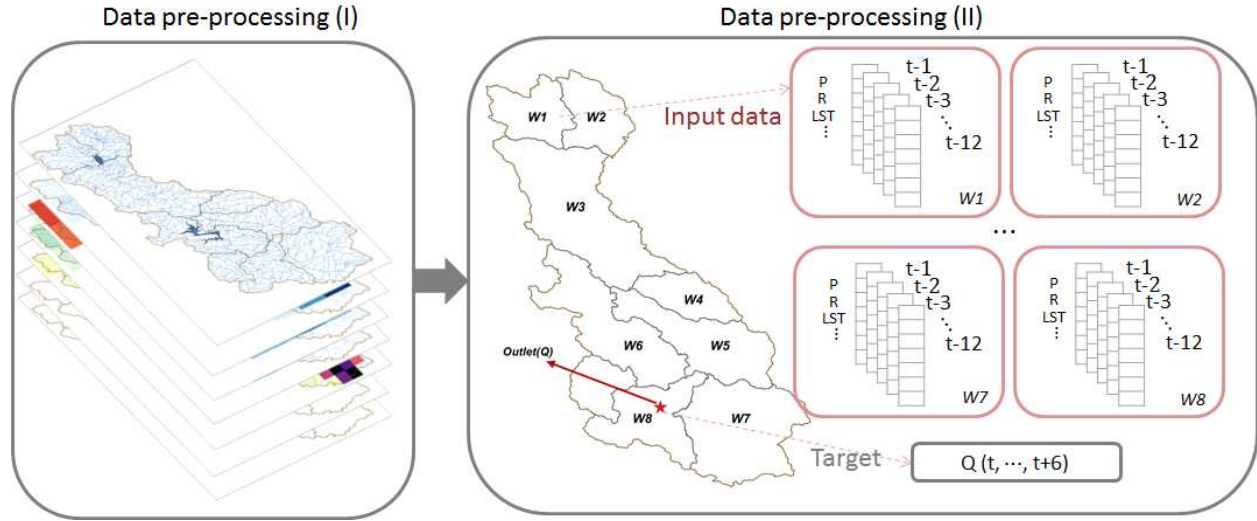
Figure 6.3: Diagram of model design using NLDAS-based distributed forcing data for eight sub-watersheds.

In order to operate the data-driven models, collected input datasets require two pre-processing steps. The first step is to supplement the missing observed data to enhance the continuity of the data. For instance, in the case of the LSTM, since the temporal continuity of the data is important, the process of supplementing the missing value is necessary. Thus, this study corrected the missing values as the average value of the runoff one hour before and after.

The second pre-processing step is the normalization of the datasets. Because the units and ranges of datasets are different, the predictive performance will be low due to the divergence of function values when training models. Thus, input data need to be converted to values between 0 and 1 through the normalization process such as Eq (6.3).

$$Y_i = \frac{X_i - X_{min}}{X_{max} - X_{min}} \tag{6.3}$$

where, Y_i denotes normalized value of variables, X_i represents original value in time i. X_{max} and X_{min} denote the maximum and minimum value in the datasets.

6.3 Results

6.3.1 Performance of Data-Driven Models for Runoff Prediction

In this section, the predicted hourly runoff from three data-driven models was compared with observed runoff over the test period from January 2017 to December 2019 to evaluate the predictive ability of the models. Figure 6.4 shows the comparison results of predicted runoff with observations for 1 hour of lead time. The left panels represent the time-series of hourly runoff predicted from three data-driven models and observations and right panels indicate the scatter plots for two runoff datasets. As shown in Figure 6.4, the performance of each model was excellent for entire time period. In particular, it seems that the performance of runoff forecasting was good when the volume of observation was large (for example, 01/2017 – 04/2017 and 12/2018 – 04/2019). The R^2 values of each model were 0.63 for ANN and 0.92 for both SVR and LSTM models.

From the scatter plots (right panels in Figure 6.4), all three models somewhat underestimated runoff compared with observations. Particularly, the ANN model showed overestimated runoff predictions for flows over 1,250 cms. The maximum difference in peak runoff from ANN and observation was about 2,000 cms (approximately 80% of peak value), which means that ANN has relatively low ability to simulate the peak value. In contrast, both the SVR and LSTM models particularly underestimated runoff for flows over 1,250 cms. However, the differences in peak runoff values between predicted and observed runoff are less than 400 cms (approximately 20% of peak runoff), and the models show good performance in predicting

the trend of observations. ANN has a somewhat lower performance than the other two models for simulating trend and peak values.
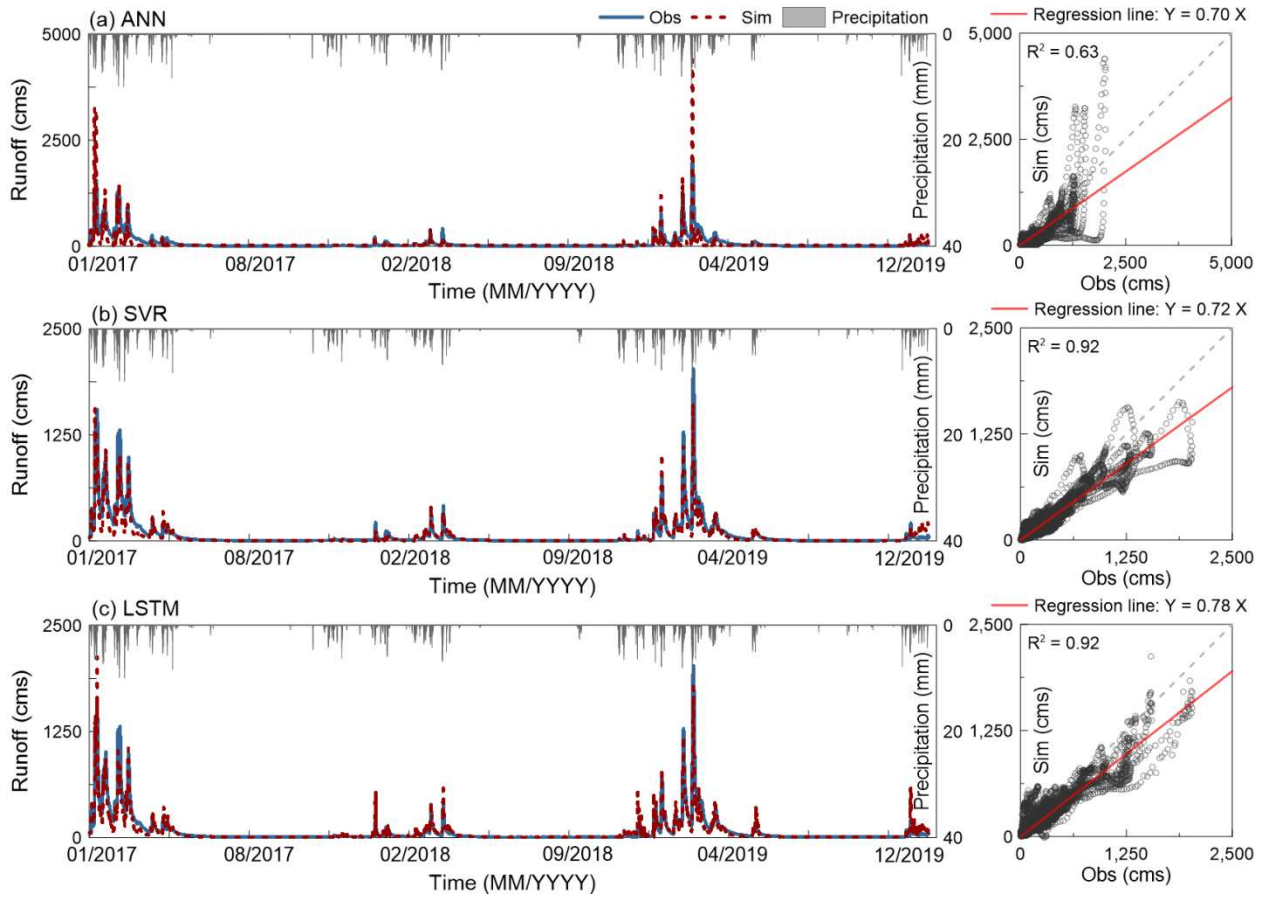
Figure 6.4: Comparison results of observed and predicted runoff from three data-driven models for 1 hour of lead time. Left panels show time-series and right panels represent scatter plots of two runoff datasets.

Figure 6.5 represents errors in prediction results of three models, with the left panels indicating the time-series of errors between predicted and observed runoff, and right panels showing distributions of the error values. As shown in Figure 6.5, the predicted runoff from the SVR and LSTM models were smaller and it showed similar patterns compared to the ANN model. Particularly, the range of error in runoff for SVR and LSTM models was -1,250 cms to

1,250 cms, whereas the error in ANN model ranged from -2,500 cms to 1,500 cms. Moreover, the errors in the SVR and LSTM models were nearly always positive, further highlighting the model`s tendency to underestimate runoff.
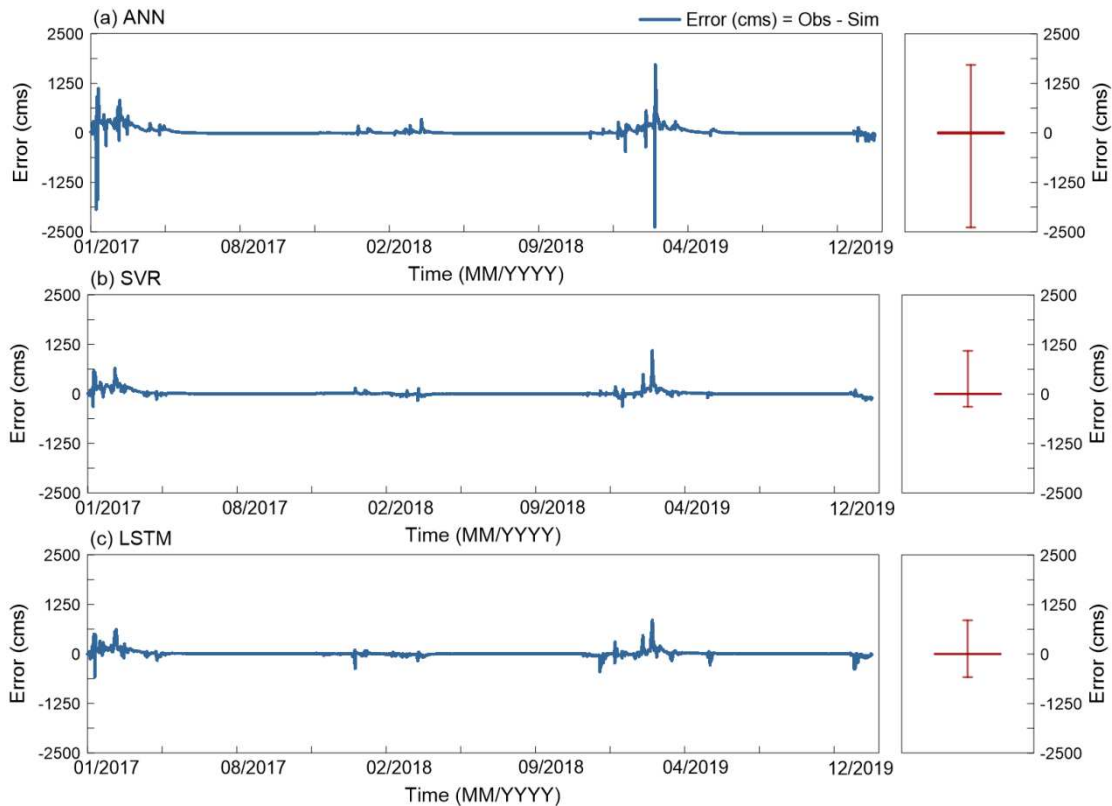
Figure 6.5: Errors in predicted runoff from three models.

Table 6.2 lists the evaluation metrics for each data-driven model with lead times from 1 to 6 hours. The five indices, including CC, NSE, PBIAS, BIAS, and RMSE, were estimated to evaluate the performance of each model to simulate the variability and volumes of runoff from various input variables. As shown in Table 6.2, the predictive power of all three models tended to decrease as the lead time increased. This trend was most evident in the ANN results, in which

the RMSE increased by nearly 20 cms between 1- and 6-hour lead times, and the PBIAS increased by nearly 10% between same lead times.

The ranges of CC and NSE, showing the performance of models in terms of trends of predicted runoff and overall predictive power, were between 0.78 to 0.95 for CC and 0.56 to 0.88 for NSE. According to the Moriasi et al. (2007), the results with NSE > 0.5 can be acceptable. This means that the predicted results from three data-driven models are acceptable compared to the observations. In addition, the values of PBIAS, BIAS and RMSE, which indicate the errors in predicted runoff volume, were much larger for the ANN model compared to the other models. The SVR and LSTM showed that the PBIAS errors of 19% and 17%, whereas the PBAIS of the ANN model was from 30% to 40% at all lead times. The RMSE also was higher for the ANN model, representing a low prediction performance in terms of volume of runoff. Among the three models, the LSTM generated the best ability for all lead times.

Table. 6.2: Evaluation metrics for each data-driven model with lead times from 1 to 6 hours.

Lead time	CC	NSE	PBIAS(%)	BIAS	RMSE(cms)
ANN					
1	0.835	0.681	29.107	1.080	105.615
2	0.827	0.678	33.924	1.246	106.065
3	0.824	0.665	31.979	0.991	108.109
4	0.824	0.669	32.690	1.099	107.438
5	0.821	0.657	32.586	0.998	109.363
6	0.771	0.559	39.882	1.481	124.052
SVR					
1	0.953	0.858	19.365	1.285	70.500
2	0.952	0.857	19.387	1.285	70.659
3	0.951	0.855	19.484	1.286	71.152
4	0.949	0.852	19.552	1.288	71.771
5	0.948	0.850	19.670	1.292	72.413
6	0.947	0.846	19.793	1.295	73.244
LSTM					
1	0.950	0.878	17.180	1.134	65.163
2	0.950	0.880	17.155	1.133	64.838
3	0.951	0.880	17.165	1.133	64.677
4	0.951	0.880	17.198	1.132	64.686
5	0.951	0.879	17.274	1.132	64.937
6	0.950	0.877	17.389	1.133	65.462

6.3.2 Seasonal Based Runoff Prediction Performance of Data-Driven Models

It is necessary to analyze the reliability of the data-driven models at seasonal time-scales because water management strategies, such as developing flood warning system, drought analysis, are often tied to these time periods. In this study, based on the climate characteristics and typical water management activities of the Russian River basin, four seasonal periods were considered and were defined as season I (Mar-May), season II (Jun-Aug), season III (Sep-Nov) and season IV (Dec-Feb). For the Russian River basin, runoff during wet seasons (i.e., season I,

IV) is used for flood forecasting and analysis, and runoff during the dry seasons (i.e., season II, III) is important for drought analysis and irrigation deliveries.

Figure 6.6 shows the whiskers-box plots and cumulative density functions of the observed and predicted runoff for season IV, which has the largest amount of runoff among the four seasons. The results of seasonal based evaluation showed that the ANN model predicted larger median values of runoff compared to observations, and the predicted median runoff from the SVR model was smaller than observed runoff. The predicted quartile runoff values from the LSTM model were most similar to the observed value.

As shown in Figure 6.6 (b), the cumulative distribution of predicted runoff values from LSTM results the best approximates the distribution of observations. Both the SVR and LSTM models predict that 90% of season IV runoff was 550 cms or less, compared to 600 cms or less for the observed runoff. The ANN model, however, predicts a 90% cumulative runoff value of 300 cms or less.
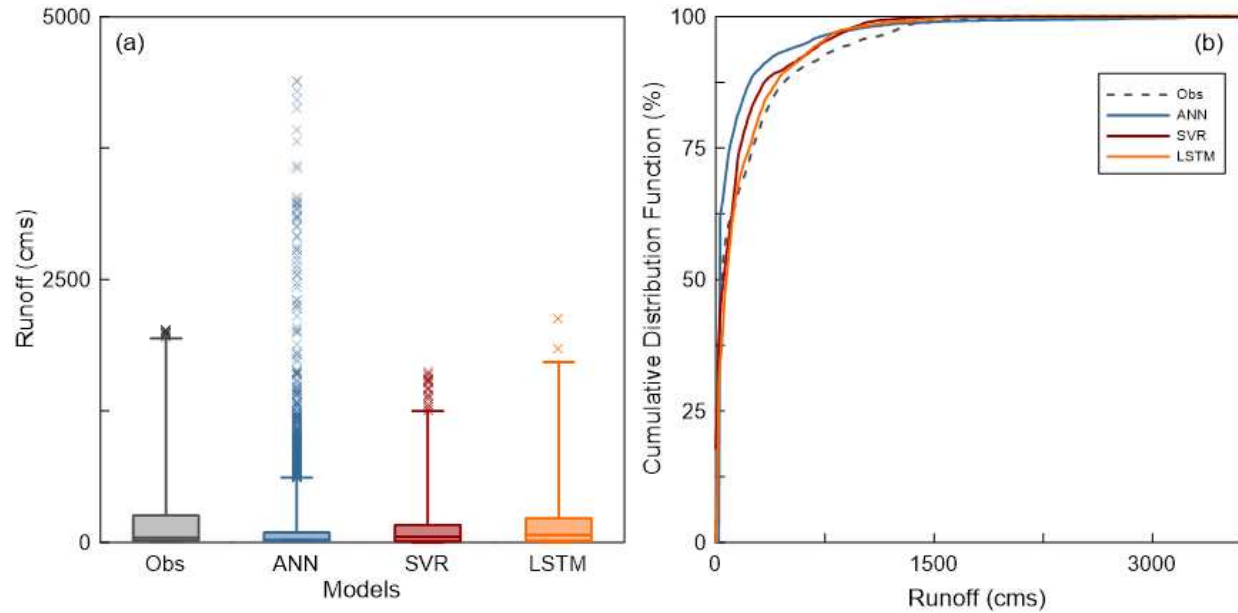
Figure 6.6: Whiskers-box plots and cumulative density functions of the observed and predicted runoff for season IV.

Table 6.3 represents the error estimations for seasonal predictive ability of each model with a 1 hour of predictive lead time. The performance of runoff prediction was obviously different amount the four seasons. All models showed the relatively better performance during the wet seasons (i.e., I, IV) and poor ability during the dry seasons (i.e., II, III). For the wet season, the average values of CC and NSE for the three models were 0.87 and 0.65, respectively, while the average values for the dry season were 0.53 and -4.1. There was a significant difference in the NSE values between dry and wet seasons, indicating predicted runoff from the data-driven model is much more useful for flood forecasting during wet season, whereas it is less useful for drought analysis and water resources management during the dry season. In addition, in the case of ANN, NSE was estimated as a negative value during the dry season, and the CC value was very low. In season IV, which has the highest runoff utilization for flood analysis, both SVR and LSTM showed high performance, with CC and NSE values of 0.95 and 0.83, and PBIAS and BIAS values are less than 20% and 1.3.

108

Table. 6.3: Error estimations for seasonal predictive ability of each model with a 1 hour of predictive lead time.

Models	Season I (Mar-May)					Season II (Jun-Aug)				
	CC	NSE	PBIAS(%)	BIAS	RMSE(cms)	CC	NSE	PBIAS(%)	BIAS	RMSE(cms)
ANN	0.73	0.15	49.47	2.78	103.48	0.00	-11.4	55.38	0.29	14.86
SVR	0.91	0.78	17.80	1.22	53.02	0.91	0.79	13.44	1.14	1.92
LSTM	0.87	0.74	18.46	1.14	57.35	0.91	0.72	15.06	1.21	2.24
Models	Season III (Sep-Nov)					Season IV (Dec-Feb)				
	CC	NSE	PBIAS(%)	BIAS	RMSE(cms)	CC	NSE	PBIAS(%)	BIAS	RMSE(cms)
ANN	0.16	-14.6	56.96	0.28	15.23	0.78	0.51	33.57	1.53	226.06
SVR	0.39	-0.21	23.43	1.31	4.25	0.95	0.83	19.86	1.32	131.41
LSTM	0.79	0.21	14.98	1.11	3.42	0.95	0.87	16.71	1.13	117.76

6.3.3 Event Based Runoff Prediction Performance of Data-Driven Models

The accurate prediction of single runoff event is essential for proper flood analysis and reservoir operations. In this study, the predictive ability of large runoff events for each model was evaluated by comparing the number of high runoff events and the discharge of each event to observations. The single runoff event including a peak runoff above the mean value of the total runoff was separated from the entire time-series of the runoff. The process for identifying high flow events included the following four steps:

1) The runoff time series was smoothed using a moving average algorithm to eliminate small discharge fluctuations.

2) The start of a high flow event was determined based on six hours of continuous increasing discharge values (indicated by a positive slope in the discharge time series),

and the point at which the slope was converted from negative to positive was determined as the end point of a high flow event.

3) After these two points were determined, the peak value was found at the point with the maximum runoff value.

4) A single high flow event was recorded.

For event based evaluation, the runoff volume, peak value and peak time from all models were compared to the observed values. Each model predicted a total of 44 runoff events, which matched the number of events from the observed data (Table 6.4).

Table. 6.4 List of 44 single runoff events predicted from three data-driven models.

Events	Begin (m/d/yyyy hh:mm)	End (m/d/yyyy hh:mm)	Duration (hr)	Peak (cms)			
				Obs	ANN	SVR	LSTM
1	1/3/2017 9:00	1/7/2017 5:00	93	385.1	373.7	391.3	462.5
2	1/7/2017 6:00	1/10/2017 12:00	79	1362.0	3254.1	1561.4	1422.0
3	1/10/2017 13:00	1/15/2017 20:00	128	1551.8	3226.3	1254.3	2125.8
4	1/18/2017 10:00	1/20/2017 3:00	42	739.1	504.3	571.3	679.1
5	1/20/2017 4:00	1/22/2017 0:00	45	841.0	759.3	743.9	810.3
6	1/22/2017 1:00	1/27/2017 5:00	125	1008.1	1339.3	1090.4	921.7
7	2/2/2017 5:00	2/5/2017 19:00	87	427.6	319.6	399.3	349.4
8	2/5/2017 20:00	2/9/2017 11:00	88	1271.4	1200.4	928.4	1022.0
9	2/9/2017 12:00	2/14/2017 14:00	123	1308.2	1485.5	1012.4	832.0
10	2/17/2017 11:00	2/19/2017 16:00	54	526.7	299.8	397.7	566.9
11	2/19/2017 17:00	2/25/2017 22:00	150	988.3	988.2	894.3	1051.6
12	3/20/2017 16:00	3/24/2017 4:00	85	106.5	20.2	142.3	139.7
13	3/24/2017 5:00	3/29/2017 12:00	128	260.2	180.5	314.3	314.6
14	4/6/2017 14:00	4/8/2017 15:00	50	220.6	262.5	346.4	338.7
15	4/12/2017 17:00	4/17/2017 23:00	127	193.7	105.7	243.7	263.5
16	1/8/2018 4:00	1/13/2018 19:00	136	218.3	233.4	136.5	531.9
17	1/21/2018 19:00	1/24/2018 15:00	69	120.1	78.6	76.3	146.1
18	1/24/2018 16:00	1/30/2018 1:00	130	105.3	43.5	90.8	136.2
19	3/12/2018 20:00	3/14/2018 17:00	46	65.7	53.0	113.2	121.0
20	3/15/2018 10:00	3/20/2018 18:00	129	120.6	98.0	146.7	183.5
21	3/20/2018 19:00	3/27/2018 2:00	152	393.6	377.3	410.9	422.6
22	4/5/2018 23:00	4/12/2018 4:00	150	416.3	146.4	335.8	582.1
23	12/15/2018 8:00	12/20/2018 6:00	138	119.5	105.7	92.4	538.8
24	1/5/2019 11:00	1/8/2019 22:00	84	328.5	432.5	272.7	531.7
25	1/8/2019 23:00	1/14/2019 6:00	128	356.8	382.0	384.5	415.6
26	1/15/2019 15:00	1/20/2019 12:00	118	756.1	1194.5	994.6	804.0
27	1/20/2019 13:00	1/26/2019 3:00	135	275.2	169.0	317.4	302.5
28	2/1/2019 16:00	2/3/2019 21:00	54	170.5	163.5	226.4	250.9
29	2/3/2019 22:00	2/9/2019 1:00	124	320.0	258.8	354.1	438.8
30	2/9/2019 12:00	2/12/2019 22:00	83	196.2	87.9	178.7	234.7
31	2/12/2019 23:00	2/19/2019 4:00	150	1282.8	1622.9	1111.6	1163.8
32	2/25/2019 13:00	3/3/2019 21:00	153	2024.7	4393.2	1623.9	1838.4
33	3/5/2019 22:00	3/9/2019 10:00	85	512.5	371.6	466.6	580.0
34	3/9/2019 11:00	3/14/2019 21:00	131	436.1	305.6	318.9	344.1
35	3/22/2019 13:00	3/25/2019 9:00	69	172.7	62.7	179.7	182.1
36	3/25/2019 10:00	3/27/2019 5:00	44	217.5	75.8	240.4	302.2
37	3/27/2019 6:00	3/28/2019 17:00	36	317.2	164.9	317.1	457.7
38	4/5/2019 7:00	4/10/2019 10:00	124	125.2	66.5	156.2	135.1
39	5/15/2019 7:00	5/17/2019 5:00	47	73.3	111.6	145.7	106.2
40	5/18/2019 15:00	5/22/2019 8:00	90	116.1	20.2	131.4	397.2
41	5/22/2019 9:00	5/27/2019 5:00	117	85.2	20.2	94.2	209.1
42	11/30/2019 11:00	12/6/2019 13:00	147	88.4	122.0	48.6	109.2
43	12/6/2019 14:00	12/11/2019 20:00	127	208.7	299.5	152.4	592.5
44	12/29/2019 13:00	12/31/2019 14:00	50	69.7	267.8	212.7	106.0

Figure 6.7 represents the predicted and observed single hydrographs of six flood events with peak runoff ranging from 400 cms to 4,000 cms, and the simulated peak runoff generally showed high performance compared to the observations. For hydrographs event (a), (e), and (f), the ANN model poorly predicted peak runoff compared to other models and tended to overestimated peak value compared to the observed value. In these three cases, the PE of ANN results varied from -21% to -54%, whereas the SVR and LSTM results were from -6% to 24%, indicating better predictive ability than the ANN model. However, as shown in events (a) and (f), the SVR and LSTM models slightly underestimated runoff compared to observed runoff.

The prediction results for events (b), (c), and (d) showed acceptable quality performance in all three models. The PE and PTE values of these three events were both less than 15% and 8 hours, and the R^2 values were ranged from 0.72 and 0.97, showing comparable performance with observed runoff events. For six events, the averaged value of R^2 was 0.72 for the ANN model, 0.86 for the SVR model, and 0.91 for the LSTM model. The averaged value of PE was -19% for the ANN model, 2.5% for the SVR model, and -2.1% for the LSTM model. In addition, the PTE was 5.8 hours for the ANN model, 7 hours for the SVR model, and 4.5 hours for the LSTM model. These results indicated that the LSTM model outperformed the ANN and SVR models for forecasting runoff event.
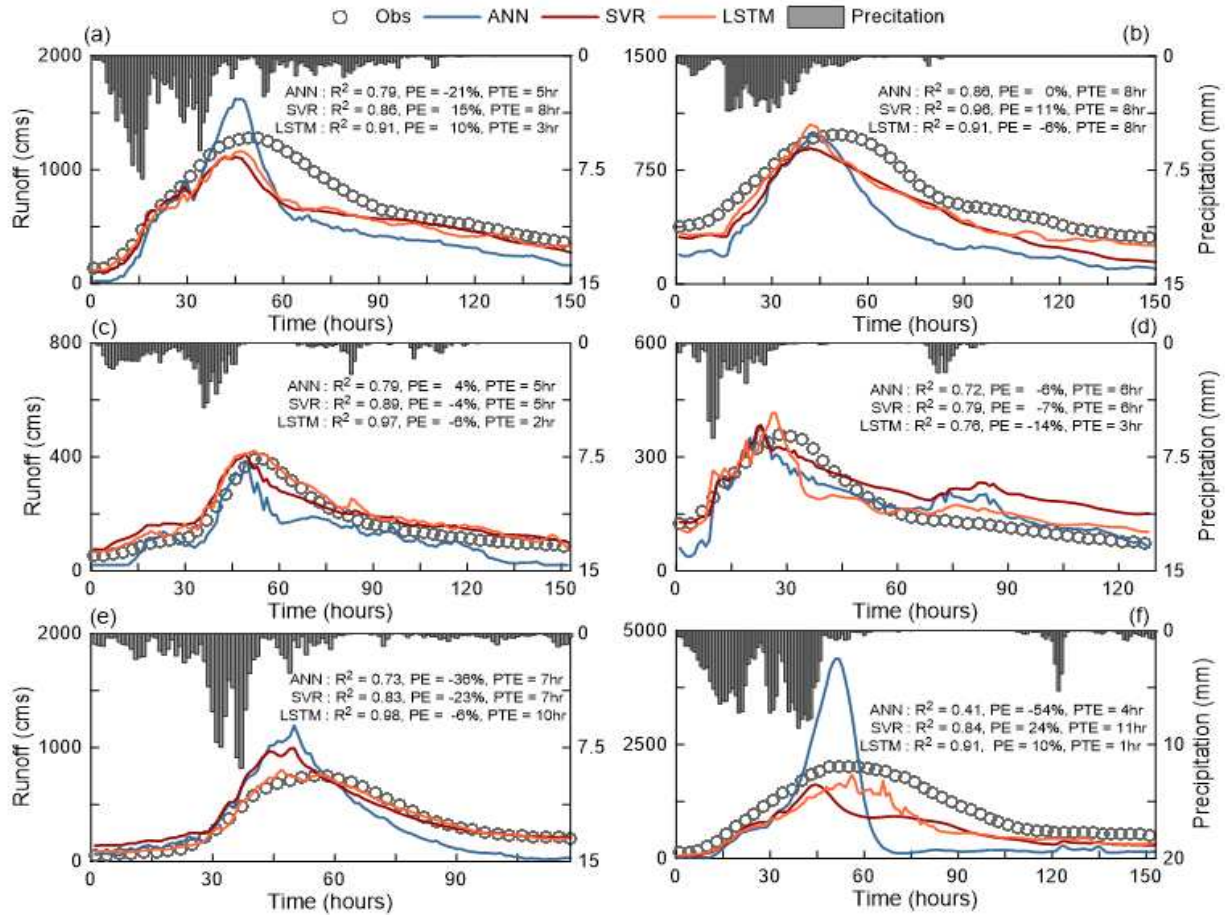
Figure 6.7: Event based evaluation results. (a) – (f) illustrate predicted and observed single hydrographs of six flood events.

Figure 6.8 illustrates the whiskers-box plots of seven error indices for all 44 events predicted from the three data-driven models. As shown in Figure 6.8, the distribution ranges of the seven indices were similar for the SVR and LSTM models, and the ANN model showed poor results according to most indices when compared to the other models. The SVR and LSTM models showed better predictive performance for predicting runoff events when compared to the ANN model in terms of event tendency, volume, peak value, and peak time. There were stark difference in ranges of CC, BIAS, and NSE between ANN and other models. The ranges of CC were between 0.5 and 0.8 for ANN, whereas the SVR and LSTM have the CC values ranged

from 0.75 to 0.9. The ranges of BIAS were between 0.15 and 0.3, whereas the SVR and LSTM

showed the BIAS ranging from 0.7 to 0.12. Moreover, the ANN has the NSE values ranged from

-6.0 to 0.0, but the SVR and LSTM models showed better performance, with the NSE ranging

from -2.0 to 1.0.
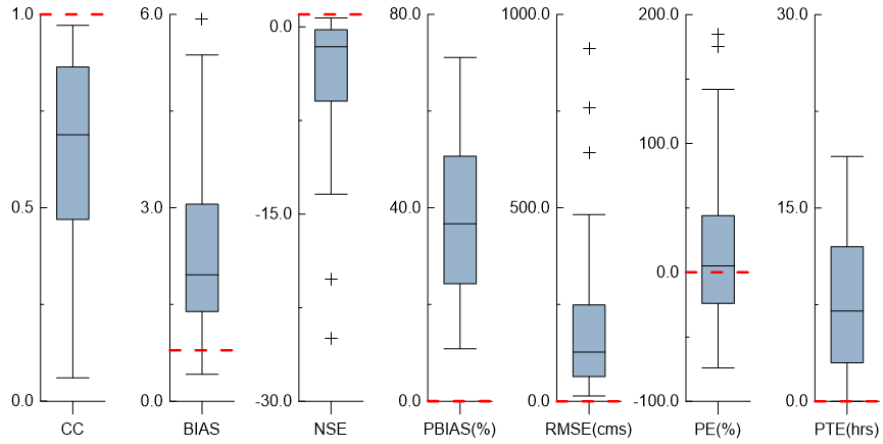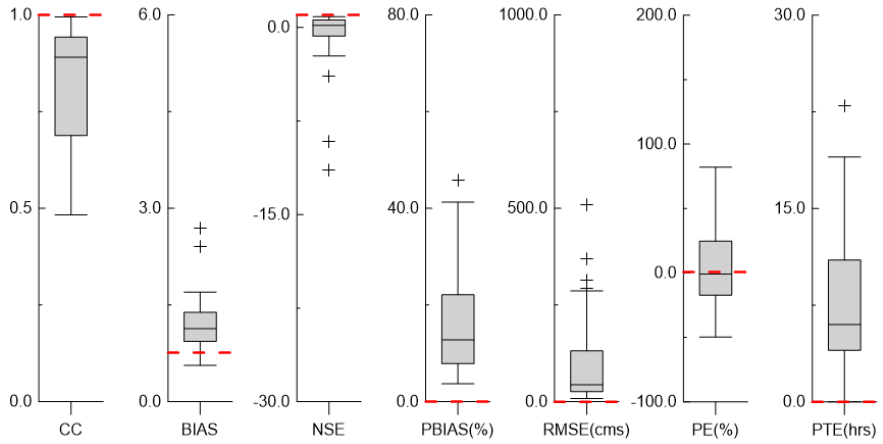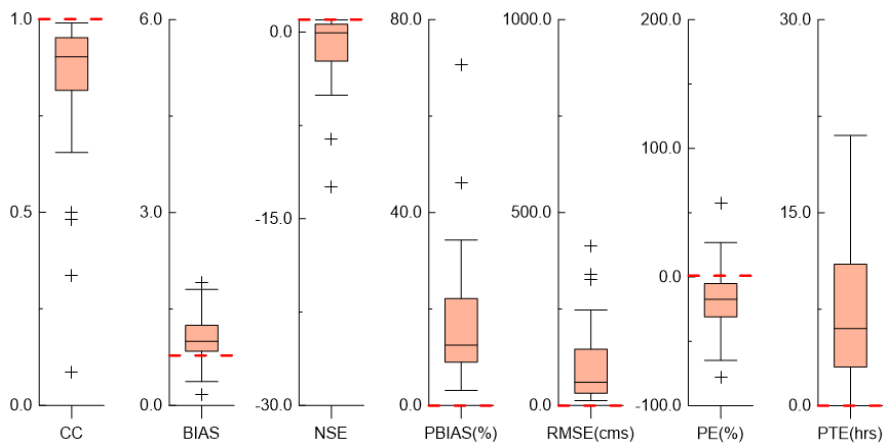
Figure 6.8: Whiskers-box plots of seven error indices for all 44 events predicted from the three data-driven models. (a), (b), and (c) denote the result of ANN, SVR, and LSTM models.

6.3.4 Comparison with Physically-Based Hydrological Model

This study compared the results from three data-driven models to the results from the physically-based hydrologic model (i.e., NWM), which is currently used for flood warning system in the United States, to further evaluate the predictive performance for runoff forecasting. The detailed information about the NWM was described in 4.2.2. For evaluation, predicted results of hourly runoff from the three data-driven models (i.e., ANN, SVR, and LSTM) were compared to the results from the NWM for 1 and 6 hours of lead time during 2019. Taylor diagram, which was introduced by Taylor (2001), was used for evaluation in this study. The Taylor diagram is a one of the mathematical diagrams can be used to evaluate differences in reference and simulated datasets and provides visual indicators in terms of pattern and magnitude of the variability. The diagram manipulated the comparative evaluation of different models. Here, the diagram showed a summary of the relative skill with which four models predict the runoff and quantify the degree of correspondence between the modeled and observations in terms of three statistical metrics, CC, standard deviation (SD) and RMSE. Figure 6.9 represents the Taylor diagrams for evaluating hourly runoff prediction results from the data-driven models and the NWM.

The diagrams illustrated that the point positions of four models (i.e., ANN, SVR, LSTM, and NWM) for forecasting runoff for 1 and 6 hours of lead time. As shown in Figure 6.9, overall result showed that the NWM model is closer to the observations than data-driven models, and the SD points of the data-driven models are slightly smaller than observations. The CC values of the SVR, LSTM and NWM models were located between 0.95 and 0.99, and the ANN model had the CC value of 0.75. In addition, the RMSE values of the models were less than 100 cms, while the ANN model had the RMSE value which is approximately 130 cms. Among the four models,

the NWM provided SD, CC, and RMSE values most similar to the observations, and the LSTM

and SVR models also demonstrated acceptable performances compared to the observed data.

(a)   (b)
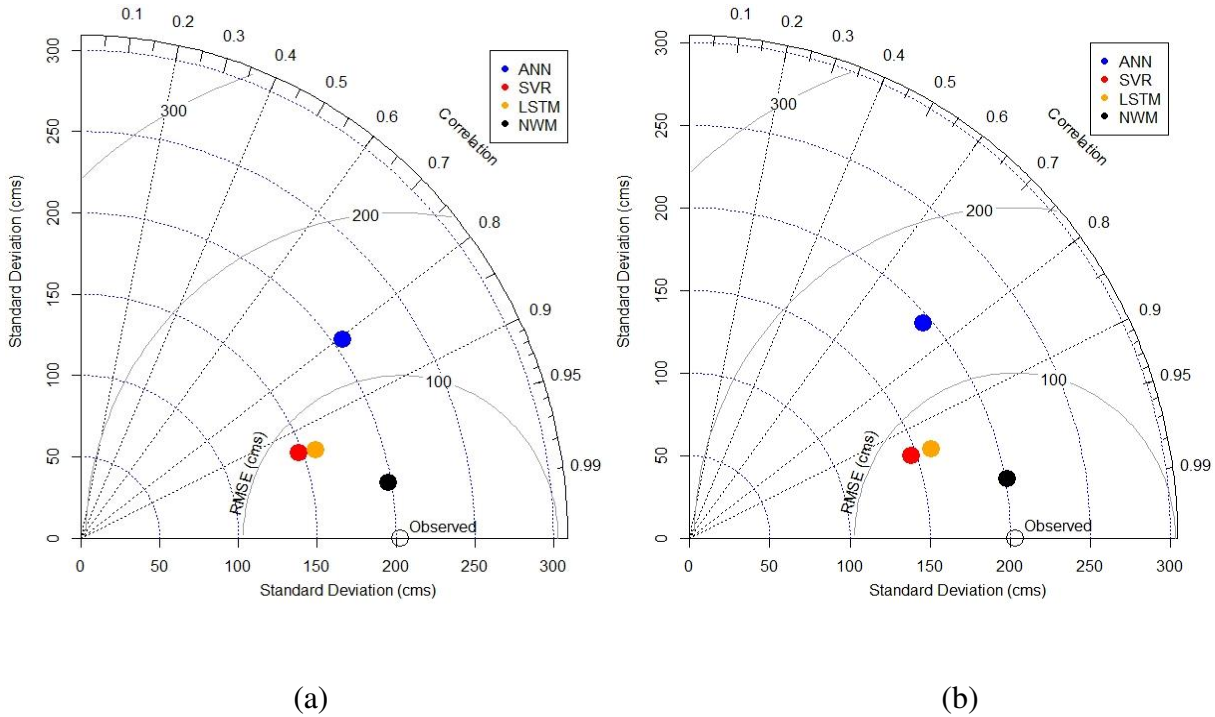
Figure 6.9: Taylor diagrams for evaluating hourly runoff prediction results from the data-driven models and the NWM.

Table 6.5 indicates the evaluation metrics for single runoff events in 2019 predicted by

each model. All models produced 15 single events during 2019. Among the four models, the

ANN model demonstrated the poorest performance whereas the NWM showed the best

prediction result. Similar to the result from NWM, the SVR and LSTM also demonstrated

acceptable performances, with the CC values of 0.81 and PBIAS values less than 20%. In the

case of PE indicating the error in simulated peak runoff, the NWM showed the best performance

with 0.9% of PE value. The SVR model also showed high predictive ability with a PE value of

about 5%. The four models had similar performance according to PTE with values ranging from

117

7 to 8 hours. Generally, the SVR and LSTM demonstrated similar performance in predicting runoff events when compared to the NWM, highlighting the effective use of data-driven models for runoff forecasting.

Table. 6.5: Evaluation metrics for single runoff events in 2019 predicted by each model.

Models	CC	BIAS	PBIAS(%)	RMSE(cms)	PE(%)	PTE(hour)
ANN	0.554	2.566	41.788	165.155	27.847	8.684
SVR	0.808	1.117	12.057	77.248	5.402	7.684
LSTM	0.812	0.995	16.681	93.629	-20.659	7.053
NWM	0.853	1.039	7.403	48.632	0.954	7.111

6.4 Discussion

In this study, the predictive performances of ANN, SVR and LSTM data-driven models were evaluated for runoff forecasting. The distributed forcing datasets from the NLDAS, including precipitation, land surface temperature, soil moisture contents, and base flow, were used to consider the contribution of eight sub-watersheds to runoff generations at outlet point. Similar to recent works, the results of this study showed that LSTM model produced the best performance for hourly runoff prediction.

Recently, Fan et al. (2020) proposed a data-driven approach using LSTM model to simulate rainfall-runoff process using various meteorological variables. This study applied the proposed approach and compared the simulated results with an ANN network model. They concluded that the LSTM model can achieve accurate results with NSE ranged from 0.60 to 0.94.

In addition, the ANN model showed lower performance than the LSTM model. Another study conducted by Hu et al. (2018) used ANN and LSTM models for simulating runoff. This study resulted that the performance of the LSTM for simulating rainfall-runoff process was the best with values of NSE ranging from 0.85 to 0.96 compared with the ANN model. It also represented that the LSTM model outperformed the ANN model for simulating runoff event with values of R^2 ranging from 0.94 to 0.97 (R^2 for ANN model was from 0.76 to 0.88). Xiang et al. (2020) proposed the LSTM based model for estimating runoff and found that the LSTM model outperformed several methods, including linear regression, SVR, Gaussian processes regression and lasso regression. Also, they concluded that the input datasets with distributed structure can increase the model performance compared to using averaged datasets for an entire watershed.

Similar to previous studies, this study demonstrates that LSTM model outperforms other models such as ANN, SVR for runoff predictions. Although they showed different values of evaluation statistics (e.g. NSE, R^2 etc.) due to various factors, such as quality of the input datasets, parameters, structure of the model, and temporal and spatial resolution of the datasets, it is obvious that the LSTM model outperforms other popular data-driven model approaches. Furthermore, this study confirms that the data-driven models with distributed forcing datasets can be more effective alternative to the physically-based hydrologic model for time-series predictions in hydrology field.

This study predicted hourly runoff using three data-driven models with distributed forcing datasets. These models achieved comparable prediction results in hourly runoff. Because the data-driven models forecast time-series data using the information learned from the relationships between input and output datasets, the quality of training data significantly affects the modeling results (Shen, 2018; Fan et al., 2020). In this study, four meteorological variables

119

generated from the NLDAS were used as input data of each data-driven model. Many studies have demonstrated the high accuracy of NLDAS datasets, but the temporal and spatial uncertainties inherent in the data cannot be neglected (Cai et al., 2014; Zhuo et al., 2015; Xia et al., 2015; Espinoza-Dávalos et al., 2016). These uncertainties in the NLDAS datasets not only affect the training process of each data-driven model, but also translate into errors in the model outputs (Abebe and price, 2003; 2004). The analysis of uncertainty in the input datasets was out of the scope of this study and will be an important task for future study.

The prediction results of this study indicated that the SVR and LSTM models produce comparable performance in runoff forecasting with $1 - 6$ hours of lead time and represented the proposed models can be an alternative approach for runoff forecasting. Based on the results of the seasonal evaluation, both SVR and LSTM models are expected to be efficient tools for flood warning system during wet season, from December to May, in the Russian River basin, CA. The results of this study can contribute to various fields such as drought analysis, water resources management for irrigation, and environmental flow assessments based on daily or monthly runoff predictions even though this study focused on investigating the short-term runoff forecasting. In addition, the results of this study showed that the distributed data-based data-driven models are also expected to contribute greatly to the operation of flood warning systems in regions where installation of observation systems is difficult, or in areas with low spatial density of data collection. In addition, it is expected that the using the data-driven models for runoff analysis will become convenient as the quality of forcing data and computing systems are improved compared to traditional systems.

Chapter 7

Conclusions and Summary

This chapter presents the overall conclusions and summary drawn from the research, particularly assessment, error correction, and runoff predictions of hydrologic models. It also provides recommendations on the use data-driven models for hydrologic assessment in future studies.

Data-driven models have shown high potential in a wide variety of applications, such as image classification, computer vision, language translation, and time-series prediction, where it is difficult to develop conventional algorithms to perform the required evaluation. Specifically, in water-related fields, including environmental, agricultural, water quality, and hydrologic studies, data-driven models have shown outstanding performances recently. Additionally, in hydrologic studies, with the advancement of computational systems and algorithms, data-driven models have shown good performance in analyzing hydrologic problems by considering various hydrological, meteorological, and topographical factors with multiple time steps from sub-hourly

to monthly. In this research, multiple data-driven approaches were used to effectively achieve three tasks: 1) hydrologic assessment of a physically-based model, 2) performance improvement of a hydrologic model by error prediction as a post-processor tool, and 3) hydrologic forecasting with distributed forcing data. The notable results and conclusions of this study are as follows.

7.1 Assessment of a Physically-Based Hydrologic Model

1) This study applied a hybrid framework consisting of two data-driven models, namely, unsupervised and supervised learning techniques, to develop a new HAT for a single-event based hydrologic assessment. The HAT was applied to evaluate the quality of the retrospective simulated streamflow of the NWM in the San Francisco Bay area, California. For the evaluation, the HAT provides four performance ratings, which are composite and easy-to-understand for model users.

2) For the hydrological assessment of a physically-based hydrologic model, the data-driven models can be an effective alternative to the traditional statistical and graphical assessment methods. Specifically, this research represented that the features of data-driven models such as clustering, classification are appropriate to provide evaluation results for hydrological performance.

3) A new HAT has been developed to provide four ratings, namely, VG, G, S, and US. The HAT has apparent statistical and graphical features. It can accurately diagnose the quality and status of outcomes from the hydrologic models using each rating objectively, and it is expected to be used for determining the necessity, strategy, and extent of calibration.

4) The performance of the HAT was proven through the training and testing processes. The results showed that the HAT can objectively and accurately evaluate the quality of the model in terms of two components of a single event, i.e., the rising and recession limbs, as well as for the entire hydrograph. In addition, it provides ratings that indicate the performance of the hydrologic models, which are easy-to-understand and can help in interpreting and using the assessment results for various purposes.

5) The HAT was applied to evaluate the performance of the NWM in simulating the streamflow at 57 gages in the San Francisco Bay area. The evaluation results showed that the NWM has VG and G ratings for at least 46% of the hydrographs simulated from October 2013 to February 2017.

6) Even though this study used four ratings for hydrologic assessment, the HAT can extend the range of evaluation by adding new groups. As the HAT is very flexible, it can be applied for various purposes. For instance, during a flash flood, if an hourly or sub-hourly based evaluation of the hydrologic model is required, it can be implemented by training the HAT using hourly or sub-hourly time step datasets. In addition, the HAT can be applied to various models, such as flood forecasting and hydrologic models, as well as any geophysical data driven by physically pulsed phenomena.

7) This research showed how to develop a hydrological assessment to using hybrid framework which is combination of two data-driven models. Developed assessment tool provided reasonable and easy-to-understand performance ratings, from US to VG, for each single hydrograph. It should be an effective tool for users of hydrologic models for various applications such as dam operation, water resource management,

and flood forecasting which require a magnitude of reliability of hydrological modeling. Although this study focused on evaluation of NWM for hourly runoff simulation, the HAT can be applied for evaluation of various types of model and with multiple temporal-resolutions from sub-hourly to monthly as future studies.

7.2 Performance Improvement of a Hydrologic Model by Error Prediction as a Post-Processor Tool

1) This study proposed a LSTM-s2s model, which is one of the deep-learning based data-driven models, to improve the predictive performance of the NWM as post-processor. The proposed method was applied in the Russian River basin, CA. The impacts of potential factors such as sequence time-step and parameters in prediction accuracy were tested for the models` training and improved performance of NWM with the LSTM-s2s model.

2) The LSTM-s2s model provided error predictions indicating differences between the predicted runoff and observations for 1–18 h of lead times. The presented model used observed precipitation and runoff errors coming from upstream regions as input variables of the model.

3) The performance of NWM for forecasting runoff for 1–18 hours was evaluated using various statistical metrics. It was shown that average metrics of CC, NSE, PBAIS, and RMSE were 0.65, 0.55, 10%, and 40 cms, respectively, for lead times from 12 to 18 hours. In addition, overall predictive performances of NWM at three stations were found to be lower compared to the actual runoff, which means that a post-process is needed to improve the prediction performance of the NWM.

4) Three factors, including lag time of input data, number of layers, and batch size, have effects on the performance of LSTM-s2s model. The result indicates that the performance decreases as sequence length and number of layers increase. In addition, the change in batch size did not have a dramatic effect on simulation accuracy. The optimized model was based on 6 hours for sequence length, 32 for number of layers, and 128 for batch size, respectively.

5) The LSTM-s2s model obtained desirable results for error forecasting for each time step from 1 to 18 hours with average values of CC of 0.95, NSE of 0.88, and PBIAS of -14%, respectively. The results of prediction errors from LSTM-s2s model were used for improving predictive performance of NWM. The result showed that a post processor with a LSTM-s2s can improve the reliability of the prediction and performance of a physically-based hydrologic model (i.e., NWM). Moreover, the LSTM-s2s based post-processor can improve the predictive performance of NWM in terms of not only temporal pattern of runoff, but also the volume of predicted runoff.

6) The LSTM-s2s significantly improved the predictive performance of NWM as post-processor for a lead time of 1 to 18 hours. Compared to the predicted runoff from NWM, the NWM with the LSTM-s2s post-processor provided more improved runoff prediction results with R^2 values of 0.98 to 0.99.

7) It is expected that the proposed LSTM-s2s model can be applied for different basins and over 2.7 million river reaches around the United States for which the NWM provides the runoff predictions. In this research, the LSTM-s2s model includes only observed precipitation and upstream errors as input data. Thus, it may be easy to apply the post-processor tool to improve the NWMs` predictive ability for regions

with limited physical observations. This study also serves to provide understating of potential of data-driven models for solving hydrological problems.

8) With the improved NWM performance, it is expected that the proposed model can be applied to areas with high risk of floods for an efficient flood warning system. In addition, the results of this study can serve as base knowledge to improve the medium- and long-terms predictive ability of the NWM as well as short-term based performance.

7.3 Hourly-Runoff Forecasting with Distributed Forcing Data

1) This research aims to evaluate the applicability of data-driven models for hourly runoff forecasting with distributed forcing datasets. For runoff forecasting, various types of data-driven models (i.e., ANN, SVR, and LSTM) were used for runoff prediction. The predicted runoff results were compared with those of the NWM. In addition, to consider the contribution of sub-watersheds to the runoff at outlet points, several hydrologic variables from NLDAS-2 were used as input data for each model.

2) The proposed data-driven models obtained acceptable prediction results for 1–6 h of lead times compared to the those from the NWM. Among the three models, both SVR and LSTM models showed better predictive performance than AMM model for 1–6 hours of lead time. In addition, the SVR and LSTM models successfully predicted the patterns and volume of hourly runoff compared to the observed runoff. These models showed the R^2 value of 0.9, and the evaluation indices also proved high performances of the models. In the case of ANN model, although it tended to overestimated runoff

126

compared to the observations, the prediction results were acceptable in terms of runoff tendency.

3) Based on the seasonal evaluation results, all three models showed better predictive ability during the wet seasons than dry seasons. Particularly, for the dry seasons, the ANN and SVR models showed low accuracy in runoff prediction, which was obvious in dry season from Sep to Nov. This represents that predictions from the data-driven models may be useful for improving flood warning system but somewhat less in drought analysis.

4) Moreover, the event-based evaluation results indicated that these models showed high accuracy in predicting runoff event. The both LSTM and SVR models were the best at predicted runoff events compared to the ANN model. Both models not only showed high accuracy in predicting peak runoff and time to peak, but they also performed with less than errors of 20% in runoff volume.

5) Comparison results with NWM showed that the runoff prediction performances of the SVR and LSTM models are similar to the NWM in terms of CC, SD and RMSE evaluation indices.

6) The results of this research demonstrated that data-driven models for hourly runoff forecasting have sufficient predictive capability and are useful in areas where observation systems are not available. In particular, from the seasonal and single-event based evaluation, data-driven models can be effective alternatives to physically-based hydrologic models for flood forecasting with short-term time steps during wet seasons. Although only three models were evaluated in this study, we intend to apply other types of data-driven models for predictions of various types of hydrologic

variables, not limited to the runoff in the future study. In addition, for effective and reliable runoff forecasting, this research recommends the use of numerous types of input variable such as soil properties and types, land use, and meteorological factors which have strong relationship with runoff generation in the future study.

7.4 Potential Implications of Data-Driven Models for Improving Runoff Analysis

In this dissertation, the proposed data-driven models were tested for three tasks, namely, hydrologic assessment, improvement of runoff modeling performance, and hourly runoff prediction with distributed forcing data. Based on the results of each task, the data-driven models are capable of providing easy-to-understand evaluation ratings for runoff modeling, improving the accuracy and reliability of runoff prediction results, and forecasting hourly runoff data for regions with temporal and spatial limitations of ground-based observatories. In addition, data-driven models can serve as complementary methods to physically-based models, especially in underperforming regions.

The runoff simulation and prediction results from data-driven models can be used for various purposes, such as development of reliable flood forecasting systems, analysis of droughts based on long-term time scales, and proper water resources management. Although the time scale considered in this research is only hourly based, it is expected that data-driven models can contribute to improve the quality of runoff analysis with multiple time steps, from sub-hourly to monthly, for various challenges. Moreover, although this research considered only the NWM as the physically-based model, it can be expanded to other types of physically-based hydrologic models such as SWAT, HEC-HMS, and MODFLOW.

Recently, as computation systems and technologies are advancing, various data-driven models have been developed and proposed for many tasks. In this research, only six types of data-driven models (e.g., ANN, SVM, RF, K-means, LSTM, and LSTM-s2s) were introduced and applied for runoff analysis, but other techniques that are rarely applied to hydrologic analysis may have the potential for this application. Thus, for effective and reliable runoff analysis, this research recommends the applications of various data-driven models with multiple temporal/spatial input variables for numerous research fields such as water resources management, ground water analysis, agricultural and environmental studies, and natural disaster prevention.

References

Abbott, M.B., Bathurst, J.C., Cunge, J.A., O'Connell, P.E., and Rasmussen, J. (1986). An introduction to the European Hydrological System—Systeme Hydrologique Europeen, "SHE", 1: History and philosophy of a physically-based, distributed modelling system. *Journal of Hydrology,* 87(1–2), 45–59.

Abebe, A. J., and Price, R. K. (2003). Managing uncertainty in hydrological models using complementary models. *Hydrological Sciences Journal*, 48(5), 679-692.

Abebe, A. J., and Price, R. K. (2004). Information theory and neural networks for managing uncertainty in flood routing. *Journal of computing in civil engineering*, 18(4), 373-380.

Adamowski, J. and Chan, H.F. (2011). A wavelet neural network conjunction model for groundwater level forecasting. *Journal of Hydrology,* 407, 28–40.

Adnan, R., Ruslan, F.A., Samad, A.M., and Zain, Z.M. Flood Water Level Modelling and Prediction Using Artificial Neural Network: Case Study of Sungai Batu Pahat in Johor. (2012). *In Proceedings of the 2012 IEEE Control and System Graduate Research Colloquium,* Shah Alam, Malaysia, 22–25.

Agrawal, S., Barrington, L., Bromberg, C., Burge, J., Gazen, C., and Hickey, J. (2019). Machine learning for precipitation nowcasting from radar images. *arXiv preprint arXiv:1912.12132*.

Akbari Asanjan, A., Yang, T., Hsu, K., Sorooshian, S., Lin, J., and Peng, Q. (2018). Short-Term Precipitation Forecast Based on the PERSIANN System and LSTM Recurrent Neural Networks. *Journal of Geophysical Research: Atmospheres*, 123(22), 12-543.

Al-Sabhan, W., Mulligan, M., and Blackburn, G.A. (2003). A real-time hydrological model for

flood prediction using GIS and the WWW. *Computers, Environment and Urban Systems,* 27 (1), 9–32.

Arnaud, P., Lavabre, J., Fouchier, C., Diss, S., and Javelle, P. (2011). Sensitivity of hydrological models to uncertainty in rainfall input. *Hydrological Sciences Journal–Journal des Sciences Hydrologiques*, 56(3), 397-410.

Arnold, J.G., Srinivasan, R., Muttiah, R.S., and Williams, J.R. (1998). Large area hydrologic modeling and assessment part I: model development. *Journal of the American Water Resources Association*. 34 (1), 73–89.

ASCE. (1993). ASCE Task Committee on Definition of Criteria for Evaluation of Watershed Models of the Watershed Management Committee, Irrigation and Drainage Division, Criteria for evaluation of watershed models. *Journal of Irrigation and Drainage Engineering*. 119 (3), 429–442.

Ayzel, G. (2019). Does Deep Learning Advance Hourly Runoff Predictions. *In Proceedings of the V International Conference Information Technologies and High-Performance Computing (ITHPC-2019)*, Khabarovsk, Russia, 16-19.

Ba, H., Guo, S., Wang, Y., Hong, X., Zhong, Y., and Liu, Z. (2018). Improving ANN model performance in runoff forecasting by adding soil moisture input and using data preprocessing techniques. *Hydrology Research*, 49(3), 744-760.

Bishop, C.M. (2006). Pattern Recognition and Machine Learning. *Springer*.

Boyle, D.P., Gupta, H.V., and Sorooshian, S. (2000). Toward improved calibration of hydrologic models: combining the strengths of manual and automatic methods. *Water Resources Research*, 36 (12), 3663–3674.

Boyraz, C., and Engin, Ş. N. (2018). Streamflow Prediction with Deep Learning. *In 2018 6th*

International Conference on Control Engineering & Information Technology (CEIT), 1-5.

Breiman, L. (2001). Random forests. *Machine Learning*, 45 (1), 5–32.

Bui, D. T., Hoang, N. D., Martínez-Álvarez, F., Ngo, P. T. T., Hoa, P. V., Pham, T. D., Samuim P., and Costache, R. (2020). A novel deep learning neural network approach for predicting flash flood susceptibility: A case study at a high frequency tropical storm area. *Science of the Total Environment*, 701, 134413.

Cai, X., Yang, Z. L., Xia, Y., Huang, M., Wei, H., Leung, L. R., and Ek, M. B. (2014). Assessment of simulated water balance from Noah, Noah-MP, CLM, and VIC over CONUS using the NLDAS test bed. *Journal of Geophysical Research: Atmospheres*, 119(24), 13-751.

Castelletti, A., Galelli, S., Restelli, M., and Soncini-Sessa, R. (2010). Tree-based reinforcement learning for optimal water reservoir operation. *Water Resources Research*, 46(9).

Chang, F. J., and Tsai, M. J. (2016). A nonlinear spatio-temporal lumping of radar rainfall for modeling multi-step-ahead inflow forecasts by data-driven techniques. *Journal of Hydrology*, 535, 256-269.

Cho, K., Van Merriënboer, B., Gulcehre, C., Bahdanau, D., Bougares, F., Schwenk, H., and Bengio, Y. (2014). Learning phrase representations using RNN encoder-decoder for statistical machine translation. *arXiv preprint arXiv:1406.1078.*

Choi, C., Kim, J., Han, H., Han, D., and Kim, H. S. (2020). Development of Water Level Prediction Models Using Machine Learning in Wetlands: A Case Study of Upo Wetland in South Korea. *Water*, 12(1), 93.

Cifelli, R., Chandrasekar, V., Chen, H., and Johnson, L.E. (2018). High resolution radar quantitative precipitation estimation in the San Francisco Bay area: Rainfall monitoring for

the urban environment. *Journal of the Meteorological Society of Japan. Ser. II,* 96, 141–155.

Coffey, M.E., Workman, S.R., Taraba, J.L., and Fogle, A.W. (2004). Statistical procedures for evaluating daily and monthly hydrologic model predictions. *Transactions of the ASAE*, 47 (1), 59.

Cosgrove, B.A., Lohmann, D., Mitchell, K.E., Houser, P.R., Wood, E.F., Schaake, J.C., Robock, A., Marshall, C., Sheffield, J., Duan, Q., Luo, L., Higgins, R.W., Pinker, R.T., Tarpley, and J.D., Meng, J. (2003). Real time and retrospective forcing in the North American Land Data Assimilation System (NLDAS) project. *Journal of Geophysical Research: Atmospheres*, 108(D22).

Cosgrove, B.A., Gochis, D.J., Graziano, T., Clark, and E., Flowers, T. (2018). An update on the NOAA National Water Model and Related Activities. *In: 98th Annual Meeting American Meteorological Society*, Austin, 7–11 January 2018.

Coulibaly, P., and Anctil, F. (1999). Real-time short-term natural water inflows forecasting using recurrent neural networks. *International Joint Conference on Neural Networks. Proceedings (Cat. No. 99CH36339)*, 3802-3805.

Couta, D., Zhang, Y. K., and Li, Y. M. (2019). River Flow Forecasting Using Long Short-term Memory. *DEStech Transactions on Computer Science and Engineering, (icaic).*

Cutler, D. R., Edwards Jr, T. C., Beard, K. H., Cutler, A., Hess, K. T., Gibson, J., and Lawler, J. J. (2007). Random forests for classification in ecology. *Ecology*, 88(11), 2783-2792.

da Silva Chagas, C., de Carvalho Junior, W., Bhering, S.B., and Calderano Filho, B. (2016). Spatial prediction of soil surface texture in a semiarid region using random forest and multiple linear regressions. *Catena*, 139, 232–240.

Datta, A. R., and Bolisetti, T. (2016). Uncertainty analysis of a spatially-distributed hydrological model with rainfall multipliers. *Canadian Journal of Civil Engineering*, 43(12), 1062-1074.

Demissie, Y. K., Valocchi, A. J., Minsker, B. S., and Bailey, B. A. (2009). Integrating a calibrated groundwater flow model with error-correcting data-driven models to improve predictions. *Journal of Hydrology*, 364(3-4), 257-271.

Devia, G. K., Ganasri, B. P., and Dwarakish, G. S. (2015). A review on hydrological models. *Aquatic Procedia*, 4, 1001-1007.

Donigian Jr, A.S., Imhoff, J.C., and Bicknell, B.R. (1983). Predicting water quality resulting from agricultural nonpoint source pollution via simulation: HSPF. *Agricultural Management Practices for Water Quality,* 200–249.

Doycheva, K., Horn, G., Koch, C., Schumann, A., and König, M. (2017). Assessment and weighting of meteorological ensemble forecast members based on supervised machine learning with application to runoff simulations and flood warning. *Advanced Engineering Informatics*, 33, 427-439.

Drucker, H., Burges, C. J., Kaufman, L., Smola, A., and Vapnik, V. (1997). Support vector regression machines. *Advances in neural information processing systems*, 9, 155-161.

Dutta, D., Herath, S., and Musiake, K. (2003). A mathematical model for flood loss estimation. *Journal of Hydrology*, 277(1–2), 24–49.

Elsafi, S. H. (2014). Artificial neural networks (ANNs) for flood forecasting at Dongola Station in the River Nile, Sudan. *Alexandria Engineering Journal*, 53(3), 655-662.

Espinoza-Dávalos, G. E., Arctur, D. K., Teng, W., Maidment, D. R., García-Martí, I., and Comair, G. (2016), Studying soil moisture at a national level through statistical analysis of NASA NLDAS data. *Journal of hydroinformatics*, 18(2), 277-287.

Ester, M., Kriegel, H.P., Sander, J., and Xu, X. (1996). A density-based algorithm for discovering clusters in large spatial databases with noise. *In Kdd,* 96(34), 226–231.

Everitt, B.S., Landau, S., Leese, M., and Stahl, D. (2001). Cluster Analysis, *fourth ed. Arnold, London.*

Fan, H., Jiang, M., Xu, L., Zhu, H., Cheng, J., and Jiang, J. (2020). Comparison of Long Short Term Memory Networks and the Hydrological Model in Runoff Simulation. *Water*, 12(1), 175.

Fang, K., Shen, C., and Kifer, D. (2019). Evaluating aleatoric and epistemic uncertainties of time series deep learning models for soil moisture predictions. *arXiv preprint arXiv:1906.04595.*

Feng, Y., Cui, N., Hao, W., Gao, L., and Gong, D. (2019). Estimation of soil temperature from meteorological data using different machine learning models. *Geoderma*, 338, 67-77.

Frame, J., Nearing, G., Kratzert, F., and Rahman, M. (2020). Post processing the US National Water Model with a Long Short-Term Memory network.

Gholami VCKW, Chau KW, Fadaee F, Torkaman J, and Ghaffari A (2015) Modeling of groundwater level fluctuations using dendrochronology in alluvial aquifers. *Journal of Hydrology*, 529:1060-1069.

Green, I.R.A., and Stephenson, D. (1986). Criteria for comparison of single event models. *Hydrological Sciences Journal*, 31 (3), 395–411.

Gupta, H.V., Kling, H., Yilmaz, K.K., and Martinez, G.F. (2009). Decomposition of the mean squared error and NSE performance criteria: Implications for improving hydrological modelling. *Journal of Hydrology*, 377 (1–2), 80–91.

Han, H., Kim, J., Chandrasekar, V., Choi, J., and Lim, S. (2019). Modeling Streamflow Enhanced by Precipitation from Atmospheric River Using the NOAA National Water

Model: A Case Study of the Russian River Basin for February 2004. *Atmosphere*, 10(8), 466.

Hao, Z., Hao, F., Xia, Y., Singh, V. P., Hong, Y., Shen, X., and Ouyang, W. (2016). A statistical method for categorical drought prediction based on NLDAS-2. *Journal of Applied Meteorology and Climatology*, 55(4), 1049-1061.

Harr, M. E. (1989). Probabilistic estimates for multivariate analyses. *Applied Mathematical Modelling*, 13(5), 313-318.

Hartigan, J.A., and Wong, M.A. (1979). Algorithm AS 136: a k-means clustering algorithm. *Journal of the Royal Statistical Society. Series C (Applied Statistics)*, 28(1), 100-108.

Haydon, S., and Deletic, A. (2009). Model output uncertainty of a coupled pathogen indicator–hydrologic catchment model due to input data uncertainty. *Environmental Modelling & Software*, 24(3), 322-328.

Hidayat, H., Hoitink, A. J. F., Sassi, M. G., and Torfs, P. J. J. F. (2014). Prediction of discharge in a tidal river using artificial neural networks. *Journal of Hydrologic Engineering*, 19(8), 04014006.

Hu, C., Wu, Q., Li, H., Jian, S., Li, N., and Lou, Z. (2018). Deep learning with a long short-term memory networks approach for rainfall-runoff simulation. *Water*, 10(11), 1543.

Huang, Y., Chen, X., Li, Y. P., Huang, G. H., and Liu, T. (2010). A fuzzy-based simulation method for modelling hydrological processes under uncertainty. *Hydrological processes,* 24(25), 3718-3732.

Hochreiter, S., and Schmidhuber, J. (1997). Long short-term memory. *Neural computation*, 9(8), 1735-1780.

Hong, Y., Hsu, K. L., Moradkhani, H., and Sorooshian, S. (2006). Uncertainty quantification of

satellite precipitation estimation and Monte Carlo assessment of the error propagation into hydrologic response. *Water Resources Research*, 42(8).

Hong, W.C. (2008). Rainfall forecasting by technological machine learning models. *Applied Mathematics and Computation*. 200 (1), 41–57.

Hrnjica, B., and Bonacci, O. (2019). Lake Level Prediction using Feed Forward and Recurrent Neural Networks. *Water Resources Management*, 33(7), 2471-2484.

Hsieh, N.C. (2005). Hybrid mining approach in the design of credit scoring models. *Expert Systems with Applications*, 28 (4), 655–665.

Huysmans, J., Baesens, B., Vanthienen, J., and Van Gestel, T. (2006). Failure prediction with self organizing maps. *Expert Systems with Applications*, 30(3), 479-487.

Jin, X., Xu, C. Y., Zhang, Q., and Singh, V. P. (2010). Parameter and modeling uncertainty simulated by GLUE and a formal Bayesian method for a conceptual hydrological model. *Journal of Hydrology*, 383(3-4), 147-155.

Johnson, S.C. (1967). Hierarchical clustering schemes. *Psychometrika*, 32 (3), 241–254.

Johnson LE, Hsu C, Zamora R, and Cifelli R (2016). Assessment and applications of distributed hydrologic model-Russian-Napa River Basins, CA. *NOAA Technical Memorandum PSD-316, NOAA Printing Office, Silver Spring, MD.*

Jothiprakash, V., and Magar, R. B. (2012). Multi-time-step ahead daily and hourly intermittent reservoir inflow prediction by artificial intelligent techniques using lumped and distributed data. *Journal of Hydrology*, 450, 293-307.

Kang, H., and Sridhar, V. (2017). Combined statistical and spatially distributed hydrological model for evaluating future drought indices in Virginia. *Journal of Hydrology: Regional Studies*, 12, 253-272.

Kim, J., Han, H., Johnson, L. E., Lim, S., and Cifelli, R. (2019). Hybrid machine learning framework for hydrological assessment. *Journal of Hydrology*, 577, 123913.

Kobold, M., and Sušelj, K. (2005). Precipitation forecasts and their uncertainty as input into hydrological models. *Hydrology and Earth System Sciences*, 9(4), 322-332.

Kohonen, T., 1982. Self-organized formation of topologically correct feature maps. *Biological Cybernetics*. 43 (1), 59–69.

Kuczera, G., and Parent, E. (1998). Monte Carlo assessment of parameter uncertainty in conceptual catchment models: the Metropolis algorithm. *Journal of Hydrology*, 211(1-4), 69-85.

Kratzert, F., Klotz, D., Brenner, C., Schulz, K., and Herrnegger, M. (2018). Rainfall–runoff modelling using long short-term memory (LSTM) networks. *Hydrology and Earth System Sciences*, 22(11), 6005-6022.

Krzysztofowicz, R. (1999). Bayesian theory of probabilistic forecasting via deterministic hydrologic model. *Water Resources Research*, 35(9), 2739-2750.

Krzysztofowicz, R. (2001). The case for probabilistic forecasting in hydrology. *Journal of hydrology*, 249(1-4), 2-9.

Le, X. H., Ho, H. V., Lee, G., and Jung, S. (2019). Application of long short-term memory (LSTM) neural network for flood forecasting. *Water*, 11(7), 1387.

Lee, H., McIntyre, N., Wheater, H., and Young, A. (2005). Selection of conceptual models for regionalisation of the rainfall-runoff relationship. *Journal of Hydrology*, 312(1-4), 125-147.

Lee, G. H., Jung, S. H., and Lee, D. E. (2018). Comparison of physics-based and data-driven models for streamflow simulation of the Mekong river. *Journal of Korea Water Resources Association*. 51(6), 503-514.

Legates, D.R., and McCabe Jr, G.J. (1999). Evaluating the use of "goodness of fit" measures in hydrologic and hydroclimatic model validation. *Water Resources Research,* 35 (1), 233–241.

Li, L., Xia, J., Xu, C. Y., and Singh, V. P. (2010). Evaluation of the subjective factors of the GLUE method and comparison with the formal Bayesian method in uncertainty assessment of hydrological models. *Journal of Hydrology*, 390(3-4), 210-221.

Liang, X., Lettenmaier, D.P., Wood, E.F., and Burges, S.J. (1994). A simple hydrologically based model of land surface water and energy fluxes for general circulation models. *Journal of Geophysical Research: Atmospheres,* 99 (D7), 14415–14428.

Liang, J., Li, W., Bradford, S. A., and Šimůnek, J. (2019). Physics-Informed Data-Driven Models to Predict Surface Runoff Water Quantity and Quality in Agricultural Fields. *Water*, 11(2), 200.

Lin, G. F., Jhong, B. C., and Chang, C. C. (2013). Development of an effective data-driven model for hourly typhoon rainfall forecasting. *Journal of Hydrology*, 495, 52-63.

MacQueen, J. (1967). Some methods for classification and analysis of multivariate observations. *In: Proceedings of the fifth Berkeley symposium on mathematical statistics and probability*, 1(14), 281–297.

Maskey, S., and Guinot, V. (2003). Improved first-order second moment method for uncertainty estimation in flood forecasting. *Hydrological Sciences Journal*, 48(2), 183-196.

Maskey, S., Guinot, V., and Price, R. K. (2004). Treatment of precipitation uncertainty in rainfall-runoff modelling: a fuzzy set approach. *Advances in Water Resources*, 27(9), 889-898.

McCulloch, W.S., and Pitts, W. (1943). A logical calculus of the ideas immanent in nervous

activity. *The bulletin of mathematical biophysics*. 5 (4), 115–133.

McMillan, H., Jackson, B., Clark, M., Kavetski, D., and Woods, R. (2011). Input uncertainty in hydrological models: an evaluation of error models for rainfall. *Journal of Hydrology*, 400(1-2), 83-94.

Mehdizadeh, S., Fathian, F., and Adamowski, J. F. (2019). Hybrid artificial intelligence-time series models for monthly streamflow modeling. *Applied Soft Computing*, 80, 873-887.

Melching, C. S. (1992). An improved first-order reliability approach for assessing uncertainties in hydrologic modeling. *Journal of Hydrology*, 132(1-4), 157-177.

Montanari, A., and Brath, A. (2004). A stochastic approach for assessing the uncertainty of rainfall-runoff simulations. *Water Resources Research*, 40(1).

Montanari, A. (2007). What do we mean by 'uncertainty'? The need for a consistent wording about uncertainty assessment in hydrology. *Hydrological Processes: An International Journal*, 21(6), 841-845.

Moriasi, D. N., Arnold, J. G., Van Liew, M. W., Bingner, R. L., Harmel, R. D., and Veith, T. L. (2007). Model evaluation guidelines for systematic quantification of accuracy in watershed simulations. *Transactions of the ASABE*, 50(3), 885-900.

Mosavi, A., Ozturk, P., and Chau, K. W. (2018). Flood prediction using machine learning models: Literature review. *Water*, 10(11), 1536.

Muñoz, P., Orellana-Alvear, J., Willems, P., and Célleri, R. (2018). Flash-flood forecasting in an Andean mountain catchment—Development of a step-wise methodology based on the random forest algorithm. *Water*, 10(11), 1519.

Muñoz, E., Tume, P., and Ortíz, G. (2014). Uncertainty in rainfall input data in a conceptual water balance model: effects on outputs and implications for predictability. *Earth Sciences*

Research Journal, 18(1), 69-75.

Nearing, G., Sampson, A. K., Kratzert, F., and Frame, J. (2020). Post-processing a Conceptual Rainfall-runoff Model with an LSTM.

Neitsch, S. L., Arnold, J. G., Kiniry, J. R., and Williams, J. R. (2011). Soil and water assessment tool theoretical documentation version 2009. *Texas Water Resources Institute.*

Olden, J.D., Kennard, M.J., and Pusey, B.J. (2012). A framework for hydrologic classification with a review of methodologies and applications in ecohydrology. *Ecohydrology*, 5(4), 503–518.

Ott, M., Su, Z., Schumann, A. H., and Schultz, G. A. (1991). Development of a distributed hydrological model for flood forecasting and impact assessment of land-use change in the International Mosel river basin. *In Proc. of the Vienna Symposium. IAHS Pub (No. 201).*

Partal, T., and Cigizoglu, H.K. (2008). Estimation and forecasting of daily suspended sediment data using wavelet-neural networks. *Journal of Hydrology*, 358, 317–331.

Poornima, S., and Pushpalatha, M. (2019). Drought prediction based on SPI and SPEI with varying timescales using LSTM recurrent neural network. *Soft Computing*, 23(18), 8399-8412.

Rajaee, T., Nourani, V., Mohammad, Z.K., and Kisi, O. (2011). River suspended sediment load prediction: Application of ANN and wavelet conjunction model. *Journal of Hydrologic Engineering*, 16, 613–627.

Ralph, F.M., Neiman, P.J., Wick, G.A., Gutman, S.I., Dettinger, M.D., Cayan, D.R., and White, A.B. (2006). Flooding on California's Russian River: role of atmospheric rivers. *Geophysical Research Letters*, 33(13).

Ralph, F.M., Coleman, T., Neiman, P.J., Zamora, R., and Dettinger, M.D. (2012). Observed

impacts of duration and seasonality of atmospheric-river landfalls on soil moisture and runoff in coastal northern California. *Journal of Hydrometeorology*, 14 (2), 443–459.

Ramanarayanan, T.S., Williams, J.R., Dugas, W.A., Hauck, L.M., and McFarland, A.M.S. (1997). Using APEX to identify alternative practices for animal waste management (No. 972209). *ASAE Paper.*

Ramirez, J.A. (2000). Prediction and modeling of flood hydrology and hydraulics. Inland flood hazards: Human, riparian and aquatic communities. *Cambridge University Press.*

Refsgaard, J. C., and Storm, B. (1990). Construction, calibration and validation of hydrological models. *In Distributed hydrological modelling,* 41-54.

Rozalis, S., Morin, E., Yair, Y., and Price, C. (2010). Flash flood prediction using an uncalibrated hydrological model and radar rainfall data in a Mediterranean watershed under changing hydrological conditions. *Journal of Hydrology*, 394 (1–2), 245–255.

Rosenblueth, E. (1975). Point estimates for probability moments. *Proceedings of the National Academy of Sciences*, 72(10), 3812-3814.

Rosenblatt, F. (1958). The perceptron: a probabilistic model for information storage and organization in the brain. *Psychological review*, 65(6), 386.

Sahoo, S., Russo, T. A., Elliott, J., and Foster, I. (2017). Machine learning algorithms for modeling groundwater level changes in agricultural regions of the US. *Water Resources Research*, 53(5), 3878-3895.

Seo, Y., Kim, S., and Singh, V. P. (2018), Machine learning models coupled with variational mode decomposition: A new approach for modeling daily rainfall-runoff. *Atmosphere*, 9(7), 251.

Shen, C. (2018), A transdisciplinary review of deep learning research and its relevance for water

resources scientists. *Water Resources Research*, 54(11), 8558-8593.

Shortridge, J.E., Guikema, S.D., and Zaitchik, B.F. (2016). Machine learning methods for empirical streamflow simulation: a comparison of model accuracy, interpretability, and uncertainty in seasonal watersheds. *Hydrology and Earth System Sciences*, 20 (7), 2611–2628.

Shrestha, D. L. (2009). Uncertainty analysis in rainfall-runoff modelling: Application of machine learning techniques. *IHE Delft Institute for Water Education.*

Shrestha, D. L., and Solomatine, D. P. (2008). Data-driven approaches for estimating uncertainty in rainfall-runoff modelling. *International Journal of River Basin Management*, 6(2), 109-122.

Shrestha, D. L., and Solomatine, D. P. (2009). Assessing uncertainty in rainfall-runoff models: Application of data-driven models. *In Flood Risk Management: Research and Practice*, 1563-1573.

Singh, J., Knapp, H.V., Arnold, J.G., and Demissie, M. (2005). Hydrological modeling of the Iroquois river watershed using HSPF and SWAT. *Journal of the American Water Resources Association*, 41 (2), 343–360.

Singh, A. D., and Sharif, M. (2019). Bi-directional Storage Capacity and Elevation Level Calculator for Reservoir Operation Management. *American Journal of Water Resources*, 7(3), 121-127.

Singh, V.P., and Woolhiser, D.A. (2002). Mathematical modeling of watershed hydrology. *Journal of hydrologic engineering*, 7 (4), 270–292.

Solomatine, D. P., and Dulal, K. N. (2003). Model trees as an alternative to neural networks in rainfall—runoff modelling. *Hydrological Sciences Journal*, 48(3), 399-411.

Solomatine, D. P., Maskey, M., & Shrestha, D. L. (2008). Instance-based learning compared to other data-driven methods in hydrological forecasting. *Hydrological Processes: An International Journal*, 22(2), 275-287.

Solomatine, D. P., and Ostfeld, A. (2008). Data-driven modelling: some past experiences and new approaches. *Journal of Hydroinformatics*, 10(1), 3-22.

Sønderby, C. K., Espeholt, L., Heek, J., Dehghani, M., Oliver, A., Salimans, T., Agrawal, S., Hickey, J., and Kalchbrenner, N. (2020). MetNet: A Neural Weather Model for Precipitation Forecasting. *arXiv preprint arXiv:2003.12140.*

Souffront Alcantara, M. A., Kesler, C., Stealey, M. J., Nelson, E. J., Ames, D. P., and Jones, N. L. (2018). Cyberinfrastructure and web apps for managing and disseminating the national water model. *Journal of the American Water Resources Association*, 54(4), 859-871.

Taylor, K. E. (2001), Summarizing multiple aspects of model performance in a single diagram. *Journal of Geophysical Research: Atmospheres*, 106(D7), 7183-7192.

Tian, Y., Xu, Y. P., Yang, Z., Wang, G., and Zhu, Q. (2018). Integration of a parsimonious hydrological model with recurrent neural networks for improved streamflow forecasting. *Water*, 10(11), 1655.

Tokar, A.S., and Johnson, P.A. (1999). Rainfall-runoff modeling using artificial neural networks. *Journal of Hydrologic Engineering,* 4(3), 232-239.

Tran, Q. K., and Song, S. K. (2017). Water level forecasting based on deep learning: a use case of Trinity river-Texas-The United States. *Journal of KIISE*, 44(6), 607-612.

Tsai, M. J., Abrahart, R. J., Mount, N. J., and Chang, F. J. (2014). Including spatial distribution in a data-driven rainfall-runoff model to improve reservoir inflow forecasting in Taiwan. *Hydrological Processes*, 28(3), 1055-1070.

Tsai, C.F., and Chen, M.L. (2010). Credit rating by hybrid machine learning techniques. *Applied soft computing*, 10 (2), 374–380.

Tung, Y. K. (2011). Uncertainty and reliability analysis in water resources engineering. Journal of Contemporary *Water Research and Education*, 103(1), 4.

Vapnik, V. (1995). The Nature of Statistical Learning Theory, *Springer,* New York, NY, USA.

Vrugt, J. A., Ter Braak, C. J., Clark, M. P., Hyman, J. M., and Robinson, B. A. (2008). Treatment of input uncertainty in hydrologic modeling: Doing hydrology backward with Markov chain Monte Carlo simulation. *Water Resources Research*, 44(12).

Wang, W. (2006). Stochasticity, nonlinearity and forecasting of streamflow processes. *Ios Press.*

Wang L, Liu HL, Bao AM, Pan XL, and Chen X. (2014). Estimating the sensitivity of runoff to climate change in an alpine-valley watershed of Xinjiang, China. *Hydrological Sciences Journal,* 61(6), 1069–1079.

Wang, J., Shi, P., Jiang, P., Hu, J., Qu, S., Chen, X., Chen, Y., Dai, Y., and Xiao, Z. (2017). Application of BP neural network algorithm in traditional hydrological model for flood forecasting. *Water*, 9(1), 48.

Wang, Z., Lai, C., Chen, X., Yang, B., Zhao, S., and Bai, X. (2015). Flood hazard risk assessment model based on random forest. *Journal of Hydrology*, 527, 1130-1141.

Wu, J., Liu, H., Wei, G., Song, T., Zhang, C., and Zhou, H. (2019). Flash flood forecasting using support vector regression model in a small mountainous catchment. *Water*, 11(7), 1327.

Wu, R., Yang, L., Chen, C., Ahmad, S., Dascalu, S. M., and Harris Jr, F. C. (2018). Modeling Error Learning based Post-Processor Framework for Hydrologic Models Accuracy Improvement. *Geoscientific Model Development Discussions*, 1.

Wu, Z. Y., Lu, G. H., Wen, L., and Lin, C. A. (2011). Reconstructing and analyzing China's

fifty-nine year (1951-2009) drought history using hydrological model simulation. *Hydrology & Earth System Sciences Discussions*, 8(1).

Xia, Y., Hobbins, M. T., Mu, Q., and Ek, M. B. (2015), Evaluation of NLDAS-2 evapotranspiration against tower flux site observations. *Hydrological processes*, 29(7), 1757-1771.

Xia, Y., Mitchell, K., Ek, M., Sheffield, J., Cosgrove, B., Wood, E., Luo, L., Alonge, C., Wei, H., Meng, J., Livneh, B., Lettenmaier, D., Koren, V., Duan, Q., Mo, K., Fan, Y., and Mocko, D. (2012). Continentalscale water and energy flux analysis and validation for the North American Land Data Assimilation System project phase 2 (NLDAS-2): 1. Intercomparison and application of model products. *Journal of Geophysical Research: Atmospheres*, 117(D3).

Xiang, Z., Yan, J., and Demir, I. (2020). A rainfall-runoff model with LSTM-based sequence-to-sequence learning. *Water Resources Research*, 56(1), e2019WR025326.

Xu, L., Chen, N., Zhang, X., and Chen, Z. (2018). An evaluation of statistical, NMME and hybrid models for drought prediction in China. *Journal of Hydrology*, 566, 235-249.

Xu, T., Valocchi, A. J., Choi, J., and Amir, E. (2014). Use of machine learning methods to reduce predictive error of groundwater models. *Groundwater*, 52(3), 448-460.

Yan, L., Feng, J., and Hang, T. (2019). Small watershed stream-flow forecasting based on LSTM. *In International Conference on Ubiquitous Information Management and Communication*, 1006-1014.

Yilmaz, A. G., and Muttil, N. (2014). Runoff estimation by machine learning methods and application to the Euphrates Basin in Turkey. *Journal of Hydrologic Engineering*, 19(5), 1015-1025.

Young, C. C., Liu, W. C., and Wu, M. C. (2017). A physically based and machine learning hybrid approach for accurate rainfall-runoff modeling during extreme typhoon events. *Applied Soft Computing*, 53, 205-216.

Zhang, D., Lin, J., Peng, Q., Wang, D., Yang, T., Sorooshian, S., Liu, X. and Zhuang, J. (2018a). Modeling and simulating of reservoir operation using the artificial neural network, support vector regression, deep learning algorithm. *Journal of Hydrology*, 565, 720-736.

Zhang, J., Zhu, Y., Zhang, X., Ye, M., and Yang, J. (2018b). Developing a Long Short-Term Memory (LSTM) based model for predicting water table depth in agricultural areas. *Journal of Hydrology*, 561, 918-929.

Zhuo, L., Han, D., Dai, Q., Islam, T., and Srivastava, P. K. (2015). Appraisal of NLDAS-2 multi-model simulated soil moistures for hydrological modelling. *Water Resources Management*, 29(10), 3503-3517.

Zia, H., Harris, N., Merrett, G., and Rivers, M. (2015), Predicting discharge using a low complexity machine learning model. *Computers and Electronics in Agriculture*, 118, 350-360.

Appendix A

Clustering Results from K-means Clustering Technique

Table A.1: Error indices and clustering ratings determined from K-means technique.

Event	CC	NSE	PBIAS	PE	PTE	Rating	Event	CC	NSE	PBIAS	PE	PTE	Rating
1	0.75	-6.1	49.4	-66.27	2	US	23	0.66	-0.36	59.48	209.92	3	US
2	0.53	-13.94	40.04	-54.89	1	S	24	0.79	-0.15	43.49	80.69	1	G
3	0.55	-16.57	47.66	-72.75	1	S	25	0.86	0.27	29.91	171.89	0	G
4	0.74	-19.27	29.47	-74.56	1	G	26	0.72	0.43	31.28	48.12	1	G
5	0.8	-0.04	15.92	-22.36	1	VG	27	0.81	0.46	24.1	31.95	1	G
6	0.67	-0.4	60.38	209.92	3	US	28	0.7	0.28	24.65	192.08	12	S
7	0.79	-0.15	43.49	80.69	1	G	29	0.69	0.37	32.87	88.34	3	G
8	0.86	0.24	30.61	171.89	0	G	30	0.91	0.77	19.29	40.82	2	G
9	0.72	0.43	31.28	48.12	1	G	31	0.94	0.83	13.74	31.88	5	VG
10	0.81	0.46	24.1	31.95	1	G	32	0.52	0.27	25.69	117.82	2	G
11	0.68	0.25	25.28	192.08	12	S	33	0.77	0.46	13.54	8.17	2	VG
12	-0.11	-2.38	85.54	1910.5	13	US	34	0.84	0.67	11.04	78.14	0	VG
13	-0.24	-3.88	82.41	331.83	17	US	35	0.47	-57.19	70.02	-83.61	12	US
14	0.25	-1.51	64.78	270.66	2	US	36	0.81	-6.45	49.5	-66.45	3	US
15	0.08	-5.73	40.6	-53.42	2	S	37	0.84	-0.89	26.68	-49.25	2	G
16	0.1	-2.5	34.02	42.07	11	S	38	0.42	-6.08	43.69	-54.46	2	S
17	0.43	-1.64	80.29	805.97	3	US	39	0.54	-27.03	44.21	-76.86	2	S
18	0.66	-1.81	71.7	250.84	12	US	40	0.69	-7.69	33.04	-59.29	1	G
19	0.76	-2.61	55.74	214.59	1	US	41	0.34	-0.72	55.33	11.06	1	US
20	0.42	-0.22	31.71	18.91	2	S	42	0.67	0.12	45.36	144.82	2	S
21	0.57	-3.98	40.84	57.64	2	S	43	0.8	-0.11	39.48	118.03	4	G
22	0.69	-1.99	45.31	136.51	2	S	44	0.12	-10.36	53.54	-64.48	1	S

Event	CC	NSE	PBIAS	PE	PTE	Rating	Event	CC	NSE	PBIAS	PE	PTE	Rating
45	0.63	-1.58	22.52	-44.29	1	G	76	0.77	0.44	22.69	-11.99	5	G
46	0.54	-0.25	20.4	60.73	1	G	77	0.57	-0.03	37.24	-0.81	1	S
47	-0.23	-0.89	48.95	42.95	17	US	78	0.59	-1.58	21.39	-44	1	G
48	0.65	0.37	25.16	98.83	1	G	79	0.6	-2.04	31.19	-46.17	1	G
49	0.93	0.52	16.94	67.95	0	VG	80	0.86	0.71	14.82	14.84	1	VG
50	0.91	0.26	18.18	9.67	3	VG	81	0.89	0.67	16.61	100.66	1	VG
51	0.31	-0.2	43.21	532.52	5	S	82	0.68	-0.4	22.11	-8.59	5	G
52	0.7	0.36	20.69	80.64	2	G	83	0.85	0.27	19.16	6.87	1	G
53	0.56	0.06	23.92	197.99	11	S	84	0.86	0.71	13.69	15.49	1	VG
54	0.56	-6.56	50.71	-64.25	11	US	85	0.89	0.7	14.53	98.67	1	VG
55	0.69	-2.03	37.74	-53.66	2	S	86	0.69	-0.57	22.62	-13.59	5	G
56	0.74	-0.68	27.11	-46.45	2	G	87	0.88	0.33	18.31	3.43	1	VG
57	0.78	-6.01	37.25	-62.41	6	G	88	0.92	0.75	19.29	-22.12	0	G
58	0.19	-2.1	43.58	-33.28	5	S	89	0.91	0.72	18.46	9.87	1	VG
59	0.42	-3.35	34.17	-56.84	2	S	90	0.72	0.4	24.56	16.92	4	G
60	0.71	0.1	28.13	-13.67	2	G	91	0.94	0.77	19.6	44.44	0	G
61	0.49	-0.48	46.13	59.67	1	S	92	0.72	-0.64	25.87	-41.91	1	G
62	0.79	0.19	28.57	-17.75	4	G	93	0.91	-15.59	38.01	-67.69	2	G
63	0.85	0.55	23.56	14.2	6	G	94	0.78	0.48	13.65	37.19	0	VG
64	0.89	-2.41	27.92	-44.41	4	G	95	0.98	0.21	12.48	-38.4	0	VG
65	0.23	-0.03	35.74	78.43	7	S	96	0.26	-0.36	79.28	749.51	1	US
66	0.39	-0.81	36.12	-15.39	4	S	97	0.52	-0.3	59.18	542.83	1	US
67	0.61	0.28	27.6	73.34	1	G	98	0.89	0.18	44.09	320.48	1	G
68	0.78	0.4	25.97	-0.2	0	G	99	0.33	0.03	26.73	114.52	1	S
69	0.92	0.43	15.64	-35.53	1	VG	100	0.64	-0.25	31.19	24.48	4	G
70	0.9	0.7	9.36	-22.41	1	VG	101	0.48	-0.32	25.84	77.11	1	S
71	0.49	0	27.75	0.95	4	S	102	0.72	-0.52	53.13	401.98	2	US
72	0.61	-1.22	19.61	-47.18	2	G	103	0.69	-0.14	41.65	327.59	1	S
73	0.87	0.75	9.87	14.83	1	VG	104	0.88	0.28	38.46	274.26	1	G
74	0.62	0.08	39.01	17.56	6	S	105	0.75	0.41	14.31	3.54	1	VG
75	0.74	-1.56	32.27	-54.03	2	G	106	0.76	-2.37	28.37	-24.19	3	G

Event	CC	NSE	PBIAS	PE	PTE	Rating	Event	CC	NSE	PBIAS	PE	PTE	Rating
107	0.67	-0.1	21.44	65.24	9	S	138	0.6	-7.52	27.39	-59.79	3	G
108	0.8	0.34	18.04	59.44	1	VG	139	0.03	-0.72	65.13	214.93	7	US
109	0.67	-0.61	49.99	557.04	18	S	140	0.47	-0.68	45.44	51.58	8	S
110	0.86	-0.24	42.37	310.79	1	G	141	0.59	-0.46	33.7	50.72	4	G
111	0.93	0.25	38.53	218.39	1	G	142	-0.06	-1.27	46.26	-15.63	5	US
112	0.84	0.39	20.51	73.93	2	G	143	0.03	-2.09	33.08	-2.64	4	S
113	0.56	-0.68	18.84	-1.33	4	G	144	0.51	-0.27	31.22	47.82	5	S
114	0.64	-0.17	19.55	71.85	9	G	145	0.86	-3.33	32.11	-66.89	2	G
115	0.81	0.04	19.1	89.13	0	G	146	0.69	-32.82	48.38	-77.11	4	S
116	0.47	-0.2	44.05	-5.89	0	S	147	0.8	-17.98	41.58	-73.24	2	G
117	0.43	0.05	37.76	11.1	6	S	148	0.96	-20.07	42.07	-70.95	1	G
118	0.69	0.43	23.87	6.17	1	G	149	0.8	-34.18	46.73	-73.75	1	US
119	0.29	-8.67	35.03	-72.34	1	S	150	0.76	-71.77	58.35	-84.06	1	US
120	0.28	-3.07	26.61	-56.92	6	S	151	0.75	0.29	25.53	-1.49	1	G
121	0.44	-0.74	16.84	-37.88	1	G	152	0.86	-0.25	20.92	-44.63	2	G
122	0.04	-30.75	52.64	-75.66	7	S	153	0.89	0.16	15.96	-32.11	1	VG
123	0.55	-0.18	33.35	-27.1	2	G	154	0.58	-0.2	27.25	-27.6	4	G
124	0.44	-1.02	30.85	-41.34	1	S	155	0.69	-1.32	17	-51.15	2	G
125	0.34	-10.02	26.92	-67.03	3	S	156	0.88	0.67	10.81	-11.34	1	VG
126	0.46	-7.58	21.98	-62.91	1	S	157	0.88	-7.97	58.68	-51.6	3	US
127	0.88	-4.65	44.65	-61.76	0	G	158	0.9	-39.81	62.6	-76.56	3	US
128	0.82	-0.21	24.3	-34.47	0	G	159	0.89	-25.9	49.94	-71.57	5	US
129	0.89	-0.95	25.82	-23.41	3	G	160	0.93	-17.81	59.73	-68.82	1	US
130	0.68	-29.65	44.35	-61.75	2	S	161	0.64	-48.08	61.35	-67.58	4	US
131	0.81	-4.12	23.53	-42.89	0	G	162	0.9	-19.63	56.99	-64.36	3	US
132	0.84	-0.1	15.4	-7.57	2	VG	163	0.87	0.5	26.72	102.22	4	G
133	0.63	-27.8	50.14	-85.64	2	S	164	0.95	-0.65	22.09	-49.24	4	G
134	0.47	-4.35	39.81	-69.86	7	S	165	0.99	0.98	4.58	-1.49	1	VG
135	0.52	-11.76	41.37	-68.09	3	S	166	0.94	0.76	13.77	57.24	1	VG
136	0.48	-2.07	32.03	-51.39	2	S	167	0.68	-0.34	14.64	44.33	4	G
137	0.48	-5.05	23.03	-62.52	2	S	168	0.98	0.84	8.49	-9.41	0	VG

Event	CC	NSE	PBIAS	PE	PTE	Rating	Event	CC	NSE	PBIAS	PE	PTE	Rating
169	0.63	0.23	33.37	3.9	2	G	200	0.92	-0.38	28.65	-40.14	1	G
170	0.91	0.78	13.92	-14.22	4	VG	201	0.95	0.87	13.82	2.92	0	VG
171	0.84	0.63	15.29	-14.73	2	VG	202	0.89	-2.59	28.14	-51.55	0	G
172	-0.02	-1.14	29.57	-11.06	5	S	203	0.88	-1.45	26.03	-46.37	1	G
173	0.28	-1.25	11.75	-31.55	4	S	204	0.26	-0.18	45.8	201.54	7	S
174	0.82	0.63	10.65	-12.63	3	VG	205	0.82	0.61	22.8	-13.98	1	G
175	0.47	-1.65	37.41	-53.57	7	S	206	0.96	0.77	14.49	38.83	1	VG
176	0.43	-0.89	32.86	-38.19	16	S	207	0.61	0.16	12.73	-9.24	3	G
177	0.61	-0.68	23.59	-45.23	10	S	208	0.85	0.61	15.4	11.51	3	VG
178	-0.3	-5.5	38.18	-53.42	8	US	209	0.76	-1.41	26.51	-49.68	7	G
179	0.05	-5.84	15.19	-54.54	7	S	210	0.81	-2.05	23.47	-57.97	3	G
180	0.69	-0.3	13.66	-39.36	6	G	211	0.5	-11.93	31	-67.15	3	S
181	0.78	0.59	12.66	23.14	1	VG	212	0.67	-3.4	7.61	-36.39	3	G
182	0.81	0.64	13.69	12.65	2	VG	213	0.92	-1.2	14.54	-51.76	1	VG
183	0.89	-19.04	34.14	-59.25	1	G	214	0.65	-2.5	28.9	-54.85	12	S
184	0.92	-4.49	33.13	-49.87	0	G	215	0.72	-3.75	24.96	-61.53	8	S
185	0.71	0.35	10.6	-6.08	1	G	216	0.46	-14.12	29.93	-66.45	4	S
186	0.77	0.57	15.09	44.13	1	VG	217	0.54	-7.88	6.84	-35.19	4	G
187	0.79	-35.56	31.6	-64.95	1	G	218	0.9	-2.33	15.52	-51.72	3	VG
188	0.89	-2.62	29.92	-50.43	0	G	219	0.53	-2.37	27.24	-56.01	18	S
189	0.79	-1.65	35.15	-52.36	5	G	220	0.74	-0.9	25.18	-50.54	16	S
190	0.83	-1.27	33.3	-48.09	6	G	221	0.6	-4.45	5.64	-5.04	10	G
191	0.51	-3.11	22.92	-49.38	4	G	222	0.85	-0.87	18.69	-42.46	14	S
192	0.84	-0.59	18.91	-44.56	4	G	223	0.86	-10.05	46.66	-68.62	4	US
193	0.52	-10.59	52.96	-69.36	8	US	224	0.98	-5.73	47.67	-64.59	1	US
194	0.64	-4.77	39.46	-70.14	4	S	225	0.75	-4.75	27.51	-39.5	1	G
195	0.78	-4.42	32.72	-62.35	1	G	226	0.7	-25.1	40.6	-66.75	15	S
196	0.02	-9.59	38.41	-67.57	3	S	227	0.91	-4.53	34.7	-55.27	5	G
197	0.54	-13.27	29.33	-68.16	4	G	228	0.98	-0.6	31.69	-40.42	1	G
198	0.75	-7.83	24.11	-68.58	2	G	229	0.88	-9.43	22.79	-39.9	1	G
199	0.88	-1.02	28.03	-48.59	3	G	230	0.78	-37.48	40.69	-71.66	16	S

Event	CC	NSE	PBIAS	PE	PTE	Rating	Event	CC	NSE	PBIAS	PE	PTE	Rating
231	0.75	0.23	32.33	-20.14	16	S	262	0.41	-13.92	59.74	-74.77	2	US
232	0.11	-2.08	66.91	-40.48	20	US	263	0.65	-3.1	75.48	280.77	1	US
233	0.55	0.3	40.65	36.34	3	S	264	-0.45	-3.47	33.14	200.45	41	US
234	0.56	-13.57	63.51	-84.32	0	US	265	0.64	-3.3	14.87	-58.41	1	G
235	0.63	-115.4	75.67	-86.01	1	US	266	0.89	-393.3	57.72	-93.45	1	US
236	0.71	-335.5	74.49	-84.13	8	US	267	0.38	-0.81	75.87	491.88	20	US
237	0.6	-0.64	31.8	-43.63	9	G	268	0.39	-0.1	47.5	66.52	1	S
238	0.87	-46.3	67.23	-81.9	1	US	269	0.66	-1.02	61.87	456.58	12	US
239	0.79	0.08	41.54	49.27	1	G	270	0.63	-0.93	19.65	53.25	3	G
240	0.61	-4.96	33.5	30	0	G	271	0.62	-0.52	16.79	-1.9	5	G
241	0.84	-8.38	58.77	-64.65	0	US	272	0.47	-9.7	27.73	-56.57	6	S
242	0.74	-39.01	73.89	-78.84	2	US	273	0.72	0.12	37.35	8.59	4	S
243	0.6	-0.1	77.2	407.41	1	US	274	0.7	0.12	42.06	-8.56	7	S
244	0.56	0.22	43.89	19.16	2	S	275	-0.14	-6.39	85.33	-54.5	4	US
245	0.05	-0.09	81.77	661.02	19	US	276	-0.04	-3.52	77.81	-4.54	15	US
246	0.5	-0.11	77	1870.8	1	US	277	0.39	-0.89	65.67	26.78	1	US
247	0.73	0.22	46.21	-37.79	1	S	278	0.17	-3.62	63.76	-60.62	3	US
248	0.5	-1.91	90.16	845.87	4	US	279	0.67	0.12	65.1	10.03	1	US
249	0.08	-2.37	97.93	2448.5	10	US	280	-0.17	-0.31	83.02	2462.7	24	US
250	0.74	-0.39	73.87	199.6	1	US	281	0.67	-1.42	81.84	354.42	27	US
251	0.52	-1.85	94.63	1668.0	1	US	282	0.82	0	60.24	749.51	2	US
252	-0.18	-5.33	72.89	1071.7	39	US	283	0.85	-1.69	73.42	813.23	7	US
253	0.3	-4.28	68.95	466.34	0	US	284	0.63	0.13	19.56	84.06	2	G
254	0.7	0.28	44.82	7.85	2	S	285	0.31	0.05	20.43	52.48	5	S
255	0.24	-1.63	96.78	3055.3	8	US	286	0.35	-0.5	53.45	616.25	4	US
256	0.16	-1.67	99.04	3981.2	11	US	287	0.95	-0.23	58.16	405.76	2	US
257	-0.15	-1.75	84.41	693.53	3	US	288	-0.08	-0.39	48.81	132.2	7	US
258	0.09	-3.45	95.83	2154.0	9	US	289	-0.08	-0.83	44.43	-9.74	5	US
259	-0.01	-14.8	81.24	320.59	3	US	290	0.65	0.06	29.96	-37.15	29	S
260	0.47	-1.37	60.4	131.07	1	US	291	0.3	-3.99	50.03	-62.29	5	S
261	0.03	-1.22	68.42	3.03	29	US	292	0.66	0.31	29.28	15.06	9	G

Event	CC	NSE	PBIAS	PE	PTE	Rating	Event	CC	NSE	PBIAS	PE	PTE	Rating
293	0.38	-9.1	28.66	-64.97	5	S	324	0.62	-0.38	25.9	-41.3	2	G
294	0.37	-18.3	34.07	-73.45	6	S	325	0.65	-3.24	21.2	-65.33	1	G
295	0.71	-13.37	29.64	-72.02	2	G	326	0.01	-6.09	16.44	-56.45	11	S
296	0.52	-8.76	38.34	-74.09	5	S	327	0.73	0.24	41.64	-2.36	1	S
297	0.6	0.27	39.47	3.98	2	S	328	0.83	-0.77	46.26	-57.58	0	US
298	0.91	0.6	47.43	144.03	0	US	329	0.14	-0.57	69.03	18.12	8	US
299	0.69	0.35	41.19	-16.49	3	S	330	0.61	0.34	42.2	82.77	1	S
300	0.87	0.7	31.13	34.86	2	G	331	0.8	-3.47	47.41	-69.84	0	US
301	0.38	-0.42	66.84	152.72	29	US	332	0.19	-8.52	40.46	-42.99	6	S
302	0.25	-0.08	42.69	134.38	6	S	333	0.51	-0.05	39.82	258.08	35	S
303	0.57	-1.1	38.93	-31.72	2	S	334	0.65	0.42	33.65	48.91	1	G
304	0.47	-0.23	32.97	119.42	12	S	335	0.88	0.62	28.91	-24.69	0	G
305	0.75	-3.26	14.47	-48.02	1	VG	336	0.07	-0.14	45.89	191.86	2	S
306	0.81	-0.82	10.63	-29.08	0	VG	337	0.67	0.44	37.14	25.18	0	S
307	0.84	-0.94	29.75	-26.06	0	G	338	0.43	0.16	41.43	84.87	1	S
308	0.83	-0.34	36.8	-35.95	2	G	339	0	-9.09	93.25	3770	78	US
309	0.62	0.27	41.93	82.13	2	S	340	0	-29.04	93.94	3552.9	63	US
310	0.86	0.7	32.83	26.42	1	G	341	0	-19.15	93.53	3628.4	63	US
311	0.9	0.59	34.28	76.76	1	G	342	0.15	-0.89	85.08	942.61	33	US
312	0.57	-0.3	53.77	45.64	20	US	343	-0.27	-2.19	66.41	-4.72	7	US
313	0.5	-0.01	22.02	18.5	8	G	344	0.22	-2.25	81.02	972.67	13	US
314	0.74	0.1	36.23	-25.43	1	G	345	0	-8.87	44.99	18.6	7	S
315	0.51	-0.77	48.21	154.45	11	S	346	0.11	-2.77	31.2	-49.64	7	S
316	0.75	0.12	16.78	-11.19	1	G	347	0.65	0.2	51.25	101.63	2	US
317	0.87	0.31	25.55	34.84	1	G	348	0.51	0.19	52.87	52.06	2	US
318	0.89	0.68	17.67	19.31	1	VG	349	0.35	0	55.16	26.12	3	US
319	0.78	0.21	38.87	-26.9	2	G	350	0.76	0.29	49.48	88.62	2	US
320	0.8	0.2	43.53	0.85	2	G	351	0.69	-0.12	45.55	10.99	20	S
321	-0.14	-2.1	37.94	245.73	4	US	352	0.65	-0.72	16.81	-5.96	11	S
322	0.21	-5.99	62.22	-65.4	3	US	353	0.78	0.14	31.86	-24.78	2	G
323	0.5	-0.33	19.84	-36.94	1	G	354	0.66	0.03	29.03	60.24	11	S

Event	CC	NSE	PBIAS	PE	PTE	Rating	Event	CC	NSE	PBIAS	PE	PTE	Rating
355	0.77	-0.11	13.06	-32.34	2	VG	386	0.62	-2.18	31.52	25.73	29	S
356	0.86	0.64	17.19	10.62	1	VG	387	0.98	-0.31	22.04	43.94	3	G
357	0.96	0.7	15.66	-4.57	0	VG	388	0.9	0.24	15.25	43.27	5	VG
358	0.8	-0.13	31.82	-48.4	1	G	389	0.79	-3.33	20.38	-12.09	9	S
359	0.68	0.31	13.69	76.87	6	G	390	0.97	0.3	16.12	-38.5	2	VG
360	0.32	-0.65	49.69	43.26	33	S	391	0.85	0.45	31.41	270.94	1	G
361	0.9	-0.05	17.39	-38.23	0	VG	392	0.15	-0.11	49.79	446.23	4	S
362	0.69	-7.02	40.41	73.91	7	S	393	0.94	0.69	23.9	22.02	1	G
363	0.87	-1.65	25.71	36.43	7	G	394	0.02	-0.54	67.22	1807.5	65	US
364	0.86	-0.2	65.14	251.12	3	US	395	0.91	0.31	23.64	-41.1	1	G
365	-0.52	-4.33	45.63	320.78	64	US	396	0.87	-0.15	38.81	64.82	2	G
366	0.71	0.43	22.49	28.86	5	G	397	0.93	0.78	24.48	23.03	2	G
367	0.47	-1.27	59.51	395.86	9	US	398	0.92	0.69	29.29	-23.73	1	G
368	0.52	-0.7	59.94	347.05	7	US	399	0.8	0.43	28.13	322.52	2	G
369	0.71	-0.7	37.33	214.19	7	S	400	0.44	-0.22	16.52	29.89	53	S
370	0.53	-0.32	53.51	432.21	9	US	401	0.13	-0.6	53.28	610.17	3	S
371	0.65	0.37	26.4	-14.18	1	G	402	0.96	0.65	25.09	51.24	1	G
372	-0.14	-39.7	58.21	-82.02	6	US	403	-0.35	-0.38	64.01	1539.7	84	US
373	-0.07	-1.77	31.75	-29.41	16	S	404	-0.92	-17.78	37.15	-44.56	16	US
374	-0.14	-355.6	57.94	-81.84	9	US	405	0.91	0.2	21.5	54.96	2	G
375	-0.01	-38.74	45.67	-82.6	7	S	406	0.79	-0.16	31.38	21.04	5	G
376	0.46	-298.6	45.48	-90.72	1	US	407	0.96	0.87	26.31	29.76	0	G
377	0	-15.16	47.82	-77.71	7	S	408	0.74	-0.02	34.98	-44.88	5	G
378	0.31	-1.13	34.31	-47.1	27	S	409	0.41	0.07	57.59	204.1	5	US
379	-0.22	-32.68	57.93	-85.95	11	US	410	0.98	0.16	22.85	-39.08	1	G
380	-0.21	-1.4	30.75	-39.22	19	S	411	0.4	0.05	32.72	216.48	2	S
381	-0.05	-73.94	51.34	-85.53	12	US	412	0.9	-12.88	49.12	-67.95	0	US
382	-0.39	-40.42	54.65	-85.95	12	US	413	0.94	0.82	23.59	33.5	0	G
383	0.81	-67.69	74.92	-84.65	0	US	414	0.86	-43.38	35.6	-81.6	0	G
384	0.07	-4.25	93.57	286.53	7	US	415	0.9	0.68	20.51	-21.29	2	G
385	0.7	0.19	35.67	-25.53	15	S	416	0.89	-3.94	32.96	-68.8	0	G

Event	CC	NSE	PBIAS	PE	PTE	Rating	Event	CC	NSE	PBIAS	PE	PTE	Rating
417	0.87	0.4	16.23	-33.81	2	VG	448	0.56	-0.33	48.77	169.21	1	S
418	0.88	-83.95	51.13	-89.12	1	US	449	0.53	-21.05	57.71	-80.78	5	US
419	0.79	-19.11	49.66	-77.66	7	US	450	0.65	-1.88	56.64	-30.6	4	US
420	0.84	-4.18	46.61	-60.55	2	US	451	0.97	-0.47	35.21	-50.07	0	G
421	-0.08	-0.29	85.4	263.25	8	US	452	0.29	-3.47	40.65	-64.4	9	S
422	0.48	0.03	54.55	42.54	5	US	453	0.54	-1.23	32.26	-25.66	1	G
423	0.83	0.1	59.26	202.44	0	US	454	0.68	-165.4	40.9	-90.69	1	S
424	0.43	-0.47	75.51	1384.6	1	US	455	-0.36	-116.1	63.35	-90.65	7	US
425	0.9	-0.16	62.35	78.29	0	US	456	0.63	-25.81	56.86	-79.35	0	US
426	0.72	-0.81	75.2	96.42	1	US	457	0.62	0.1	60.2	229.12	1	US
427	0.67	-1.05	79.38	733.1	0	US	458	0.43	-0.17	41.35	113.66	1	S
428	0.92	0.27	47.13	86.79	1	US	459	0.91	0.55	29.41	116.58	1	G
429	0.78	-0.27	44.69	21.8	0	G	460	0.77	0.14	18.81	7.12	1	G
430	0.5	-0.34	28.3	-43.32	1	S	461	0.84	-0.62	23.5	-35.72	1	G
431	0.76	0.12	39.98	202.7	0	G	462	0.97	0.29	21.31	-30.19	0	G
432	0.83	0.18	54.07	57.61	0	US	463	0.45	-0.71	34.81	-37.75	7	S
433	0.32	-0.15	40.39	433.49	17	S	464	0.45	0.15	23.15	28.76	1	S
434	-0.38	-2.74	81.07	-3.3	5	US	465	0.94	0.7	14.42	54.3	1	VG
435	0.35	-1.91	93.16	527.02	1	US	466	-0.05	-8.59	90.6	-69.83	3	US
436	-0.11	-2.08	97.8	4321.8	2	US	467	0.33	-2.17	68.78	-61.31	1	US
437	0.31	-1.79	76.98	100.31	9	US	468	0.59	0.17	57.07	-1.71	2	US
438	0.01	-3.84	84.87	34.69	12	US	469	0.81	0.56	32.67	74.5	1	G
439	-0.04	-5.02	81.34	169.47	4	US	470	0.01	-15.18	38.37	-70.12	2	S
440	-0.2	-1.43	63.63	17.24	3	US	471	0.49	-4.78	28.4	-57.43	1	S
441	0.66	-0.55	91.79	1271.1	1	US	472	0.62	-2.24	38.3	-51.62	0	S
442	-0.04	-4.03	91.63	578.21	4	US	473	0.44	-0.21	54.17	11.09	11	US
443	0.97	-0.22	68.52	380.12	0	US	474	0.12	-8.81	64.19	-54.87	13	US
444	0.66	-1.56	62.7	92.62	1	US	475	0.18	-0.26	89.1	3705.8	5	US
445	0.62	-1.79	70.51	804.63	1	US	476	0.77	-0.09	75.52	746.94	1	US
446	0.68	-0.01	43.35	40.65	1	S	477	0.46	0.02	59.66	365.66	1	US
447	0	-1.11	38.22	166.92	12	S	478	0.77	0.13	68.28	760.3	0	US

Event	CC	NSE	PBIAS	PE	PTE	Rating	Event	CC	NSE	PBIAS	PE	PTE	Rating
479	0.85	0.2	55.84	261.41	1	US	510	0.83	0.48	21.02	174.8	1	G
480	0.93	-0.61	71.34	700.84	0	US	511	0.75	0.4	31.74	-11.76	3	G
481	0.81	0.02	63.13	541.56	3	US	512	0.67	-1.79	41.09	-49.93	1	S
482	0.46	0.12	39.44	97.37	0	S	513	0.32	-0.08	43.8	28.41	2	S
483	0.51	0.18	21.49	145.23	2	G	514	0.94	0.66	29.14	33.55	0	G
484	0.85	0.62	15.52	40.59	2	VG	515	0.97	0.75	12.2	-20.08	0	VG
485	0.87	0.72	17.51	18.5	1	VG	516	0.86	0.52	29.74	-32.76	0	G
486	0.87	-0.08	54.73	134.81	0	US	517	0.68	0.3	31.47	-5.69	4	G
487	0.74	-0.74	61.5	392.64	2	US	518	0.87	0.68	19.24	-8.42	0	G
488	0.38	-0.32	48.48	653.89	4	S	519	0.72	0.38	16.36	-16.34	1	G
489	0.28	0.02	30.29	507.24	11	S	520	0.71	-0.57	18.02	-46	2	G
490	0.59	-6.01	45.32	-71.29	3	S	521	0.78	-0.16	18.09	-49.17	2	VG
491	0.25	-19.12	53.46	-80.75	8	S	522	0.69	-4.7	44.98	-67.68	7	S
492	0.79	-1.41	24.27	-64.2	1	G	523	0.74	-1.68	24.32	-43.06	1	G
493	0.55	-4.75	37.48	-54.89	3	S	524	0.96	0.44	17.62	136.89	5	VG
494	0.48	-6.66	36.99	-69.75	3	S	525	0.5	-0.36	54.92	-34.23	2	US
495	0.68	-8.31	42.69	-75.54	1	S	526	0.52	-0.77	47.94	-41.5	2	S
496	0.24	-98.74	70.8	-89.53	8	US	527	0.88	0.76	19.62	5.09	1	G
497	-0.31	-21.7	53.26	-72.71	4	US	528	0.18	-7.62	22.61	-61.23	3	S
498	0.62	0.01	38.06	294.39	5	S	529	0.59	-0.74	25.1	-50.71	1	G
499	0.75	0.22	32.62	-38.62	1	G	530	0.42	-0.69	46.82	-31.66	6	S
500	0.68	-3.49	47.87	-62.15	1	S	531	0.41	-8.84	30.87	-64.72	3	S
501	0.93	0.74	23.68	39.99	1	G	532	0.57	-0.04	68.59	234.83	1	US
502	0.94	-1.02	30.78	-50.32	0	G	533	-0.08	-0.29	51.45	122.76	15	US
503	0.88	0.59	23.05	-25.89	1	G	534	0.56	-0.01	62.92	201.83	1	US
504	0.66	0.33	27.85	-0.11	0	G	535	0.83	-0.51	25.22	-19.65	1	G
505	0.64	0.41	28.65	5.39	3	G	536	0.75	-0.19	20.35	3.76	1	G
506	0.51	-0.71	34.15	1.92	3	S	537	0.79	-2.52	26.12	-54.16	2	G
507	0.52	-0.7	34.98	-24.32	4	S	538	-0.07	-0.3	48.92	135.55	9	US
508	0.61	-0.85	41.49	-36.24	3	S	539	-0.08	-2.47	68.71	-57.33	16	US
509	0.78	-5.41	46.54	-65.19	1	US	540	0.71	0.22	46.43	155.16	7	S

Event	CC	NSE	PBIAS	PE	PTE	Rating	Event	CC	NSE	PBIAS	PE	PTE	Rating
541	0.69	0.44	24.39	53.97	6	G	572	0.57	-10.07	29.82	-55.46	0	G
542	0.67	0.35	30.45	40.29	1	G	573	0.9	-7.55	21.66	-48.51	2	G
543	0.16	-2.45	34.96	-21.51	2	S	574	0.88	-43.45	47.28	-80.53	1	US
544	0.26	-3.67	75.03	-62.74	6	US	575	0.77	-34.96	60.43	-83.26	8	US
545	0.03	-0.32	74.86	177.35	1	US	576	0.81	-23.19	38.96	-79.77	0	G
546	0.07	-0.86	62.22	-25.13	3	US	577	0.33	-27.04	33.68	-37.73	17	S
547	0.26	-0.25	69.22	677.63	17	US	578	0.22	-0.22	55.72	34.19	2	S
548	0.38	0.12	57.81	171.51	0	US	579	0.61	0.2	47.62	34.04	2	S
549	0.38	0.07	53.45	160.19	8	US	580	0.37	-1.32	52.65	-50.12	4	US
550	0.64	0.2	30.86	-20.46	1	G	581	0.84	0.15	57.91	370.4	0	US
551	0.83	-0.34	29.03	-43.22	2	G	582	0.85	0.45	37.56	70.56	1	G
552	0.85	0.47	19.92	-14.92	3	G	583	0.78	0.51	18.94	-11.21	1	G
553	0.59	0.25	33.52	21.92	1	G	584	0.76	0.06	28.64	-38.66	2	G
554	0.89	0.68	19.05	69.8	3	G	585	0.74	0.35	25.49	-25.18	1	G
555	0.89	0.38	15.04	-23.93	5	VG	586	0.88	0.68	21.62	-10.82	1	G
556	0.83	0.66	17.46	91.44	2	VG	587	0.57	-0.46	25.58	-10.84	3	G
557	0.76	0.12	11.1	-14.96	0	VG	588	0.5	-1.59	23.81	-40.73	4	S
558	0.85	0.61	21.83	-22.6	3	G	589	0.48	-2.3	21.95	-49.67	3	G
559	0.58	0.12	34.98	43.17	2	S	590	0.66	-9.33	49.88	-75.11	8	S
560	0.19	-2.18	34.44	181.15	24	S	591	0.56	-5.16	29.14	-49.53	2	G
561	0.2	-0.47	61.94	1044.0	27	US	592	0.97	0.74	11.61	45.62	7	VG
562	0.44	-0.23	70.1	282.1	6	US	593	0.81	-2.13	24.27	-33.8	1	G
563	0.15	-3.18	55.3	109.13	7	S	594	0.86	-1.99	22.3	26.13	6	G
564	0.8	0.42	42.57	48.12	4	G	595	0.98	-2.28	33.57	-56.98	2	G
565	0.29	-1.42	38.27	-46.61	6	S	596	0.36	-2.79	39.46	2.28	25	S
566	0.07	-1.6	61.04	236.02	5	US	597	0.96	-7.11	39.29	-62.84	4	G
567	0.15	-1.18	43.11	-38.32	6	S	598	0.08	-0.97	76.88	1985.1	23	US
568	-0.34	-3.01	46.72	-40.68	11	US	599	0.73	0.19	43.54	189.19	5	S
569	-0.05	-1.98	62.51	-13.08	5	US	600	0.81	-0.19	33.72	48.32	4	G
570	0.83	-1.24	37.23	-41.1	3	G	601	-0.33	-11.64	48.87	262.66	34	US
571	0.88	-3.77	38.71	-67.28	1	G	602	0.96	0.86	14.16	24.68	2	VG

Event	CC	NSE	PBIAS	PE	PTE	Rating	Event	CC	NSE	PBIAS	PE	PTE	Rating
603	0.83	0.12	19.68	69.55	5	G	634	0.69	0.01	21.7	-15.05	11	S
604	0.8	0.46	10.83	2.46	4	VG	635	0.92	-0.64	22.32	-51.37	4	G
605	0.95	0.86	12.86	-19.37	4	VG	636	0.95	0.55	19.91	7.53	2	G
606	0.82	0.3	22.83	-10.27	3	G	637	0.59	-1.5	35.99	-57.13	12	S
607	0.14	-3.56	47.75	-71.84	8	S	638	0.97	-2.61	13.1	-24.88	1	VG
608	0.36	-6.05	42.25	-63.87	3	S	639	0.87	-8.16	12.37	-34.74	2	VG
609	0.88	0.61	21.84	-24.29	4	G	640	0.89	-3.61	19.98	-53.83	4	G
610	0.15	-1.84	30.5	-44.4	4	S	641	0.55	-4.05	37.51	-63.07	16	S
611	0.47	-5.28	28.47	-62.49	4	S	642	0.72	0.09	20.33	-23.48	20	S
612	0.26	-8.85	31.41	-73.3	5	S	643	0.59	0.26	35.99	-7.69	0	S
613	-0.21	-4.34	55.33	-55.42	12	US	644	0.57	-0.14	58.53	1027.6	4	US
614	0.53	-1.75	27.21	-47.86	16	S	645	0.92	0.83	22.43	16.31	0	G
615	0.56	-0.8	28.92	-53.59	11	S	646	0.89	0.72	19.68	78.71	19	S
616	-0.21	-8.09	35.53	-64.56	9	US	647	0.94	-0.44	31.01	-43.31	1	G
617	0.27	-16.14	33.76	-78.2	7	S	648	0.66	-2	40.61	-45.97	2	S
618	0.22	-30.08	40.22	-85.62	9	S	649	0.33	-0.46	33.64	-13.18	34	S
619	-0.44	-29.32	69.06	-82.1	14	US	650	0.59	-0.22	56.7	1236.8	2	US
620	0.24	-3.24	21.15	-63.95	21	S	651	0.77	0.58	24.33	20.78	1	G
621	0.59	0.01	63.38	341.91	0	US	652	0.91	0.75	18.5	70.13	2	VG
622	0.86	-1.28	32.11	-19.34	0	G	653	0.85	0.4	25.65	-12.63	3	G
623	0.79	-1.37	21.26	-19.25	3	G	654	0.97	-1.05	31.65	-37.19	0	G
624	0.89	-1.78	34.58	-44.27	0	G	655	0.93	-29.01	60.01	-74.67	0	US
625	-0.15	-1.03	51.23	48.22	9	US	656	0.76	0.56	20.19	-2.75	40	S
626	0.65	0	59.65	430.94	0	US	657	0.66	-290.2	85.13	-93.19	1	US
627	0.83	-3.75	33.92	-32.4	0	G	658	0.87	-95.87	76.81	-87.58	0	US
628	0.76	-2.16	29.19	-17.69	4	G	659	0.94	-276.4	87.57	-92.21	0	US
629	0.87	-8.83	42.73	-60.13	1	G	660	0.64	-24.93	72.85	-79.21	2	US
630	-0.16	-1.69	49.53	37.93	16	US	661	0.12	-18.34	50.76	-72.31	4	S
631	0.88	-20.32	51.06	-83.26	0	US	662	0.87	-57.37	65.68	-86.28	0	US
632	0.16	-2.87	32.57	-35.07	6	S	663	0.9	-13.57	51.04	-69.37	1	US
633	0.56	-48.53	50.01	-82.94	5	US	664	0.9	-5.1	37.66	-71.2	0	G

Event	CC	NSE	PBIAS	PE	PTE	Rating	Event	CC	NSE	PBIAS	PE	PTE	Rating
665	0.8	-534.4	74	-94.35	1	US	696	0.66	-0.43	22.66	102.67	3	G
666	0.66	-22.49	37.37	-45.49	0	S	697	0.75	-10.93	37.94	-27.15	1	G
667	0.73	-42.66	57.9	-80.79	3	US	698	-0.23	-1.09	99.38	1293.6	3	US
668	0.8	-62.6	67.53	-87.87	0	US	699	-0.09	-2.27	97.77	1406.7	14	US
669	0.82	-98.08	83.21	-88.42	2	US	700	-0.08	-7.22	90.62	86.3	4	US
670	0.82	-50.13	80.96	-65.05	0	US	701	-0.16	-5.71	93.94	4875.7	30	US
671	0.8	-74.2	70.67	-87.46	0	US	702	0.08	-3.36	94.68	1590.8	4	US
672	0.83	-34.25	54.21	-83.37	1	US	703	0.07	-3.34	83.65	97.62	2	US
673	0.3	-25.71	44.55	-72.41	20	S	704	-0.1	-3.92	77.67	947.73	3	US
674	0.97	-39.22	34.51	-63.71	0	G	705	-0.04	-2.23	80.01	238.53	3	US
675	0.71	-9.06	23.34	-44.05	2	G	706	-0.27	-9.91	86.85	552.04	6	US
676	0.87	-46.44	45.64	-39.6	1	US	707	0.04	-3.58	86.43	737.54	1	US
677	0.89	0.59	44	86.95	0	G	708	-0.31	-8.04	68.47	525.95	5	US
678	0.72	0.21	58.57	52.44	0	US	709	0.13	-1.88	91.77	667.88	13	US
679	0.92	0.57	47.42	105.61	0	US	710	0.51	-0.67	83.91	605.5	1	US
680	0.55	-0.82	62.27	-5.02	0	US	711	0.46	-2.08	77.08	338.03	1	US
681	0.46	-0.01	22.54	334.2	23	S	712	0.07	-1.66	59.34	114.59	2	US
682	0.78	-0.32	72.59	123.79	0	US	713	-0.15	-8.74	66.85	466.34	4	US
683	0.73	-0.5	64.85	37.1	1	US	714	0.59	-1.1	80.43	919.81	5	US
684	0.7	-0.12	37.68	-18.16	1	S	715	0.4	-0.85	61.87	189.23	2	US
685	0.05	-6.15	49.2	157.09	3	S	716	0.1	-16.99	69.47	506.14	9	US
686	0.61	-0.74	60.91	224.71	4	US	717	0.05	-7.01	54.77	364.98	17	US
687	0.53	-0.04	39.52	1.77	1	S	718	0.53	-0.31	63.97	163.17	2	US
688	0.15	-0.6	11.78	31.94	17	S	719	0.17	-10.62	85.03	837.94	2	US
689	0.52	-16.58	34.14	-48.16	3	S	720	0.04	-5.61	76.4	509.79	21	US
690	0.86	0.54	29.25	44.36	1	G	721	0.39	-3.78	52.67	-66.65	13	US
691	0.67	0.07	36.37	82.41	0	S	722	0.46	-136.0	64.33	-93.03	14	US
692	0.65	-0.06	56.87	69.63	1	US	723	0.67	-4.1	36.57	-68.41	3	S
693	0.55	-1.98	71.82	114.13	0	US	724	0.44	-104.9	52.26	-89.57	2	US
694	0.44	-0.62	38.52	21.55	1	S	725	0.52	-4.48	21.47	-15.52	1	G
695	0.22	-2.47	48.55	167.27	1	S	726	-0.41	-2.65	12.53	-2.71	13	S

Event	CC	NSE	PBIAS	PE	PTE	Rating	Event	CC	NSE	PBIAS	PE	PTE	Rating
727	0.81	-11.24	37.2	-70.11	3	G	758	0.12	-4.95	31.34	34.44	2	S
728	0.72	-14.41	44.67	-74.98	1	S	759	0.05	-7.22	18.24	-34.6	4	S
729	-0.22	-7.79	26.66	-52.09	19	S	760	0.65	-0.25	27.91	-37.01	1	G
730	0.85	-15.54	36.03	-69.04	1	G	761	0.54	-3.43	39.78	-55.19	1	S
731	0.13	-14.42	63.22	-77.33	0	US	762	0.17	-2.16	39.97	-0.33	2	S
732	0.3	-2.5	44.73	-34.66	5	S	763	0.43	-5.99	42.27	22.5	4	S
733	0.36	-0.83	30.39	-8.65	20	S	764	0.24	-3.27	27.06	52.7	2	S
734	0.9	-54.34	42.48	-45.69	0	G	765	0.4	-3.52	38.34	-62	1	S
735	0.62	-0.15	58.94	119.86	4	US	766	0.38	-2.52	64.05	111.3	2	US
736	0.47	-0.26	66.36	247.16	5	US	767	0.44	-0.71	57.5	-45.65	3	US
737	0.17	-0.51	47.6	385.57	4	S	768	0.78	-1.13	62.39	71.15	2	US
738	0.31	-0.44	20.38	-16.64	4	S	769	0.26	-2.47	40.42	-21.24	8	S
739	0.33	-0.16	17.35	49.65	5	S	770	0.73	-2.03	42.72	50.95	2	S
740	-0.06	-0.38	10.44	4.34	25	S	771	0.87	-0.67	45.44	79.25	1	G
741	0.76	0.29	23.94	78.93	6	G	772	-0.17	-5.89	42.29	-32.68	4	US
742	0.83	0.61	21.66	14.91	2	G	773	0.5	-3.46	47.41	31.56	3	S
743	0.8	-13.8	30.93	-56.02	14	S	774	0	-0.27	81.6	2692.0	18	US
744	0.37	-6.82	27.47	-52.45	5	S	775	0.69	-0.04	74.23	963.46	2	US
745	0.86	0.58	30.43	83.27	1	G	776	0.28	-0.06	63.36	749.51	34	US
746	0.93	-1.22	27.95	-42.82	4	G	777	0.6	-0.08	63.12	891.09	3	US
747	0.66	0.27	15.45	9.08	17	S	778	0.74	-0.07	69.31	1617.0	0	US
748	0.85	0.68	9.84	24.07	1	VG	779	0.86	0.57	40.66	115.86	1	G
749	0.9	0.78	10.52	27.71	6	VG	780	0.62	0.06	55	476.33	1	US
750	0.84	0.63	10.24	-5.86	1	VG	781	0.83	-0.05	52.93	539.63	2	US
751	0.62	-0.01	61.05	-27.94	1	US	782	0.91	-0.46	55.57	131.12	0	US
752	0.7	-0.31	59.09	-50.71	1	US	783	0.68	-0.19	42.2	188.32	5	S
753	0.5	-0.28	66.72	7.73	3	US	784	-0.12	-0.7	54.96	194.5	22	US
754	0.49	-1.67	64.09	-37.58	1	US	785	0.83	-0.73	61.26	580.96	0	US
755	0.26	-0.97	62.41	-42.33	3	US	786	-0.66	-0.87	55.55	235.27	26	US
756	0.6	-2.42	45.87	-25.65	1	S	787	0.68	0.28	25.79	16.17	1	G
757	0.19	-5.76	50.22	-71.76	2	S	788	0.7	-0.11	31.14	147.13	4	G

Event	CC	NSE	PBIAS	PE	PTE	Rating	Event	CC	NSE	PBIAS	PE	PTE	Rating
789	0.56	-0.82	27.96	101.82	0	G	820	0.54	-2.52	41.73	-42.6	0	S
790	-0.25	-0.27	42.44	274.47	11	US	821	0.89	-3.48	30.88	-60.93	0	G
791	0.88	0.59	20.61	64.1	2	G	822	0.87	0.67	26.2	16.68	1	G
792	0.53	-0.99	20.03	-9.82	0	G	823	0.21	-0.38	28.49	14.11	1	S
793	0.62	0.17	28.48	162.33	3	G	824	0.65	-9.67	38.23	-65.35	1	S
794	0.32	-0.16	29.93	106.21	19	S	825	0.67	-7.02	26.56	-40.3	1	G
795	0.74	-0.02	21.75	131.93	5	G	826	0.54	-8.14	27.26	-32.07	1	G
796	0.78	-0.12	64.75	392.47	2	US	827	0.4	0.15	33.31	85.32	5	S
797	0.52	-0.6	22	-0.11	8	G	828	0.51	0.09	36.02	5.44	3	S
798	0.03	-0.44	33.01	52.72	16	S	829	-0.15	-26.03	35.79	-73.18	18	US
799	0.55	0.1	22.52	140.03	2	G	830	0.9	-20.25	60.92	-78.96	2	US
800	0.84	0.24	21.72	71.27	7	G	831	-0.16	-2.22	12.02	-9.28	7	S
801	0.73	-0.05	25.8	331.83	1	G	832	0.51	0.23	43.35	32.01	3	S
802	0.62	-33.01	51.21	-85.86	3	US	833	0.85	-3.38	40.61	-33.16	3	G
803	0.19	-8.1	42.15	-66.33	13	S	834	0.33	-0.34	30.5	32.03	16	S
804	0.82	0.37	17.67	-26.79	1	VG	835	-0.01	-1.15	26.42	-0.85	3	S
805	-0.31	-87.79	59.06	-87.41	12	US	836	0.87	0.72	14.15	24.43	10	VG
806	0.19	-1.05	27.68	-28.8	5	S	837	0.72	-165.1	65.4	-84.23	2	US
807	-0.19	-2.82	28.43	-53.47	24	S	838	0.57	-10.82	23.85	-55.75	1	G
808	0.29	-0.52	34.53	-19.15	5	S	839	0.75	0.47	27.08	-11.3	1	G
809	0.49	-0.33	36.3	-34.71	3	S	840	0.82	-3.14	40.89	-70.08	1	G
810	0.83	-23.86	51.16	-76.83	6	US	841	0.45	-1.36	32.82	-29.95	3	S
811	0.34	-23.41	58.47	-76.11	7	US	842	0.72	0.06	33.4	-40.68	2	G
812	0.23	-1.6	60.62	-45.32	4	US	843	0.76	-0.07	27.62	-36.58	0	G
813	0.68	-5.06	33.37	-69.29	5	G	844	0.78	0.39	24.26	95.07	0	G
814	0.66	-0.09	18.17	-27.82	7	G	845	0.73	-3.97	22.88	-66.9	0	G
815	0.73	0.46	18.63	-2.55	5	G	846	0.62	-0.1	14.69	-12.3	2	G
816	0.75	-7.9	44.21	-63.51	3	S	847	0.55	0.08	10.78	-1.72	2	G
817	0.76	0.05	33.35	-30.31	1	G	848	0.66	0.4	24.14	26.32	3	G
818	0.98	-0.95	42.03	-50.3	0	G	849	0.69	0.24	27.72	-27.07	2	G
819	0.39	-2.8	58.11	-47.61	4	US	850	0.21	-48.68	37.79	-76.38	6	S

Event	CC	NSE	PBIAS	PE	PTE	Rating	Event	CC	NSE	PBIAS	PE	PTE	Rating
851	0.9	-16.47	33.86	-78.55	0	G	882	-0.03	-8.57	24.94	-39.47	6	S
852	0.59	-1.01	12.19	-45.15	1	G	883	-0.14	-2.76	53.34	-30.24	13	US
853	0.71	0.32	35.94	-25.41	2	G	884	0.29	-0.1	47.32	67.75	19	S
854	0.91	-3.01	31.89	-60.91	4	G	885	0.85	-0.04	21.1	-17.6	1	G
855	0.65	-0.22	21.57	-15.59	7	G	886	0.77	0.04	37.52	95.67	4	G
856	0.3	-3.57	21.36	-36.47	2	S	887	0.84	-0.55	24.66	-43.01	1	G
857	0.91	0.78	9.96	5.68	4	VG	888	0.78	-0.23	92.28	968.4	1	US
858	0.65	-77.1	43.99	-77.57	3	S	889	0	-2.19	98.36	34163	49	US
859	0.71	-8.11	17.51	-64.89	3	G	890	-0.09	-2.2	96.47	1614.9	3	US
860	0.25	-5.59	75.2	-68.99	3	US	891	0.24	-0.38	45.41	214.94	9	S
861	0.3	-1.38	65.62	-44.74	2	US	892	0.91	0.28	37.24	176.94	2	G
862	0.62	-0.46	70.97	232.86	2	US	893	0.68	0.38	16.86	23.57	5	G
863	0.6	-2.07	60.74	139.57	0	US	894	0.17	-7.68	25.55	-35.35	7	S
864	0.7	-0.87	73.98	228.02	1	US	895	-0.14	-2.42	53.37	-26.3	12	US
865	0.77	-0.35	19.84	-41.55	1	G	896	-0.21	-13.99	23.75	-68.96	7	S
866	0.32	-9.78	37.66	-71.5	2	S	897	0.78	0.07	36.94	107.25	1	G
867	0.63	-5.9	21.41	-48.76	1	G	898	0.82	-0.51	25.18	-35.14	2	G
868	0.43	-0.04	29.55	55.93	17	S	899	0.64	-0.07	45.44	-22.97	6	S
869	0.67	0.06	36.24	-7.13	1	S	900	0.69	0.45	39.68	25.61	1	S
870	0.6	-0.97	38.04	-46.78	2	S	901	0.56	-0.23	41.33	-33.59	2	S
871	0.71	-0.32	20.51	-29.93	2	G	902	0.77	0.56	31.69	38.06	1	G
872	0.61	-2.15	24.89	-58.69	5	G	903	0.3	0.07	43.1	221.6	4	S
873	0.18	-6.7	29.89	-49.06	2	S	904	0.87	0.75	25.19	-7.16	1	G
874	0.75	0.1	23.95	4.85	16	S	905	0.54	-0.21	53.88	831.48	5	US
875	0.09	-8.2	35.92	-27.13	4	S	906	0.97	0.1	29.61	-48.82	0	G
876	0.79	-0.17	93.15	1098.7	0	US	907	0.35	-0.3	29.55	93.5	7	S
877	0	-2.33	98.27	31331	47	US	908	0.97	0.33	43.23	120.47	1	G
878	-0.09	-2.11	96.78	2059.7	2	US	909	0.94	0.13	16.72	-38.16	1	VG
879	0.25	-0.44	48.33	220.83	9	S	910	0.78	-1.93	22.82	-44.99	2	G
880	0.92	0.25	39.07	214.63	1	G	911	0.62	0.38	17.36	-2.58	1	G
881	0.61	0.3	18.01	31.25	5	G	912	0.92	-2.43	26.12	-59.6	0	G

Event	CC	NSE	PBIAS	PE	PTE	Rating	Event	CC	NSE	PBIAS	PE	PTE	Rating
913	0.91	0.43	16.33	-39.13	1	VG	944	0.57	-212.3	63.12	-89.37	2	US
914	0.78	-1.04	21.89	3.34	3	G	945	0.86	-31.2	53.94	-76.46	2	US
915	0.83	0.49	15.13	-20.19	1	VG	946	0.93	-20.09	42.96	-73.91	1	G
916	0.88	0.32	15.93	-36.42	1	VG	947	0.92	-52.88	73.53	-86.03	0	US
917	0.91	0.53	23.24	-22.04	1	G	948	0.93	-29.4	36.09	-75.54	1	G
918	0.84	0.56	26.64	-27.02	1	G	949	0.92	-161.5	53.25	-84.73	4	US
919	0.76	-0.34	23.86	-3.02	11	S	950	-0.08	-7.48	35.65	98.81	11	S
920	0.72	0	26.83	-22.39	1	G	951	0.35	-0.8	47.97	-35.8	3	S
921	0.84	-0.16	26.79	-43.57	1	G	952	0.58	0.23	34.87	0.34	2	S
922	0.64	0.18	21.25	-22.19	0	G	953	0.72	-1.7	39.65	-64.14	1	S
923	0.92	0.35	26.11	-34.88	1	G	954	0.27	-1.56	33.86	-41.26	3	S
924	0.87	0.27	22.57	-46.03	3	G	955	0.42	-0.64	30.2	-26.76	2	S
925	0.62	-0.23	16.28	11.29	1	G	956	0.73	-0.37	27.61	-51.83	1	G
926	0.71	-3.24	25.09	-35.95	0	G	957	0.5	-0.76	26.14	-31.21	1	S
927	0.66	0.14	24.89	39.55	7	G	958	0.84	0.63	21.46	70.56	1	G
928	0.9	0.74	14.49	-16.81	0	VG	959	0.75	-0.68	18.75	-44.96	1	G
929	0.93	-0.36	25.3	-24.49	1	G	960	0.74	0.26	12.68	-15.88	1	VG
930	0.11	-0.96	64.85	16.31	17	US	961	0.56	-0.12	15.61	-10.16	2	G
931	-0.02	-0.79	62.92	18.84	8	US	962	0.62	0.31	26.79	36.54	4	G
932	0.22	-1.14	52.31	-20.67	5	S	963	0.71	0.46	23.5	-19.11	2	G
933	-0.26	-22.41	43.1	-78.9	6	US	964	0.96	-10.59	31.68	-61.11	1	G
934	-0.33	-1.55	17.03	63.68	7	S	965	0.36	-69.2	37.66	-78.14	7	S
935	0.06	-0.78	46.38	10.94	8	S	966	0.89	-6.76	30.5	-70.98	1	G
936	-0.15	-3.89	44.4	-46.07	7	US	967	0.57	-1.08	13.47	-44.98	2	G
937	-0.07	-0.18	12.06	1.89	22	S	968	0.66	0.31	39.13	-19.81	2	S
938	0	-0.59	71.27	3.89	6	US	969	0.89	-1.21	24.56	-51.76	5	G
939	0.02	-3.59	70.98	170.02	6	US	970	0.73	0.49	13.98	-19.88	7	G
940	-0.14	-2.76	55.61	157.36	24	US	971	0.05	-2.73	19.91	-23.99	3	S
941	0.91	0.75	11.39	-14.52	3	VG	972	0.86	0.72	13.51	38.46	1	VG
942	0.87	0.65	15.68	-25.39	2	VG	973	0.85	-26.7	39.67	-72.56	1	G
943	0.91	-7.4	33.11	-69.46	0	G	974	0.7	-7.7	20.36	-63.54	4	G

Event	CC	NSE	PBIAS	PE	PTE	Rating	Event	CC	NSE	PBIAS	PE	PTE	Rating
975	0.7	-0.77	25.28	-10.75	7	G	1006	0.16	-290.5	53.91	-85.7	4	US
976	0.89	-0.33	17.67	-32.87	0	VG	1007	0.48	-0.22	40.06	-30.48	4	S
977	0.33	-0.84	19.07	-16.98	24	S	1008	0.77	-4.44	34.28	-67.53	5	G
978	0.71	-2.03	11.9	-28.19	12	G	1009	0.45	-0.22	16.22	-12.38	10	G
979	0.93	-3.61	41.96	-55.6	1	G	1010	-0.27	-8.5	18.86	-48.31	4	S
980	0.42	-0.04	40.22	261.3	8	S	1011	0.81	0.14	15.21	-28.2	6	VG
981	-0.1	-0.78	80.87	1540.4	14	US	1012	0.07	-4.52	21.22	-56.09	6	S
982	-0.44	-2.29	93.04	5463.6	15	US	1013	0.23	-2.19	42.94	-68.94	10	S
983	0.64	-0.7	84.33	1222.6	10	US	1014	0.33	-1.28	31.97	-47	21	S
984	0.77	-0.18	64.56	368.27	9	US	1015	-0.06	-12.23	39.42	-67.43	13	US
985	0.67	0.18	22.08	41.67	6	G	1016	0.27	-9.19	38.74	-74.96	11	S
986	0.91	-5.5	33.76	-53.89	2	G	1017	0.39	-28.65	43.38	-73.03	17	S
987	0.74	0.41	7.56	1.48	4	VG	1018	-0.07	-288.5	60.11	-87.53	10	US
988	0.86	0.38	21.49	140.07	2	G	1019	0.26	-2.07	51.26	-61.75	9	S
989	0.92	0.83	7.67	31.91	4	VG	1020	0.65	-0.93	18.52	-54.89	9	G
990	0.67	-0.05	13.89	32.46	15	S	1021	-0.04	-1.93	18.14	-34.61	9	S
991	0.81	0.65	4.24	14.22	2	VG	1022	0.09	-11.32	21.92	-65.72	10	S
992	0.9	0.7	15.5	65.85	3	VG	1023	0.81	-0.18	84.55	1482.4	1	US
993	0.88	0.22	28.46	125.58	3	G	1024	0.73	-0.47	39.68	571.84	1	S
994	0.97	0.9	6.64	-11.47	1	VG	1025	0.2	-0.59	77.03	732.45	11	US
995	0.88	0.56	6.05	20.28	4	VG	1026	-0.13	-1.11	74.83	1145.9	3	US
996	0.7	0.46	8.19	9.59	2	G	1027	0.1	-0.38	55.06	393.81	9	S
997	0.92	0.73	11.06	71.94	11	VG	1028	0.88	0.18	39.77	356	0	G
998	0.29	-0.5	41.12	-37.42	7	S	1029	0.39	0.09	41.46	64.96	11	S
999	0.47	-0.02	34.28	14.45	14	S	1030	0.82	-0.53	29.43	-2.21	2	G
1000	-0.37	-54.52	47.46	-87.39	15	US	1031	0.81	-0.03	34.27	151.21	1	G
1001	-0.39	-90.89	45.67	-67.46	8	US	1032	0.91	0.35	16.19	-19.24	1	VG
1002	-0.74	-43.12	42.24	-60	8	US	1033	0.82	-0.18	84.53	1240.8	0	US
1003	0.33	-1.13	25.7	-34.2	9	S	1034	0.8	-1.04	50.96	682.88	0	US
1004	0.43	-1.18	33.94	-45.1	6	S	1035	0.22	-0.65	75.48	709.06	12	US
1005	0.24	-13.03	36.4	-64.24	13	S	1036	-0.19	-1.83	76.78	1148.5	3	US

Event	CC	NSE	PBIAS	PE	PTE	Rating	Event	CC	NSE	PBIAS	PE	PTE	Rating
1037	0.19	-0.44	48.78	285.79	9	S	1068	0.45	-2.81	12.02	-29.71	3	G
1038	0.88	0.24	34.54	246.61	5	G	1069	0.93	0.41	14.2	-15.47	4	VG
1039	0.36	0.04	44.34	67.61	12	S	1070	0.16	-14.72	8.63	-29.79	5	S
1040	0.88	-0.9	28.32	-17.21	4	G	1071	0.72	-0.27	10.23	13.85	10	G
1041	0.8	-0.01	30.94	101.24	1	G	1072	-0.07	-3.37	47.46	-46.51	15	US
1042	0.87	-0.38	19.69	-35.06	1	G	1073	0.65	0.09	34.81	-9.27	17	S
1043	0.89	0.19	62.68	312.69	6	US	1074	0.73	0.02	22.79	-46.54	12	S
1044	0.7	-0.17	26.39	-24.68	14	S	1075	0.69	0.16	19.51	-42.23	12	S
1045	0.86	-3.86	45.44	-51.18	2	G	1076	-0.18	-16.23	34.49	-74.24	16	US
1046	0.86	0.68	19.98	19.04	3	G	1077	-0.08	-3.59	12.18	-15.55	5	S
1047	0.81	-45.2	52.03	-73.53	18	US	1078	0.65	-1.13	21.14	-48.51	5	G
1048	0.79	-23.89	65.31	-83.18	5	US	1079	0.82	-2.2	14.19	-55.53	4	VG
1049	0.65	-8.38	36.59	-73.39	7	S	1080	0.67	-0.6	11.27	-36.27	37	S
1050	0.6	-15.99	53.25	-61.25	1	US	1081	0.71	-0.58	13.95	-17.65	3	G
1051	0.62	-13.37	38.05	-76.89	6	S	1082	0.62	-0.92	28.12	-50.29	4	G
1052	-0.01	-1.96	49.43	-39.08	14	US	1083	0.74	-0.9	34.39	0.99	4	G
1053	0.68	0.09	35.03	-0.05	17	S	1084	0.19	-6.12	19.25	-51.54	11	S
1054	-0.9	-0.55	25.36	72.18	84	US	1085	0.17	-4.56	12.35	-30.29	4	S
1055	0.77	0.44	21.65	-41.53	12	S	1086	0.92	0.33	15.3	-16.6	6	VG
1056	0.71	0.43	18.41	-33.31	12	S	1087	0.78	0.07	7.95	9.61	12	VG
1057	-0.07	-11.54	31.47	-72.31	14	S	1088	0.88	0.5	23.41	3.48	15	S
1058	0.06	-3.1	10.88	-13.15	4	S	1089	0.88	0.69	12.76	-25.97	7	VG
1059	-0.33	-31.53	17.95	-36.23	11	S	1090	0.79	-1.7	21.32	-48.59	8	S
1060	0.67	-1.57	20.22	-45.24	3	G	1091	0.93	-0.93	14.2	-43.56	8	VG
1061	0.86	-2.09	13.24	-56.04	3	VG	1092	0.78	-12.5	24.79	-35.76	1	G
1062	0.67	-0.5	9.02	-37.7	38	S	1093	0.84	-0.45	18.92	-9.79	12	S
1063	0.65	0.07	11.14	-8.03	3	G	1094	0.26	-3.63	17.62	-39.61	23	S
1064	0.84	0.63	9.02	18.33	2	VG	1095	0.9	0.17	14.39	-27.52	10	VG
1065	0.73	-0.33	24.34	-46.27	3	G	1096	0.82	-1.07	11.55	14.06	30	S
1066	0.79	-0.8	34.95	7.33	1	G	1097	0.89	-0.04	34.64	-36.22	1	G
1067	0.33	-6.09	18.62	-51.34	9	S	1098	0.75	0.44	35.52	-12.01	2	G

Event	CC	NSE	PBIAS	PE	PTE	Rating	Event	CC	NSE	PBIAS	PE	PTE	Rating
1099	0.78	0.27	47.27	142.56	4	US	1130	0.39	-4.45	38.45	-47.11	2	S
1100	0.96	0.59	32.76	104.63	0	G	1131	0.74	-7.29	24.78	-67.54	2	G
1101	0.51	-1.56	40.2	50.52	8	S	1132	0.25	-0.48	34.62	63.76	12	S
1102	0.83	0.58	26.47	50.81	5	G	1133	0.67	-18.74	28.49	-73.89	14	G
1103	0.97	-0.28	39.74	-28.76	1	G	1134	0.61	-0.44	61.58	332.31	2	US
1104	0.91	-5.71	51.37	-32.5	1	US	1135	0.79	0.49	23.01	27.07	1	G
1105	0.98	-1.05	37.28	-44.76	1	G	1136	0.14	-1.02	47.03	268.85	6	S
1106	0.99	0.42	27.9	-32.81	0	G	1137	0.72	0.01	28.76	35.07	1	G
1107	0.9	-24.16	72.72	-52.69	0	US	1138	0.14	-1.78	68.95	434.62	4	US
1108	0.9	-3.3	48.17	-66.74	1	US	1139	0.19	-1.81	46.98	61.71	3	S
1109	0.74	-11.98	51.56	-61.85	0	US	1140	-0.28	-2.59	49.01	183.17	19	US
1110	0.72	-13.79	59.98	-57.26	34	US	1141	-0.05	-3.67	50.31	-2.83	15	US
1111	0.61	-30.03	63.83	-63.96	4	US	1142	0.58	-2.17	63.22	318.28	3	US
1112	0.86	-40.41	66.09	-84.06	5	US	1143	0.68	-2.34	51.77	92.28	2	US
1113	0.91	-51.84	71.19	-71.41	11	US	1144	-0.07	-4.25	58.23	309.56	1	US
1114	0.74	-0.76	35.52	-35.1	0	G	1145	0.73	-2.31	45.82	97.86	15	S
1115	0.75	0.49	34.82	51.46	1	G	1146	0.61	-0.44	61.58	332.31	2	US
1116	0.69	0.13	44.83	150.7	3	S	1147	0.8	0.51	22.9	27.07	1	G
1117	0.66	0.09	39.31	141.03	15	S	1148	0.15	-0.9	45.54	268.85	6	S
1118	0.92	0.74	23.92	-9.75	0	G	1149	0.73	0.1	27.87	35.07	1	G
1119	0.94	0.54	32.12	103.85	1	G	1150	0.86	0.66	16.19	47.46	2	VG
1120	0.92	0.27	21.25	-30.32	3	G	1151	0.93	-2.7	17.3	-32.37	1	VG
1121	0.95	0.87	9.92	-8.3	3	VG	1152	0.85	0.55	13	-9.89	2	VG
1122	0.97	-5.31	30.17	-47.45	3	G	1153	0.79	-0.22	25.42	23.4	1	G
1123	0.84	-18.4	34.8	-40.67	1	G	1154	0.75	-0.97	32.17	152.35	0	G
1124	0.78	-5.26	50.52	-65.95	0	US	1155	0.94	0.8	6.95	9.04	0	VG
1125	0.81	-3.46	40.25	-46.06	0	G	1156	0.75	-0.09	25.2	-32.58	6	G
1126	0.95	-9.12	51.93	-62.77	2	US	1157	0.89	-22.38	32.08	-59.87	1	G
1127	0.94	-1.82	35.58	-32.82	0	G	1158	0.61	-6.56	30.89	-62.86	3	G
1128	0.85	-11.61	40.71	-71.16	7	G	1159	0.34	-0.3	25.98	12.44	14	S
1129	0.89	-1.8	8.93	-4.88	3	VG	1160	0.78	-2.31	24.08	-53.8	15	G

Event	CC	NSE	PBIAS	PE	PTE	Rating	Event	CC	NSE	PBIAS	PE	PTE	Rating
1161	0.49	-4.06	46.62	-71.05	1	S	1192	0.31	-0.52	20.42	16.2	6	S
1162	0.39	-2.35	36.86	-32.19	1	S	1193	0.86	0.53	11.4	-24.33	4	VG
1163	0.7	0.33	28.96	12.44	0	G	1194	0.79	-1.02	12.29	-27.81	5	VG
1164	0.77	0.3	32.97	-10.71	3	G	1195	0.84	-0.14	16.15	-42.14	1	VG
1165	0.53	-19.04	48.81	-76.35	2	S	1196	0.93	0.75	13.93	-18.42	1	VG
1166	0.53	-5.52	35.91	-55.28	1	S	1197	0.96	0.75	8.51	-20.56	12	VG
1167	0.69	0.08	20.21	0.64	9	S	1198	0.56	-6.55	43.99	-66.39	1	S
1168	0.95	-0.33	46.92	265.84	1	US	1199	0.48	-2.2	31.79	-7.33	2	S
1169	0.37	-4.35	53.19	106.12	3	US	1200	0.59	-0.17	34.89	77.44	5	S
1170	0.64	-1.17	62.08	730.63	5	US	1201	0.44	-4.35	25.83	28.26	8	S
1171	0.71	0.43	23.59	33.18	6	G	1202	0.77	0.17	37.45	20.26	3	G
1172	0.67	0.04	14.38	0.43	7	S	1203	0.55	-2.56	40.17	-50.7	2	S
1173	0.84	0.7	13.79	2.55	2	VG	1204	0.31	-1.43	31.13	6.26	11	S
1174	0.89	-0.39	41.07	281.1	1	G	1205	0.87	0.09	23.5	15.29	11	G
1175	0.71	-1.24	67.49	737.83	2	US	1206	0.91	0.67	22.8	106.25	1	G
1176	0.69	0.46	14.02	27.74	10	G	1207	0.88	0.46	20.83	7.59	7	G
1177	0.27	-56.78	44.86	-86.54	7	S	1208	0.91	0.48	21.61	130.97	1	G
1178	0.03	-1.85	26.78	-20.27	6	S	1209	0.84	0.29	25.34	-5.8	4	G
1179	0.62	-3.62	35.01	-58.6	6	S	1210	0.92	0.67	22.61	105.93	1	G
1180	0.62	-6.66	34.44	-52.11	3	S	1211	0.9	0.49	20.38	-0.07	7	G
1181	0.63	-5.85	38.8	-69.59	2	S	1212	0.87	0.46	21.51	91.91	0	G
1182	0.49	-1.07	30.21	-24.16	3	S	1213	0.86	0.31	24.44	-8.11	4	G
1183	0.6	-4.49	40.82	-63.51	12	S	1214	0.82	-9.15	34.99	-74.66	1	G
1184	0.09	-5.13	29.49	-58.91	7	S	1215	0.92	0.82	16.08	9.01	1	VG
1185	0.22	-0.03	24.75	106.47	7	S	1216	0.95	-0.35	20.25	-47.25	2	G
1186	0.74	0.51	21.69	17.73	5	G	1217	0.93	-0.91	30.12	-53.22	0	G
1187	0.63	-3.62	35.51	-31.85	7	S	1218	0.82	-3.32	28.37	-63.67	0	G
1188	0.64	-0.74	36.2	-40.29	4	S	1219	0.83	0.6	21.87	-8.3	1	G
1189	0.48	0.11	30.96	113.85	7	S	1220	0.77	-0.1	25.49	-32.97	0	G
1190	0.75	-0.8	28.75	-12.78	1	G	1221	0.77	0.15	36.8	129.27	3	G
1191	0.29	-4.16	25.66	-61.05	6	S	1222	0.87	0.29	30.31	133.89	7	G

Event	CC	NSE	PBIAS	PE	PTE	Rating	Event	CC	NSE	PBIAS	PE	PTE	Rating
1223	0.41	-0.35	45.54	34.07	1	S	1254	-0.19	-2.14	52.94	246.98	23	US
1224	0.72	-5.92	34.99	-49.64	5	S	1255	0.54	-0.33	33.83	25.41	17	G
1225	0.77	0.58	25.22	43.95	1	G	1256	0.75	-5.84	32.67	-60.27	1	G
1226	0.91	0.71	12.73	-14.34	0	VG	1257	0.81	-11.1	28.17	-73.63	3	G
1227	0.88	0.5	23.38	140.54	2	G	1258	0.87	-22.4	37.7	-66.51	2	G
1228	0.88	0.63	17.48	60.02	6	VG	1259	0.94	0.19	17.78	-40.13	0	VG
1229	0.94	-4.96	25.43	-49.58	1	G	1260	0.47	-7.59	23.78	-72.64	8	S
1230	0.81	0.61	18.32	32.44	1	VG	1261	0.16	-0.7	17.06	-3.38	7	S
1231	0.67	0.32	22.33	139.97	3	G	1262	0.84	-0.01	15.75	-35.27	4	VG
1232	0.93	0.41	27.38	149.65	1	G	1263	0.81	-3.16	16.78	-35.32	6	VG
1233	0.89	0.3	26.73	82.72	6	G	1264	0.84	-0.96	22.07	-50.16	2	G
1234	0.83	-1.06	51.71	254.47	2	US	1265	0.92	0.78	12.2	-21.31	1	VG
1235	0.92	0.82	10.34	44.78	0	VG	1266	0.66	0.36	17.84	1.25	0	G
1236	0.9	0.79	15.15	26.86	1	VG	1267	0.95	0.41	12.44	-38.02	11	VG
1237	0.73	0.34	34.06	114.4	2	G	1268	0.26	-17.63	59.7	-48.34	6	US
1238	0.67	0.29	21.31	-13.36	3	G	1269	0.89	-101.9	64.47	-79.87	2	US
1239	0.46	-1.16	19.55	-30.48	5	G	1270	0.48	-19.55	41.62	-42.02	2	S
1240	0.64	0.23	26.1	-0.14	3	G	1271	0.74	-39.15	56.24	-73.4	3	US
1241	0.64	0.09	26.74	-37.72	1	G	1272	0.72	-166.8	59.24	-74.36	3	US
1242	0.39	-4.35	26.31	-39.83	3	S	1273	0.85	-26.72	56.41	-73.26	2	US
1243	0.34	-1.09	20.34	6.71	1	S	1274	0.33	-10.45	55.74	-40.68	5	US
1244	0.24	-0.57	41.87	-5.5	4	S	1275	0.71	-13.37	49.54	-56.61	4	US
1245	0.94	0.77	15.42	19.08	1	VG	1276	0.92	-35.85	62.02	-77.61	3	US
1246	0.95	-1.19	21.42	-40.96	1	G	1277	0.57	-0.27	24.63	-21.07	5	G
1247	0.79	0.52	18.12	30.4	1	VG	1278	0.7	-1.65	19.82	59.44	7	G
1248	0.56	-0.17	28.82	-19.52	2	G	1279	0.95	-0.02	31.89	94.22	0	G
1249	0.72	-0.9	16.61	-52.26	3	G	1280	0.92	-5.46	26.43	82.65	2	G
1250	0.46	0.1	15.02	12.4	4	G	1281	0.98	0.59	22.48	64.05	2	G
1251	0.71	-0.22	18.42	-37.74	3	G	1282	0.63	0.38	13.69	43.82	6	G
1252	0.25	-1.25	44.03	101.89	5	S	1283	0.95	-0.88	34.22	123.72	2	G
1253	0.44	-0.43	37.87	-3.89	5	S	1284	0.84	0.24	19.24	12.48	1	G

Event	CC	NSE	PBIAS	PE	PTE	Rating	Event	CC	NSE	PBIAS	PE	PTE	Rating
1285	0.76	0.49	18.46	-11.52	4	VG	1316	0.83	0.68	16.68	16.72	1	VG
1286	0.59	-1.96	9.88	-27.97	6	G	1317	0.78	0.49	15.17	-17.64	5	VG
1287	0.75	0.24	11.73	-26.31	3	VG	1318	0.8	-0.02	33.69	269.82	1	G
1288	0.44	0.08	21.02	23.86	15	S	1319	0.92	0.82	11.9	-8.88	6	VG
1289	0.92	0.85	6.73	-4.89	2	VG	1320	0.77	-2.34	19.65	-47.98	2	G
1290	0.44	-1.55	27.62	-49.09	12	S	1321	0.83	-0.96	19.68	-56.67	2	G
1291	0.56	-2	22.74	-60.21	8	G	1322	0.51	-7.68	19.12	-51.72	14	G
1292	0.14	-0.72	20.03	-14.58	16	S	1323	0.9	0.21	12.85	-30.89	1	VG
1293	0.69	-0.23	15.82	-30.6	6	G	1324	0.73	-1.01	14.32	-2.34	4	G
1294	0.95	-1.27	18	-37.37	1	VG	1325	0.64	-5.07	18.97	-53.27	6	G
1295	0.97	-13.83	28.11	-55.48	1	G	1326	0.78	-1.91	23.56	-59.69	6	G
1296	0.9	-7.86	28.45	26.14	1	G	1327	0.47	-4.83	18.38	-39.1	14	S
1297	0.91	-18.1	34.21	-66.86	4	G	1328	0.88	-0.18	13.89	-31.63	3	VG
1298	0.96	-0.36	15.69	-31.58	1	VG	1329	0.77	0.17	13.88	-34.25	12	VG
1299	0.97	-17.35	29.25	-56.33	1	G	1330	0.8	-0.46	25.24	-34.37	9	G
1300	0.91	-5.76	24.16	11.4	0	G	1331	0.82	0.04	16.74	-25.46	19	VG
1301	0.96	-15.66	34.24	-67.61	0	G	1332	0.97	-3.11	42.93	-53.73	0	G
1302	0.84	0.17	25.91	-40.02	3	G	1333	0.69	-28.93	36.33	-67.38	7	S
1303	0.74	-2.42	22.85	-54.21	7	G	1334	0.94	-12.23	41.47	-74.27	1	G
1304	0.69	0.36	22.33	68.7	6	G	1335	0.98	-1.19	31.61	-40.19	0	G
1305	0.73	0.18	20.4	-22.78	8	S	1336	0.92	-34.68	35.02	-69.08	1	G
1306	0.35	-3.34	30.91	-45.7	5	S	1337	0.91	-5.38	35.28	-64.17	2	G
1307	0.73	0.08	16.78	-9.61	0	G	1338	0.1	-6.85	20.72	-67.78	6	S
1308	0.81	-10.56	31.34	-72.71	1	G	1339	0.03	-1.13	26.33	-4.29	6	S
1309	0.68	-0.43	22.81	108.47	25	G	1340	0.75	0.54	19.61	37.67	3	G
1310	0.31	-1.35	35.28	-28.13	6	S	1341	0.83	-1.81	13.16	-31.76	2	VG
1311	0.63	-2.97	33.08	-42.42	15	G	1342	0.73	0.26	18.22	-13.91	1	G
1312	0.84	0.61	18.93	1.82	1	G	1343	0.6	-1.81	22.83	-47.24	2	G
1313	0.92	-3.32	31.8	-63.42	2	G	1344	0.39	-0.44	27.79	46.48	3	S
1314	0.85	0.69	16.86	58.23	2	VG	1345	0.8	-0.22	10.89	-23.91	14	S
1315	0.82	0.03	24.51	-18.76	8	G	1346	0.9	0.43	8.94	-25.73	4	VG

Event	CC	NSE	PBIAS	PE	PTE	Rating	Event	CC	NSE	PBIAS	PE	PTE	Rating
1347	0.91	0.56	16.4	-31.35	4	VG	1378	0.88	-4.23	32.9	-44.72	2	G
1348	0.83	-0.06	9.72	-7.27	9	VG	1379	0.79	0.61	22.58	43.25	1	G
1349	0.96	0.83	9.2	-3.58	12	VG	1380	0.92	0.58	24.03	137.33	2	G
1350	0.66	-24.43	48.62	-76.11	1	S	1381	0.95	-0.91	21.76	-47.75	1	G
1351	0.65	-1.19	23.43	-35.93	1	G	1382	0.77	0.24	19.03	18.9	2	G
1352	0.83	0.49	21.69	21.07	2	G	1383	0.88	0.68	18.97	9.19	9	G
1353	0.6	-14.76	26.81	-56.02	7	G	1384	0.06	-35.88	40.66	-78.02	6	S
1354	0.59	-2.55	51.38	8.63	2	US	1385	0.6	-38.59	33.54	-82.49	0	G
1355	0.36	-3.63	20.76	-30.36	4	S	1386	0.92	0.5	11.31	-13.08	2	VG
1356	0.78	-9.76	46.58	-52.43	1	US	1387	0.49	-3.92	31.19	-58.78	7	S
1357	0.89	-11.97	57.59	-62.47	0	US	1388	0.56	-0.57	38.88	30.49	3	S
1358	-0.37	-4.14	92.24	877.51	20	US	1389	-0.49	-2.85	46.94	-28.34	7	US
1359	0.96	-1.99	33.29	-44.06	1	G	1390	0.31	-1.88	62.41	140.41	3	US
1360	0.91	-30.47	33.86	-68.56	3	G	1391	0.56	-7.07	59.82	95.91	2	US
1361	0.93	-19.62	18.59	-54.09	1	G	1392	0.45	-9.47	43.12	107.49	4	S
1362	0.94	-5.4	36	-60.52	0	G	1393	0.23	-1.88	46.73	43.83	2	S
1363	0.01	-1.32	79.12	171.3	7	US	1394	0.89	0.67	20.8	-2.44	2	G
1364	0.18	-2.38	60.24	157.56	5	US	1395	0.64	-0.05	13.8	45.66	9	G
1365	0.08	-2.18	41.16	-28.03	3	S	1396	0.81	0.23	20.29	-41.72	2	G
1366	0.53	-0.44	37.91	-46.59	4	S	1397	0.8	-1.82	25.06	-54.76	1	G
1367	0.93	-1.63	29.58	-43.82	1	G	1398	0.89	0.31	16.13	-12.06	1	VG
1368	0.86	-43.34	34.14	-66.38	2	G	1399	0.86	0.71	14.19	-20.89	1	VG
1369	0.97	-6.75	38.31	-59.21	0	G	1400	0.16	-2.78	43.19	-37.6	10	S
1370	0.28	-10.99	46.48	266.15	8	S	1401	0.38	-1.74	36.07	-42.15	10	S
1371	0.86	0.1	38.45	319.36	4	G	1402	0.28	-12.15	40.91	-63.59	5	S
1372	0.9	-0.38	35.39	66.18	1	G	1403	0.3	-7.74	34.06	-14.79	14	S
1373	0.89	-0.16	16.21	-12.74	1	VG	1404	0.54	-0.69	24.23	-9.29	4	G
1374	0.81	0.55	22.2	-5.61	1	G	1405	0.85	-2.22	40.91	140.17	9	S
1375	0.91	0.46	30.73	152.03	1	G	1406	0.95	0.58	15.69	-35.51	2	VG
1376	0.86	0.63	18.35	92.86	7	VG	1407	0.93	0.53	7.81	-7	2	VG
1377	0.6	-0.34	35.16	66.78	1	S	1408	0.9	-0.22	18.56	-51.23	1	G